



**ROCKSLIDES AND
ROCK AVALANCHES OF THE
KOKOMEREN RIVER BASIN
(CENTRAL TIEN SHAN)**

**ICL SUMMER SCHOOL ON ROCKSLIDES
AND RELATED PHENOMENA**

GUIDEBOOK

A.L. Strom & K.E. Abdrakhmatov

Moscow–Bishkek, 2009

CONTENT

1 INTRODUCTION.....	11
2 GEOLOGICAL BACKGROUND (FACTORS GOVERNING BEDROCK SLOPE FAILURES).....	13
2.1 GEOLOGY.....	13
2.2 GEOMORPHOLOGY AND NEOTECTONICS.....	13
2.3 SEISMICITY	20
2.4 HYDROGEOLOGICAL CONDITIONS.....	26
3 ROCKSLIDE CASE STUDIES.....	26
3.1 THE SNAKE-HEAD ROCK AVALANCHE.....	26
3.2 THE SEIT ROCK AVALANCHE.....	34
3.3 ROCKSLIDES IN THE OIGAING AND BURUNDU RIVER VALLEYS.....	41
3.4 THE CHONGSU ROCK AVALANCHE.....	42
3.5 THE SARYSU ROCK AVALANCHE.....	47
3.6 TOPPLING SITE.....	49
3.7 THE KASHKASU ROCKSLIDE AND THE UPPER TUURAKAING ROCK AVALANCHES.....	52
3.8 THE KOKOMEREN ROCKSLIDE.....	55
3.8.1 <i>Rockslide description</i>	55
3.8.2 <i>The Kokomeren rockslide 'satellites'</i>	61
3.8.3 <i>Active fault at the Kokomeren rockslide site</i>	68
3.8.4 <i>Evidence of inundation and subsequent breach</i>	72
3.9 THE DISPLACED PENEPLAIN ROCKSLIDE	77
3.10 THE MINI-KÖFELS ROCKSLIDE.....	82
3.11 THE KARAKUNGEY ROCK AVALANCHES.....	84
3.12 THE MINGTEKE ROCK AVALANCHE.....	90
3.13 LARGE LANDSLIDES IN THE NEOGENE-QUATERNARY SEDIMENTS.....	90
3.14 CALDERA-LIKE COLLAPSE AT THE NARYN RIVER BASIN DOWNSTREAM FROM THE KOKOMEREN RIVER MOUTH	94
4 CONCLUSIONS	98
5 ACKNOWLEDGEMENTS.....	98
6 REFERENCES.....	99

LIST OF FIGURES

FIGURE 1. POSITION OF THE KOKOMEREN RIVER BASIN WITHIN THE TIEN SHAN MOUNTAIN SYSTEM.....	12
FIGURE 2. LOCATION OF BEDROCK SLOPE FAILURES IN KOKOMEREN RIVER BASIN	12
FIGURE 3. GEOLOGICAL MAP OF THE STUDY REGION	14
FIGURE 4. SIMPLIFIED NEOTECTONIC SCHEME OF THE STUDY AREA.....	15
FIGURE 5. TILTED AND WARPED PLANATION SURFACE (P) AT THE EASTERN PART OF THE KYZYL-OI NEOTECTONIC DEPRESSION.....	15
FIGURE 6. FOLDING OF PRE-NEOGENE PLANATION SURFACE AND OVERLYING N-Q SEDIMENTS	16
FIGURE 7. UPLIFTED PRE-NEOGENE PLANATION SURFACE.....	16
FIGURE 8. SURFACE RUPTURES ASSOCIATED WITH LANDSLIDES AT THE NORTHERN BOUNDARY OF THE SUUSAMYR INTERMONTANE DEPRESSION.....	17
FIGURE 9. SURFACE RUPTURES ALONG THE NORTH-KYZYL-OI FAULT ZONE.	18
FIGURE 10. OUTCROP DOWNSTREAM FROM THE KYZYL-OI VILLAGE BETWEEN CHONGSUU AND KOBIIKSUU RIVER MOUTHS	18
FIGURE 11. SURFACE RUPTURE DISPLACING THE SUCCESSION OF LACUSTRINE AND FLUVIAL SEDIMENTS	19
FIGURE 12. SLICKENLINES ON THE SLIDING SURFACE OF RECENT FAULT SHOWN ON INDICATING STRIKE-SLIP SENSE OF MOTION.....	19
FIGURE 13. BOW-SHAPE SURFACE RUPTURE AT THE FAULT ZONE DIVIDING THE DJUMGAL RANGE AND THE SAME-NAME DEPRESSION	20
FIGURE 14. 2.5-KM LONG FRAGMENT OF THE NORTH-FACING ESCARPMENT OF PREHISTORIC SURFACE RUPTURE IN THE CENTRAL PART OF SUUSAMYR NEOTECTONIC DEPRESSION.....	20
FIGURE 15. STRONGEST EARTHQUAKES OF THE TIEN SHAN REGION.....	21
FIGURE 16. SURFACE RUPTURE (REVERSE FAULT) OF THE M 7.3 SUUSAMYR EARTHQUAKE	21
FIGURE 17. 1992 FAULT SCARP ABOUT 2.5 M HIGH ON THE SUUSAMYR FIRST RIVER TERRACE.....	22
FIGURE 18. LANDSLIDES TRIGGERED BY THE SUUSAMYR EARTHQUAKE	22
FIGURE 19. LANDSLIDE ON THE SOUTHERN SLOPE OF THE CHET-KORUMDY RIDGE TRIGGERED BY THE SUUSAMYR EARTHQUAKE	23
FIGURE 20. TOPPLING AT THE CENTRAL PART OF THE CHET-KORUMDU RIDGE ABOVE THE 1992 LANDSLIDE SCAR.....	23
FIGURE 21. COMPARISON OF ZOOMED SPACE IMAGES OF THE SAME SECTION OF THE CHET-KORUMDY RIDGE.....	24
FIGURE 22. ROCKSLIDE IN THE UPPER REACHES OF THE BELALDY CREEK CAUSED BY 1992 SUUSAMYR EARTHQUAKE.....	25
FIGURE 23. 1992 EARTHQUAKE INDUCED ROCKFALL ON THE RIGHT BANK OF THE KOKOMEREN RIVER VALLEY	26
FIGURE 24. LONG RUNOUT SNAKE-HEAD ROCK AVALANCHE	28
FIGURE 25. SPATIAL DISTRIBUTION OF ROCKSLIDES, LANDSLIDES AND RECENT FAULTS OF THE SUUSAMYR INTERMONTANE DEPRESSION	29
FIGURE 26. GULLY SLOPE TOTALLY AFFECTED BY LANDSLIDES	29
FIGURE 27. LANDSLIDES EAST FROM THE SNAKE-HEAD RA DOWNSTREAM FROM THE SITE SHOWN ON FIGURE 26.....	29
FIGURE 28. HEAD-SCARP OF THE SNAKE-HEAD ROCKSLIDE AND THE PROXIMAL PART OF ROCK AVALANCHE DEPOSITS	30
FIGURE 29. SCHEMATIC CROSS-SECTIONS OF THE SNAKE-HEAD ROCKSLIDE SCAR.....	30

FIGURE 30. DISTAL END OF THE SNAKE-HEAD ROCKSLIDE COMPACT PART AT THE NARROWING OF THE CREEK VALLEY.....	31
FIGURE 31. NEARLY HORIZONTAL SURFACE OF THE SNAKE-HEAD ROCK AVALANCHE UPPER PART IMMEDIATELY BELLOW ITS COMPACT PART	31
FIGURE 32. THE SNAKE-HEAD ROCK AVALANCHE PALM-LIKE DISTAL BLADE.....	31
FIGURE 33. BOUNDARY LEVEES OF THE SNAKE-HEAD ROCK AVALANCHE DISTAL BLADE	32
FIGURE 34. TRANSVERSE LEVEES AND FURROWS AT THE CENTRAL PART OF THE SNAKE-HEAD ROCK AVALANCHE DISTAL BLADE	32
FIGURE 35. RECENT AND OLD (SIGNIFICANTLY ERODED) ROCKSLIDE DAMS	33
FIGURE 36. OVERVIEW OF THE SEIT PRIMARY ROCK AVALANCHE	34
FIGURE 37. THE SCHEMATIC MAP OF THE SEIT ROCK AVALANCHE	35
FIGURE 38. LONGITUDINAL CROSS-SECTION ALONG THE SEIT ROCK AVALANCHE.....	36
FIGURE 39. THE SEIT ROCK AVALANCHE BODY FILLS THE CREEK'S CHANNEL	36
FIGURE 40. DRILLING OF THE ~300 YEARS OLD ARCHA TREE GROWING ON THE SEIT ROCK AVALANCHE DEPOSITS	37
FIGURE 41. VARIOUS LICHENS ON THE BOULDER SURFACE.....	37
FIGURE 42. SCAR AND THE TRANSITION ZONE OF THE SEIT ROCK AVALANCHE	38
FIGURE 43. TRIMLINES AT THE RIGHT SIDE OF THE SEIT ROCK AVALANCHE PATH	38
FIGURE 44. LOWER PART OF THE SEIT ROCK AVALANCHE TRANSITION ZONE	39
FIGURE 45. OVERVIEW OF THE SEIT RA (S) AND PRE-SEIT ROCKSLIDE SCAR (P-S)	39
FIGURE 46. WAVY SURFACE OF THE SEIT ROCK AVALANCHE DISTAL PART.....	39
FIGURE 47. ANGULAR FRACTURED BOULDER THAT HAD BEEN BROKEN JUST BEFORE MOTION HALTED	40
FIGURE 48. THE MOLARD-LIKE HILL ON TOP OF THE SEIT ROCK AVALANCHE DEPOSITS	40
FIGURE 49. THE OIGAING ROCKSLIDE	41
FIGURE 50. OVERVIEW OF THE CHONGSU ROCK AVALANCHE	42
FIGURE 51. NEOTECTONIC REVERSE FAULT.....	42
FIGURE 52. THE SCHEMATIC MAP OF THE CHONGSU ROCK AVALANCHE	43
FIGURE 53. PRIMARY (PS) AND SECONDARY (SS) CIRCUS-LIKE SCARS OF THE CHONGSU ROCK AVALANCHE.....	44
FIGURE 54. TRIMLINE ON THE RIGHT SLOPE OF THE CHONGSU ROCK AVALANCHE TRANSIT ZONE.....	45
FIGURE 55. ABRUPT DECREASE OF THE TRIMLINE LEVEL ON THE LEFT SLOPE OF THE CHONGSU ROCK AVALANCHE TRANSIT ZONE.....	45
FIGURE 56. ANGULAR BOULDER (BLACK ARROW) OUTSIDE THE SPLASH	46
FIGURE 57. THE CHONGSU ROCK AVALANCHE LEFT BOUNDARY JUST "DOWNSTREAM" FROM THE SITE SHOWN ON FIGURE 55	46
FIGURE 58. LATERAL AND FRONTAL EDGES OF THE CHONGSU ROCK AVALANCHE INDICATING ABRUPT HALT OF ITS MOTION.....	46
FIGURE 59. THE CHONGSU ROCK AVALANCHE FRONT OVERLAYING PRE-ROCK AVALANCHE DEBRIS FLOW	47
FIGURE 60. THE CHONGSU-2 ROCKSLIDE.....	47
FIGURE 61. THE SARYSU ROCK AVALANCHE HEADSCARP	48
FIGURE 62. UPPER PART OF THE SARYSU ROCK AVALANCHE.....	48
FIGURE 63. LOWER PART OF THE SARYSU ROCK AVALANCHE PATH.....	48
FIGURE 64. DISTAL END OF THE SARYSU ROCK AVALANCHE.....	49

FIGURE 65 . UPSLOPE-FACING SCARPS AT THE UPPER PART OF THE SLOPE.....	49
FIGURE 66. STRUCTURE OF ROCK MASSIF SHOWN ON FIGURE 65	50
FIGURE 67. UPSLOPE-FACING SCARPS AT THE MOST AFFECTED PART OF THE SLOPE, SHOWN ON FIGURE 65.....	50
FIGURE 68. SIDE VIEW ON THE TOPPLING SITE.....	51
FIGURE 69. AERIAL PHOTOGRAPH OF THE RIDGE UNDERGOING TOPPLING DEFORMATIONS	51
FIGURE 70. GENERAL SCHEME OF TOPPLING AND EXAMPLE OF SUCH PHENOMENON	52
FIGURE 71. AERIAL PHOTOGRAPH OF THE TUURAKAING RIVER BASIN AND OF THE LOWER PART OF THE KASHKASU RIVER BASIN	53
FIGURE 72. THE KASHKASU ROCKSLIDE DAM AND A PLANAR SURFACE OF THE INFILLED DAMMED LAKE	54
FIGURE 73. KASHKASU ROCKSLIDE DAM	54
FIGURE 74. LOWER WIDENED PART OF THE KASHKASU ROCKSLIDE DAM.....	55
FIGURE 75. SCHEMATIC MODEL OF A "JUMPING" ROCK AVALANCHE FORMATION.....	55
FIGURE 76. LEFT (A) AND RIGHT (B) TUURAKAING ROCK AVALANCHE.....	56
FIGURE 77. DEBRIS FLOW DEPOSITS OF THE UPPER PLEISTOCENE – HOLOCENE (?) AGE	57
FIGURE 78. AERIAL PHOTOGRAPH OF THE KOKOMEREN ROCKSLIDE	59
FIGURE 79. DISSECTED BODY OF THE KOKOMEREN ROCKSLIDE	59
FIGURE 80. THE KOKOMEREN ROCKSLIDE OVERVIEW	60
FIGURE 81. NEW GORGE OF THE KOKOMEREN RIVER THAT HAD BEEN ERODED AFTER THE BLOCKAGE.....	60
FIGURE 82. ALTERNATING BEDROCK SUCCESSION IN THE KOKOMEREN ROCKSLIDE SOURCE ZONE	61
FIGURE 83. RECONSTRUCTION OF THE KOKOMEREN ROCKSLIDE EMBLEMMENT MECHANISM ...	61
FIGURE 84. THE SCHEMATIC MAP AND CROSS-SECTIONS OF THE KOKOMEREN ROCKSLIDE BLOCKAGE	62
FIGURE 85. VERTICAL CROSS-SECTION OF THE LEFT-BANK PART OF THE KOKOMEREN ROCKSLIDE BODY	63
FIGURE 86. LOWER PART OF THE KOKOMEREN ROCKSLIDE BODY RESTING ON THE HIGH LEFT-BANK TERRACE	64
FIGURE 87. SHATTERED GRANITE DEBRIS AT THE LOWER PART OF THE KOKOMEREN ROCKSLIDE BODY	64
FIGURE 88. PLEISTOCENE CHANNEL ALLUVIUM OF THE KOKOMEREN RIVER OVERLAID BY SHATTERED	65
FIGURE 89. ALTERNATING "LAYERS" OF CRUSHED ROCKSLIDE DEBRIS ON THE RIGHT BANK OF THE KOKOMEREN RIVER.....	65
FIGURE 90. CONTACT OF THE CEMENTED ROCKSLIDE BRECCIA AND BOULDERY ALLUVIUM	66
FIGURE 91. METER-SIZE SUCCESSION OF CRUSHED BUT UNMIXED GRANITES AND METASEDIMENTS	66
FIGURE 92. TYPICAL GRAIN-SIZE COMPOSITION OF CRUSHED GRANITE (ABOVE) AND METASEDIMENTS (BELOW)	67
FIGURE 93. OVERVIEW OF THE SHATTERED ZONE OF THE KOKOMEREN ROCKSLIDE RIGHT-BANK PART.....	68
FIGURE 94. ANGULAR GRANITE BOULDERS ON THE TOP OF THE KOKOMEREN ROCKSLIDE RIGHT-BANK PART.....	68
FIGURE 95. STRONGLY ERODED ROCKSLIDE SCAR OPPOSITE THE KASHKASU RIVER MOUTH.....	69
FIGURE 96. PARTIALLY ERODED ROCKSLIDE DAM IN THE CREEK EAST FROM THE KOKOMEREN ROCKSLIDE	69

FIGURE 97. RECENT FAULT RUPTURING LEFT BANK RIVER TERRACES DOWNSTREAM FROM THE KOKOMEREN ROCKSLIDE.....	70
FIGURE 98. DISPLACED ALLUVIUM OF HIGH (PLEISTOCENE) RIVER TERRACE.....	70
FIGURE 99. DETAIL OF RECENT REVERSE FAULT SHOWN ON FIGURE 97	71
FIGURE 100. CRUSHED GRANITE (Γ) OVERTHUSTING THE ALLUVIUM (AQ)	72
FIGURE 101. LACUSTRINE SEDIMENTS OVERLY BOULDERY ALLUVIAL DEPOSITS	73
FIGURE 102. FINE BEDDED LACUSTRINE SEDIMENTS OVERLYING ALLUVIUM	74
FIGURE 103. OVERVIEW OF THE LEFT BANK OF KOKOMEREN RIVER OPPOSITE THE KYZYL-OI VILLAGE	74
FIGURE 104. BASAL UNITS OF THE LACUSTRINE SUCCESSION	75
FIGURE 105. LACUSTRINE DEPOSITS WITH BOULDERY INCLUSIONS	76
FIGURE 106. LAKE-HEAD DELTAS OF RIVERS FLOWING INTO THE TOKTOGUL RESERVOIR.....	76
FIGURE 107. DEEPLY ERODED BODY OF THE DISPLACED PENEPLAIN ROCKSLIDE	77
FIGURE 108. LANDSLIDES, ROCKSLIDES AND ROCK AVALANCHES AT THE WESTERN TERMINATION OF THE DJUMGAL INTERMOUNTAIN DEPRESSION AND THE SURROUNDING RANGES	78
FIGURE 109. HEADSCARP OF THE DISPLACED PENEPLAIN ROCKSLIDE	78
FIGURE 110. THE DISPLACED PENEPLAIN ROCKSLIDE BODY.	79
FIGURE 111. CRUSHED GNEISS OF THE DISPLACED PENEPLAIN ROCKSLIDE BODY UPPER PART RESTING OVER RED GRANITE (LOWER RIGHT CORNER OF THE PHOTOGRAPH).....	79
FIGURE 112. OUTCROP WHERE THE "STRATIFIED" INTERNAL STRUCTURE OF THE ROCKSLIDE BODY IS VISIBLE.....	80
FIGURE 113. FRAGMENT OF THE LEFT BANK OF THE ABANDONED STREAM OF THE KOKOMEREN RIVER	80
FIGURE 114. THE UPSTREAM PART OF THE ABANDONED PRE-KOKOMEREN VALLEY FILLED BY ALLUVIUM.....	81
FIGURE 115. LACUSTRINE SILT SEDIMENTS OVERLAID BY STREAM ALLUVIUM.....	81
FIGURE 116. FINE THIN-LAYERED SEDIMENTS OVERLYING STREAM ALLUVIUM	82
FIGURE 117. UPSTREAM VIEW OF THE MINI-KÖFELS ROCKSLIDE DEPOSITS	83
FIGURE 118. CENTRAL AND DOWNSTREAM PARTS OF THE MINI-KÖFELS ROCKSLIDE BODY.....	83
FIGURE 119. COMMINUTED ROCKSLIDE DEBRIS (CRUSHED GRANITE) OVERLYING ALLUVIUM	84
FIGURE 120. THE KARAKUNGEY ROCKSLIDES AND ROCK AVALANCHES AT THE WESTERN FRAME OF THE DJUMGAL DEPRESSION	84
FIGURE 121. THE SCHEMATIC MAP OF THE NORTHERN KARAKUNGEY ROCKSLIDE (RIGHT) AND SOUTHERN KARAKUNGEY ROCKSLIDE (LEFT)	85
FIGURE 122. SOUTHERN KARAKUNGEY ROCKSLIDE	86
FIGURE 123. HEADSCARP AND SHARP UPSTREAM EDGE OF THE SOUTHERN KARAKUNGEY ROCKSLIDE BODY.....	86
FIGURE 124. VIEW ON THE SOUTHERN KARAKUNGEY ROCKSLIDE FROM ITS HEADSCARP.....	87
FIGURE 125. THE FRONTAL VIEW ON THE SOUTHERN KARAKUNGEY ROCKSLIDE	87
FIGURE 126. SURFACE OF THE SOUTHERN KARAKUNGEY ROCK AVALANCHE	88
FIGURE 127. NORTHERN KARAKUNGEY ROCK AVALANCHE	88
FIGURE 128. SCHEMATIC CROSS-SECTIONS OF THE NORTHERN KARAKUNGEY ROCKSLIDE	89
FIGURE 129. UPSTREAM SEPARATE PART OF THE NORTHERN KARAKUNGEY BLOCKAGE	89
FIGURE 130. VIEW FROM UPSTREAM ON THE SEPARATE PART OF THE NORTHERN KARAKUNGEY ROCKSLIDE AND FILLED DAMMED LAKE	89
FIGURE 131. ANGULAR BOULDERS OF THE ASSUMED PLEISTOCENE PRE-KARAKUNGEY ROCK AVALANCHE	90

FIGURE 132. THE MINGTEKE ROCK AVALANCHE	91
FIGURE 133. HUGE ROTATIONAL LANDSLIDES IN THE N-Q DEPOSITS OF THE DJUMGAL INTERMONTANE DEPRESSION	91
FIGURE 134. 3-D VIEW OF THE AREA A, SHOWN ON FIGURE 133	92
FIGURE 135. PANORAMIC VIEW OF THE CHAEK LANDSLIDE.....	92
FIGURE 136. 3-D VIEW OF THE AREA B, SHOWN ON FIGURE 133.....	93
FIGURE 137. HYPOTHETICAL CROSS-SECTION OF THE WESTERN DJUMGAL LANDSLIDE.....	93
FIGURE 138. COMBINED 3D DEM AND KFA-1000 SPACE IMAGE OF THE LANDSLIDE IN THE SOUTHERN PART OF THE SUUSAMYR VALLEY.....	94
FIGURE 139. THE KYZYLKIOL CALDERA-LIKE COLLAPSE.....	95
FIGURE 140. UPPER REACHES OF THE KYZYLKIOL CREEK, ERODING THE CAVITY BOTTOM.....	96
FIGURE 141. CROSS-SECTION OF THE KYZYLKIOL CALDERA-LIKE COLLAPSE	96
FIGURE 142. TORN TOPOGRAPHIC FEATURES AT THE NORTHERN EDGE OF THE KYZYLKIOL CAVITY	97
FIGURE 143. VIEW OF THE SANTASH RIDGE AT THE KYZYLKIOL SECTION FROM THE NORTH.....	97
FIGURE 144. SCHEMATIC MODEL OF THE 'TECTONIC CAVE' FORMATION	97

1 INTRODUCTION

Large-scale catastrophic bedrock slope failures is one of the most hazardous natural phenomena that endanger people living in mountainous regions. Unlike "common" landslides and rockfalls, which affect just collapsing slopes themselves and areas directly at their feet, simultaneous failure of millions and, sometimes, billions of cubic meters of rocks can devastate vast areas, spreading up to 5-10 km and even more from the source zone. Moreover, they often have disastrous secondary effects like valley inundation due to river damming and subsequent outburst floods. It can be exemplified by the 1786 earthquake triggered Dadu rockslide in China that formed a dam, which failure killed about 100,000 people downstream, thus being the most disastrous rockslide catastrophe ever reported [Lee & Dai in press]. In 1841 and 1858 catastrophic floods occurred due to failure of rockslide dams that had blocked the Indus River and its large tributary, the Hunza River, correspondingly [Hewitt 2002]. In 1881 rock avalanche destroyed the Elm village and it was the first time when long runout event was described scientifically [Heim 1882, Hsü 1975]. In 1911 the Usoi rockslide dammed the Murgab River in Pamirs and formed the 500-m deep Sarez Lake that still poses a potential threat for the large part of the Amu-Daria River basin [Gaziev 1984, Alford and Schuster 2000]. In 1949 the Khait rock avalanche caused by strong M7.4 earthquake buried the Khait town with several thousands of its inhabitants [Leonov 1960], thus being the most disastrous landslide event in Central Asia region. In 1963 breach of the Issyk Lake rockslide dam near Almaty City in Kazakhstan produced debris flow that devastated the entire valley and caused numerous casualties [Litovchenko 1964]. This tragic list was extended by the 2008 M8 Wenchuan earthquake in Sichuan (China) where thousands of people were buried by numerous large-scale rockslides. Besides, about 30 blockages were formed and only enormous efforts undertaken by Chinese authorities prevented catastrophic outburst floods [Yin, et al 2008, Wang, et al. 2009, Cui, et al 2009].

Such phenomena attract researchers' attention for many years, starting from the pioneering study of the Elm rock avalanche by A. Heim [1882]. The main objective of Summer School on Rockslides and Related Phenomena in Kokomeran River Valley in Kyrgyzstan is to acquaint participants with various types of bedrock landslides and with basic methods used for their study. High emphasis will be placed on geological and neotectonic framework in which large rock massifs fail catastrophically, on surface ruptures in particular. The latter, especially those accompanied by rock slope failures can be considered as traces of strong past earthquakes, which, as we assume, repeatedly shook the study region and, therefore, can occur here in future.

We also hope that joint fieldwork that will be carried out during this training course will promote participants' long-term personal and professional co-operation.

Why this particular area – the Kokomeran River basin (Figure 1) – was selected for the proposed training course? Our choice is based on extremely favorable combination of several factors:

- Presence of numerous rockslides and rock avalanches ranging from several millions to more than one billion cubic meters in volume within a limited area about 40 km from North to South and from East to West (Figure 2).
- Variability of types and morphologies of the phenomena in question. There are rockslides with compact bodies that form high natural dams and those transformed into long runout rock avalanches; confined and unconfined events; rockslides deeply incised by erosion that provides excellent opportunity to study their internal structure. Expressive evidences of river valley inundation are visible, as well as deposits that can be interpreted as outburst flood accumulations.
- Arid climate of the Tien Shan, favorable to very good exposure of both overall morphology of rockslides and other geomorphic phenomena and of minor topographic features, which are not masked by forestation.
- Very expressive neotectonic structure, presence of numerous active faults and surface ruptures, which allow better understanding of geological and seismotectonic framework in which rockslides have occurred.

- Accessibility of the study area located near the road at one-day trip distance from the Bishkek City – capital of Kyrgyzstan. Bishkek is connected by direct flights with Moscow, Istanbul and London. It also possible to arrive via Almaty – former capital of Kazakhstan.

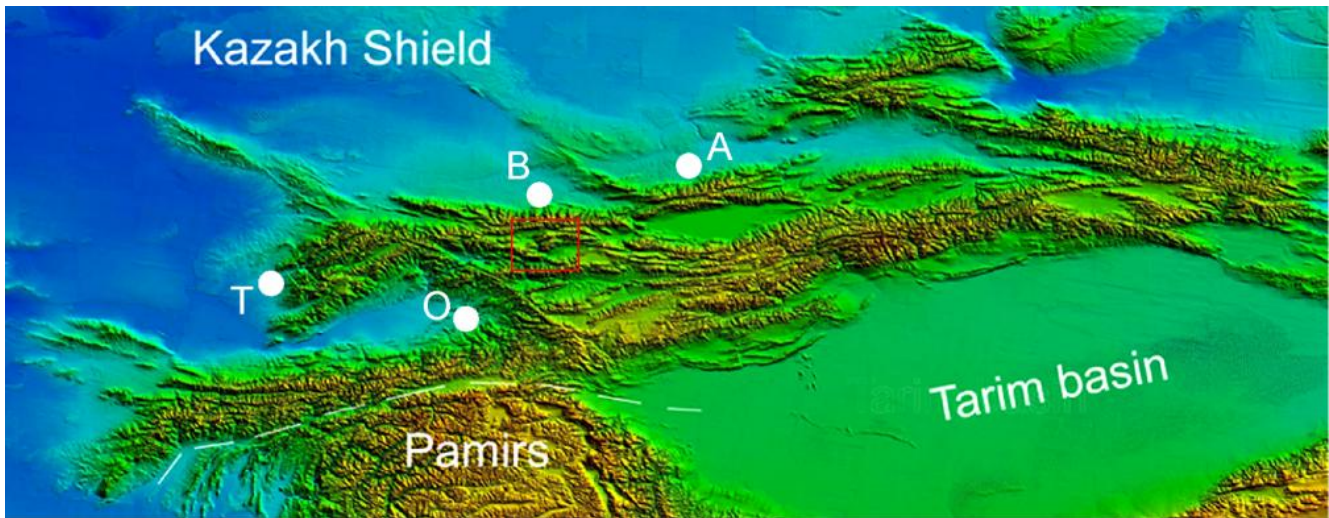


Figure 1. Position of the Kokomeren River basin within the Tien Shan Mountain system. Study region is marked by red rectangle. B – Bishkek, O – Osh, A – Almaty, T - Tashkent

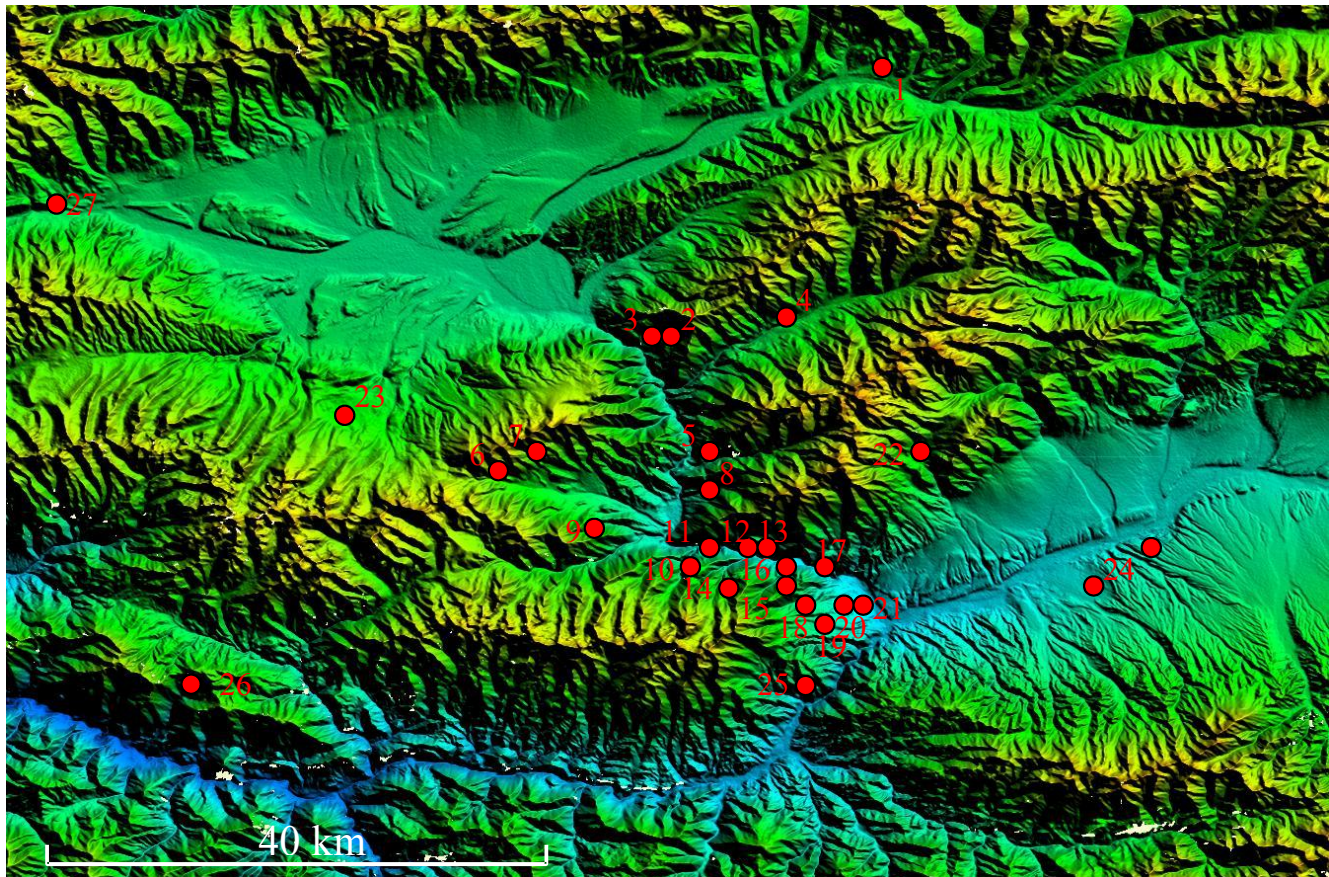


Figure 2. Location of bedrock slope failures in Kokomeren River basin between the Sausamyr and Djungal intermontane depression – the target area of the field training course. Fragment of the 3" SRTM DEM as the background. Three general types of slope failures are selected – landslides in unconsolidated N-Q sediments (LS), bedrock landslides with compact bodies – rockslides (RS), bedrock landslides transformed into long runout rock avalanches (RA). The Kyzylkiol caldera-like collapse is marked as well (site No 26). 1 – Snake-head RA; 2 – Seit RA; 3 – Pre-Seit RS; 4 – Oigaing RS; 5 – Burundu RS; 6 – Chongsu RA; 7 – Chongsu-2 RS; 8 – Sarysu RA; 9 – Toppling site; 10 – Kashkasu RS; 11 – Kashkasu mouth RS; 12 – Kokomeren RS; 13 – Kokomeren-satellite RS; 14 – Upper-Toruaigyr (left & right) RA; 15 – Displaced Peneplain RS and its frontal part (16); 17 – Mini-Köfels RS; 18 – Northern Kara-Kungey RA; 19 – Southern Kara-Kungey RA; 20 – Pre-Southern Kara-Kungey RA deposits; 21 – Western Djungal LS; 22 – Mingteke RA; 23 – South-Sausamyr LS; 24 – Chaek-1 and Chaek-2 LS; 25 – South-Aral RS; 27 – 1992 Chet-Kurumdu LS

This Guidebook presents brief description of the sites with which participants of the Summer School will be acquainted. Authors will be grateful for any comments, corrections and suggestions, which will help its improvement.

2 GEOLOGICAL BACKGROUND (FACTORS GOVERNING BEDROCK SLOPE FAILURES)

2.1 GEOLOGY

The Tien Shan is a typical basin-and-range mountain system that has been formed in Cenozoic Era due to north-south compression after long period of planation, which lasted almost all Mesozoic Era and up to Eocene [Makarov, 1977, Chedia, 1986]. In Proterozoic and Paleozoic Eras this region had been subjected to intensive tectonic deformations of Caledonian and Varissian stages that formed complex structure of its basement. Region in question, in particular, had been formed during Caledonian stage. Rocks representing Caledonian basement compose mountain ranges that rise up to 4000 m.a.s.l. They are divided by intermontane depressions filled by Neogene and Quaternary sediments (Figure 3).

Most widely developed types of basement rocks within the study area are Paleozoic granites of Ordovician and, locally, Silurian ages. Between the Kysyl-Oi and Djungal depressions there is a rock massif composed of Late Precambrian metasediments and gneiss intruded by the above granites. Devonian sandstone present at the extreme northeast of the study region, north from the Suusamyrdarya depression.

Neogene deposits are widely developed in the depressions and, locally, remain on high altitude within the ridges. They are represented by terrigenous red beds (sandstone, conglomerate, siltstone, mudstone) of the Kyrgyz series overlaid by whitish sandstone, siltstone and mudstone of the Tien Shan series, which, in its turn, is overlaid by much coarser upper molasse deposits of the Sharpyldak series. Presence of the Kyrgyz and, likely, Tien Shan series deposits at some sites within mountain ranges indicates that they were accumulated in the shallow basins before neotectonic orogeny had started in Late Pliocene or in Pleistocene. In contrast, the Sharpyldak conglomerates can be found in depressions only. At several outcrops outside the study region, however, one can find the reverse sedimentation order, with coarse debris flow deposits at the base overlaid by finer Miocene strata, which, likely, indicate penultimate orogenic movements [Abdrakhmatov, et al., 1994].

Quaternary deposits are represented by the glacial moraine, alluvial deposits of Middle, Late Pleistocene and Holocene and talus. Locally rockslide bodies and lacustrine sediments of rockslide dammed lakes present.

2.2 GEOMORPHOLOGY AND NEOTECTONICS

As mentioned above, the Tien Shan is a typical basin-and-range mountain system (Figure 4) that has been formed during the Neogene-Quaternary periods due to north-south compression. It should be noted that neotectonic features in the Tien Shan are, may be, world-best expressed. Moreover, the concept of Neotectonics itself was developed by S.S. Shultz [1948] based on his field studies carried out just in this mountain system. Later on V.I. Makarov [1977] and O.K. Chedia [1986] studied and described the Tien Shan neotectonics on more regular basis.

The extreme expressiveness of neotectonic features in the Tien Shan is stipulated by the presence of the Pre-Neogene planation surface overlaid by the sequence of variegated Cenozoic sediments, which deformation reflect post-Neogene tectonic movements. In general one can see fragments of this surface that were tilted and ruptured (Figure 5), though sometimes intensive folding affected both Paleozoic basement and overlaying Cenozoic sediments (Figure 6). Intensive neotectonic deformations resulted in presence of similar Neogene deposits both in neotectonic depressions and, locally, on the planar surfaces inside high ridges raised sometimes about 1 km above present-day river valleys and intermontane depressions (Figure 7).

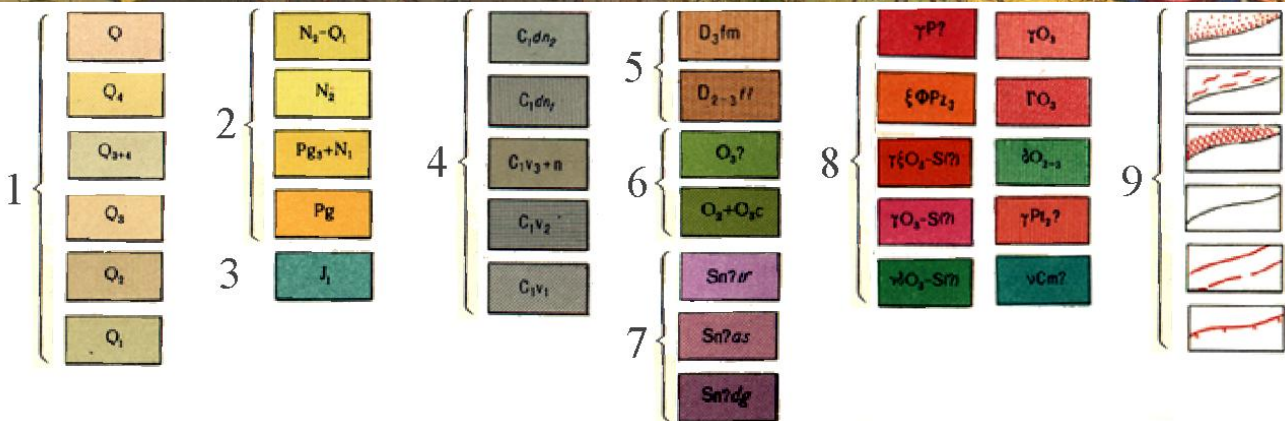
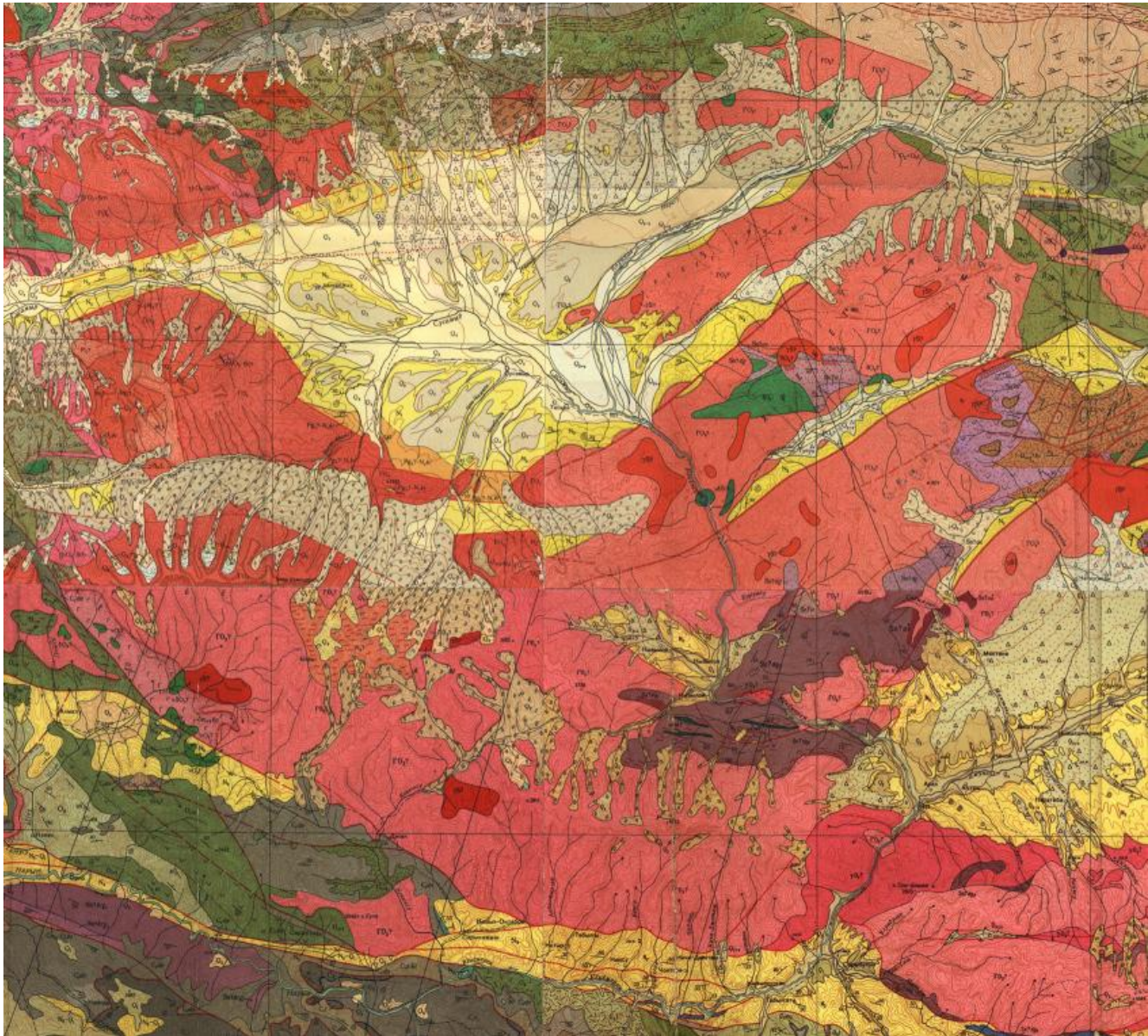


Figure 3. Geological map of the study region

Compiled from 1:200 000 State Geological Maps, sheets K-43-XIV, XV, XX, XXI.

Simplified Legend: 1 – Quaternary sediments; 2 – Cenozoic deposits; 3 – Jurassic deposits; 4 – Carboniferous deposits; 5 – Devonian deposits; 6 – Ordovician deposits; 7 – Precambrian metasediments; 8 – Igneous rocks; 9 – zones of contact metamorphism, geological boundaries and faults

Large basement folds feature distinct asymmetry and series of them forms systems characterized by either northward or southward vergence [Sadybakasov 1972, 1990].

Steeper fold limbs are usually associated with neotectonic reverse faults, some of which also have significant strike-slip component indicating the transpression style of deformations [Delvaux, et

al. 2000]. Many of large faults that divide neotectonic uplifts and depressions feature evidences of Late Pleistocene – Holocene surface rupturing.

Expressive faults displacing minor topographic features and/or recent sediments can be found at the northern boundary of the Suusamyр depression (Figure 8), along northern (Figure 9) and south-eastern (Figure 10 – Figure 12) boundaries of small Kyzyl-Oi depression, at the boundary between the Djungal Range and the same-name depression (Figure 13). Some of them, such as the fault shown on Figure 11 demonstrate clear evidences of strike-slip movements (Figure 12) while others are predominantly reverse faults, though, rather often, are represented by up-slope facing scarps (see Figure 8 or Figure 13). Several recent faults that pass near rockslide sites will be mentioned later in the corresponding sections of the Guidebook.

Slightly running ahead, we should note that recent faults shown on Figure 10 and Figure 11 had ruptured fine lacustrine sediments that, likely, had been accumulated in the lake dammed by huge rockslide downstream.

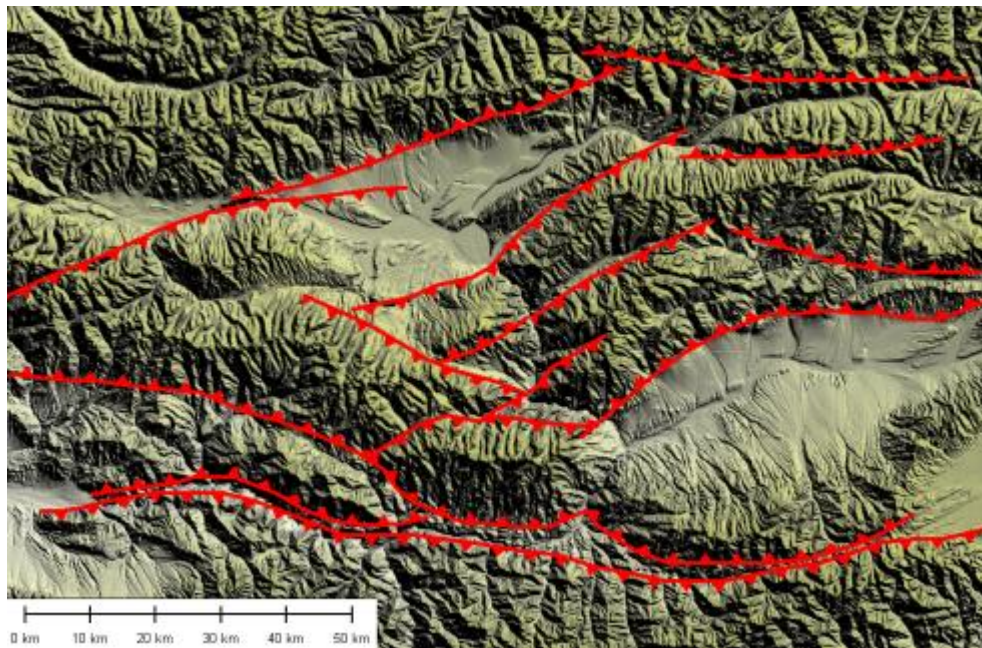


Figure 4. Simplified neotectonic scheme of the study area
Red lines – main active faults. Triangles are on the upthrown sides

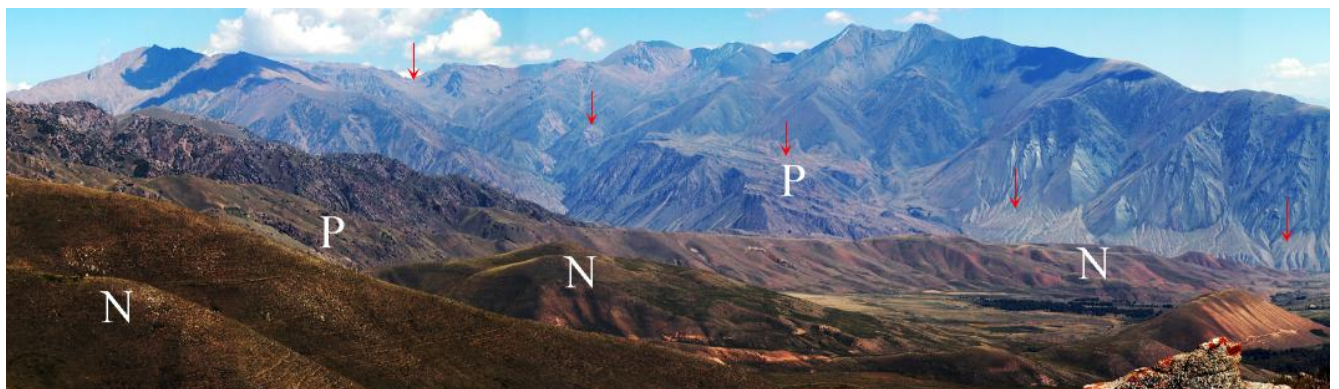


Figure 5. Tilted and warped planation surface (P) at the eastern part of the Kyzyl-Oi neotectonic depression
Fault bounding the depression is marked by red arrows. Planation surface inclination increases at the left part of the panorama foreground where it is overlaid by Neogene red beds (N)

Several active faults can be traced inside intermountain depressions. One of them, in particular, can be considered as an eastern extension of active fault that was ruptured during the 1992 Suusamyр earthquake. It displaces recent sediments and form north-facing scarp that stretches along the central part of the Suusamyр valley (Figure 14).

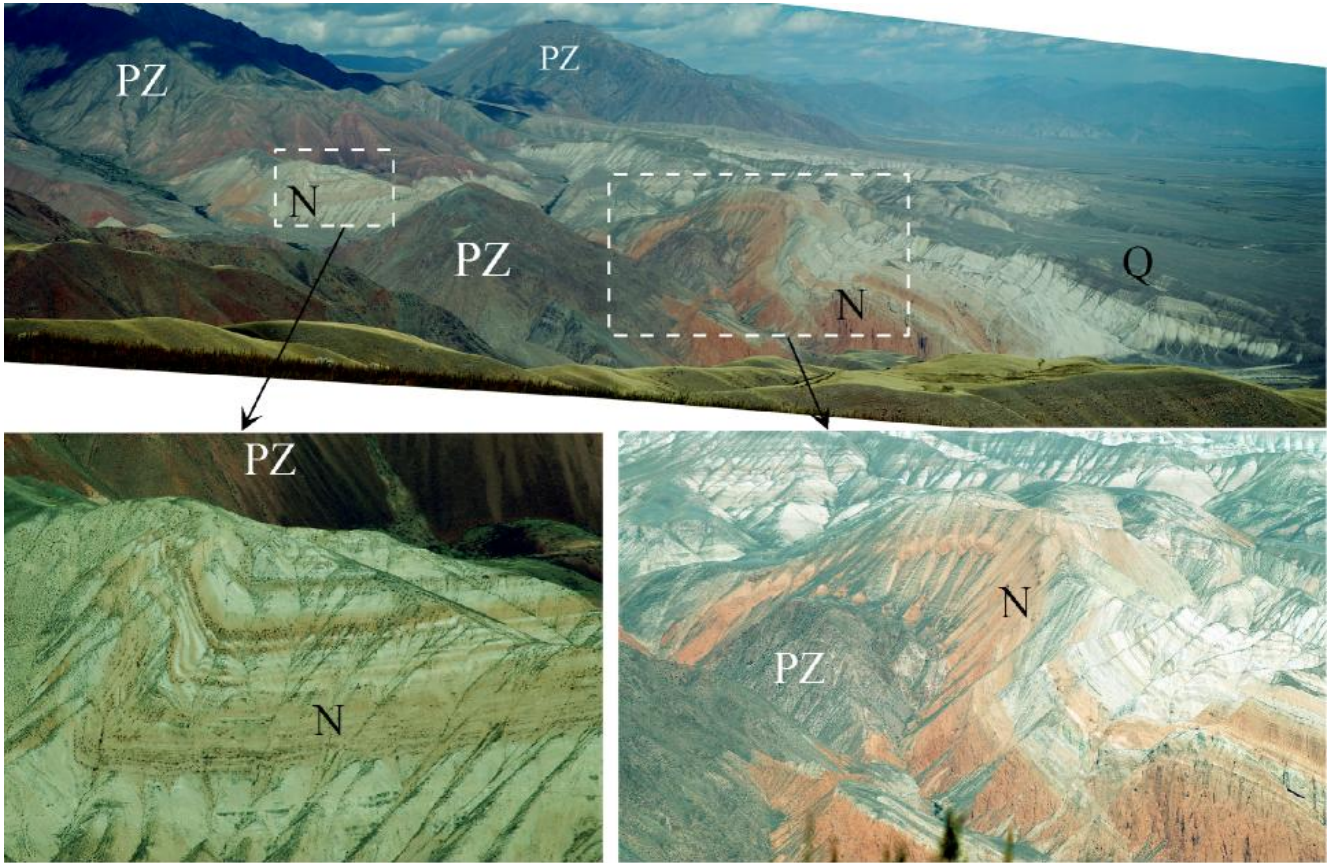


Figure 6. Folding of pre-Neogene planation surface and overlying N-Q sediments
 The north-western part of the Djungal intermontane depression. Note that Quaternary alluvial fan in the right part of panorama overlay folded Neogene sediments with distinct angular unconformity being tilted at a smaller angle



Figure 7. Uplifted pre-Neogene planation surface
 Remnants of the overlaying red beds are visible on the right bank of the Kokomeran River gorge between the Djungal and Suusamur Ranges raised about 1000 m above the same planation surface level in the adjacent Kyzyl-Oi depression filled by Neogene sediments several hundreds meters thick (on the foreground). Arrows mark the reverse fault that divides the Suusamur (Suu) and Djungal (Dj) neotectonic anticlines (ridges)

It is likely that above mentioned surface ruptures have been associated with strong past earthquakes. Outcrop shown on Figure 10, in particular, demonstrate direct and indirect evidences of multiple Quaternary seismotectonic events. First one can be revealed from the presence of angular boulders (2 on Figure 10) that could originate from the opposite slope of the Kokomeran River only.

Large distance from the source zone that is atypical of such deposits allows assumption that slope failure was associated with strong earthquake. It is supported by the following observations:

1 – Quaternary sediments rest on the crushed and milonitised Paleozoic bedrock (1 on Figure 10) indicating presence of large long-living fault zone. 2 – Scree material is mixed partially with alluvial boulders and this unit is overlaid by fine lacustrine sediments with gravel-pebble interbeds (3 on Figure 10) accumulated in the lake dammed several kilometers downstream by giant Pleistocene Kokomeren rockslide (see section 3.8). Thus, scree failure at the site in question had occurred simultaneously with large rockslide formation [Strom, Stepanchikova, 2008].

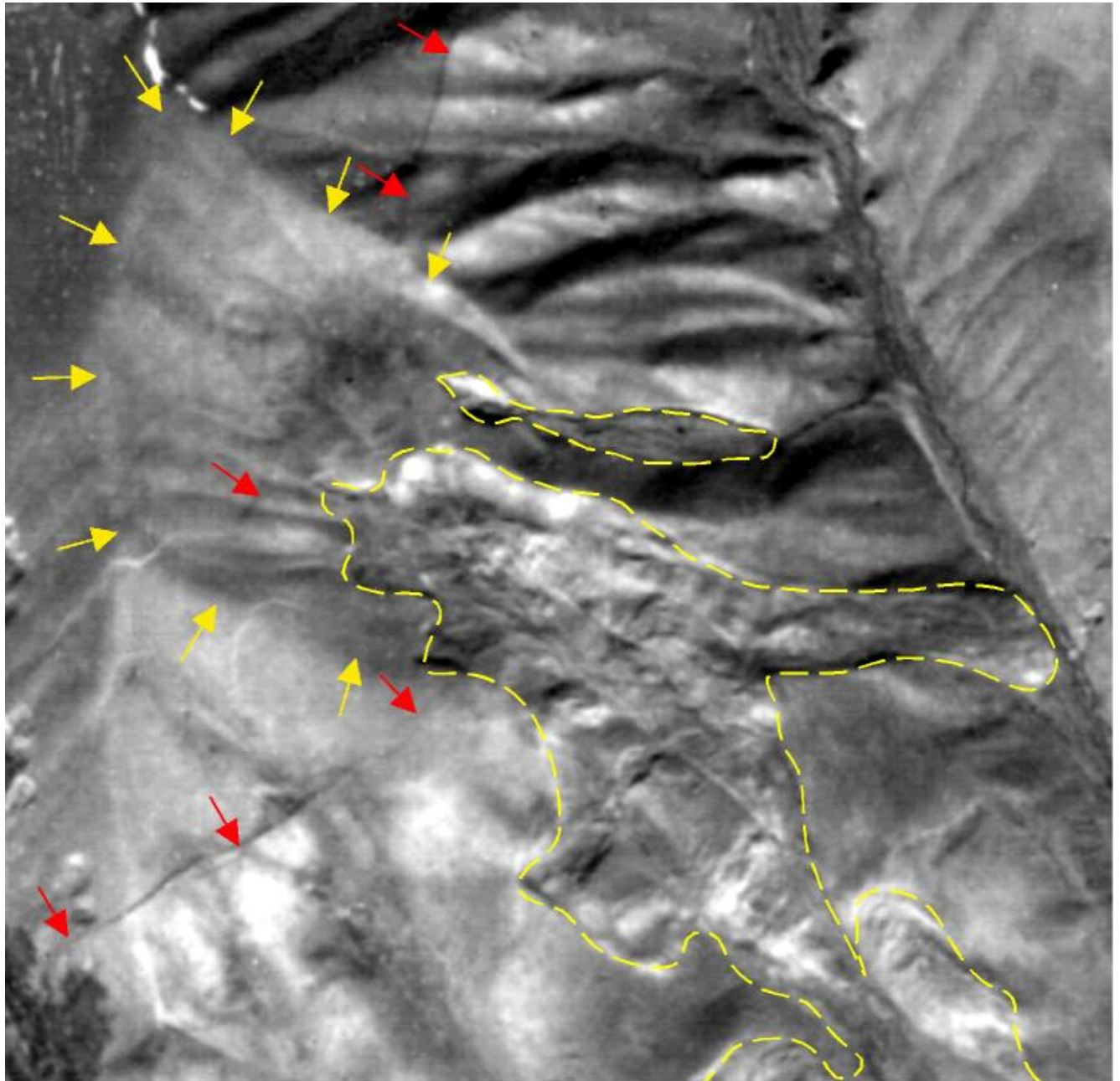


Figure 8. Surface ruptures associated with landslides at the northern boundary of the Suusamyр intermontane depression
Red arrows mark surface ruptures, orange arrows – assumed scar of old bedrock landslide, dashed yellow lines – boundaries of the more recent (modern) landslides. Fragment of high-resolution space photograph

The significant tilting of the above succession including fine well-bedded silt sediments that could accumulate initially as horizontal layers only, indicates the next tectonic event. 20-30° tilting could result from the significant vertical deformations.

Since recent fault shown on Figure 11 is characterized by the predominantly strike-slip kinematics (see Figure 12), this offset should occur during the third, most recent tectonic event.

One of the most promising ways to verify the assumption of simultaneous tectonic and rock slope deformations is to date surface ruptures and rock slope failures located nearby [Bull, 1996]. Their ages' coincidence should be a strong argument in favor of seismic origin of both features.

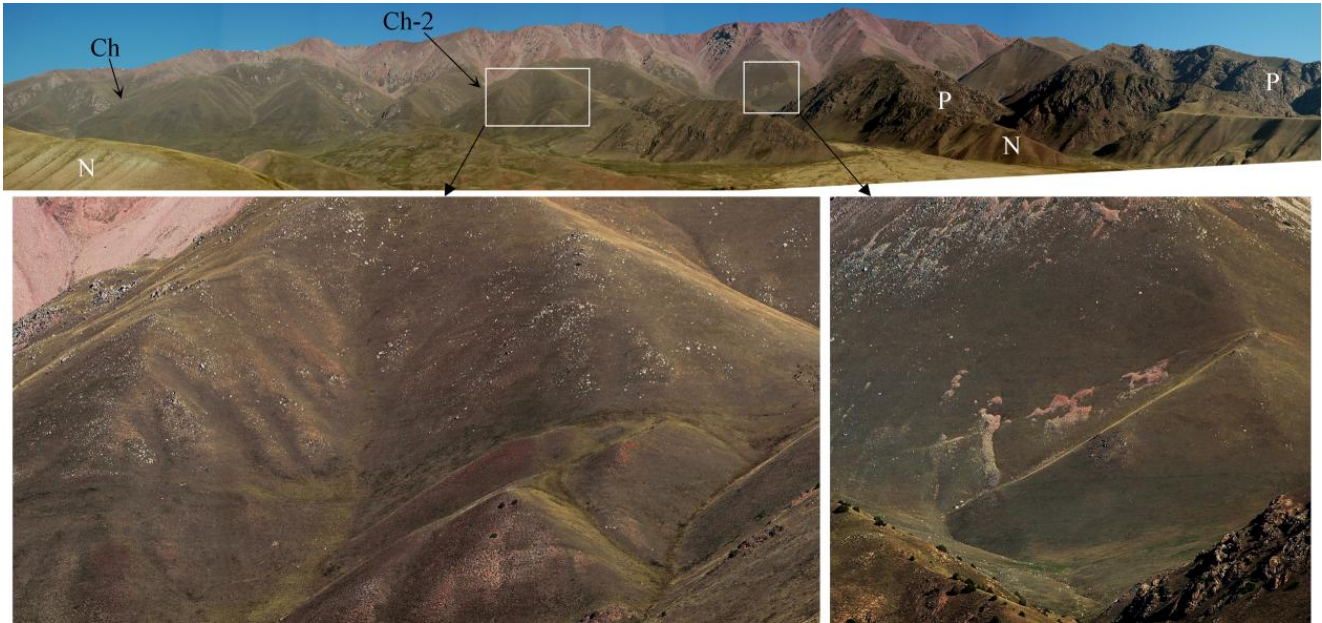


Figure 9. Surface ruptures along the North-Kyzyl-Oi fault zone.

Ch and Ch-2 – the Chongsu and Chongsu-2 rockslides. Rocky hills at the panorama foreground represent the steeply tilted and intensively eroded Pre-Neogene planation surface (P) overlaid by Neogene red beds (N)



Figure 10. Outcrop downstream from the Kyzyl-Oi village between Chongsuu and Kobiuksuu River mouths (41.93° N, 74.15° E) with evidence of multiple recent tectonic movements. 1 – crushed and milonitised Paleozoic bedrock – fault zone material; 2 – angular boulders of Paleozoic metasediments – ancient scree that could fell from the opposite slope of the Kokomerren River valley only; 3 – tilted and ruptured succession of the lacustrine and fluvial sediments accumulated in the lake, which had been formed by the Kokomerren rockslide (see section 3.8); outlined fragment with the most recent rupture is shown on Figure 11; 4 - younger alluvium overlying this succession.



Figure 11. Surface rupture displacing the succession of lacustrine and fluvial sediments. Vertical separation of layers visible in the outcrop resulted from the significant left-lateral offset of tilted layers that is proved by the presence of nearly horizontal striae of the rupture surface (Figure 12).



Figure 12. Slickenlines on the sliding surface of recent fault shown on indicating strike-slip sense of motion

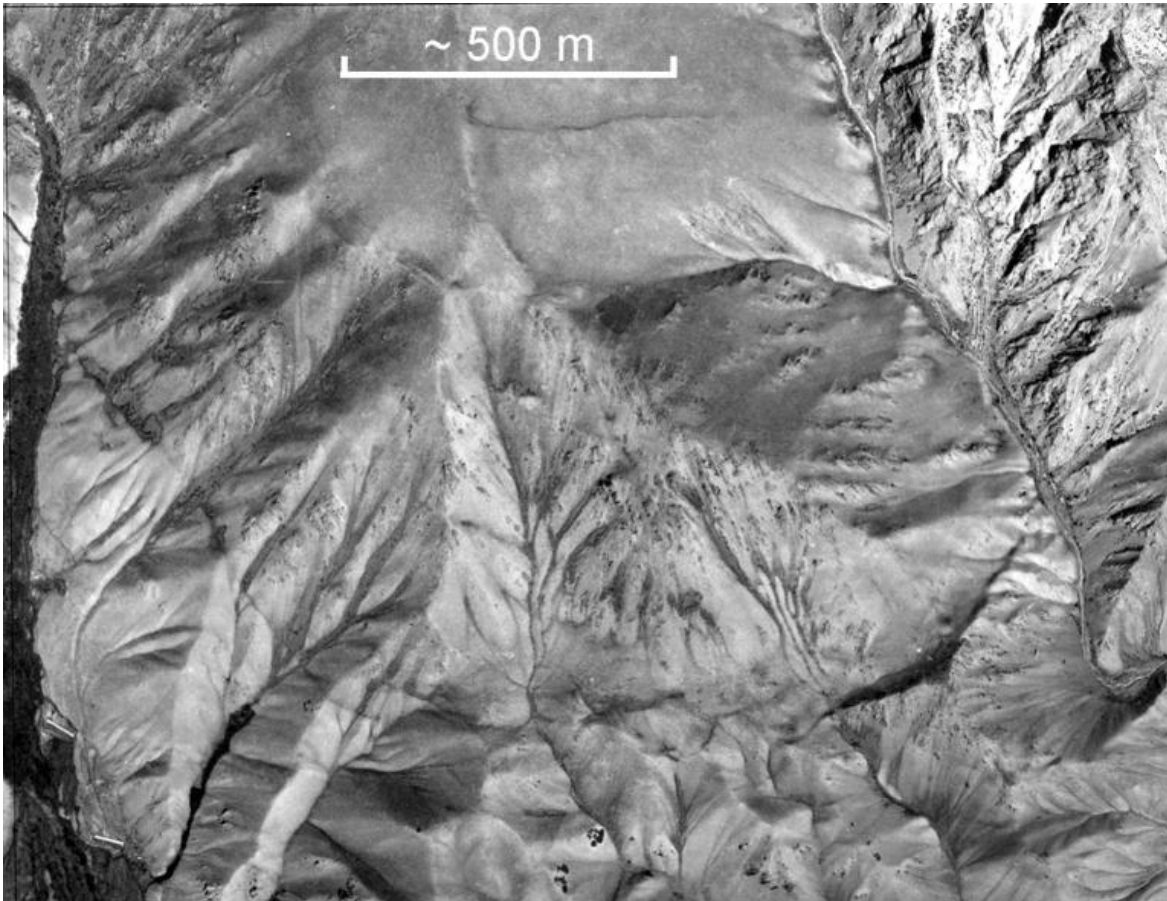


Figure 13. Bow-shape surface rupture at the fault zone dividing the Djumgal Range and the same-name depression west from the Mingteke rock avalanche. Take notice of up-slope facing escarpments, most expressive at its eastern part

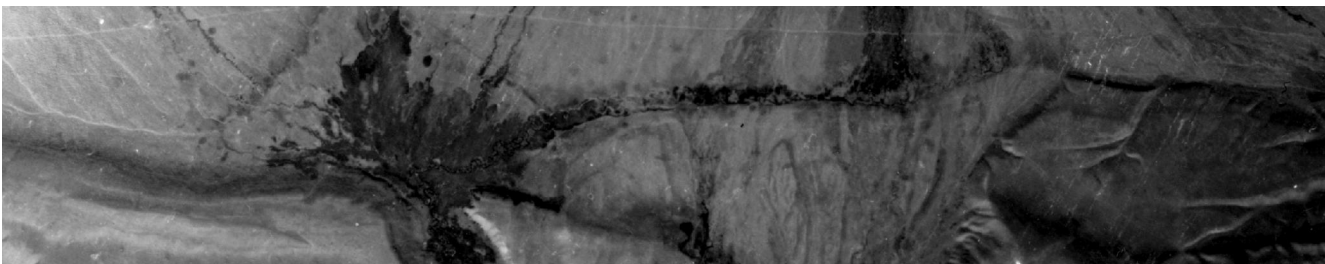


Figure 14. 2.5-km long fragment of the north-facing escarpment of prehistoric surface rupture in the central part of Sausamyr neotectonic depression

2.3 SEISMICITY

Tien Shan is a seismically active zone where numerous strong earthquakes have occurred in XIX-XX Centuries (Figure 15). Most of them have happened along the northern and southern limits of this mountain system and west from the diagonal Talas-Fergana fault. As far as most of the Tien Shan mountains were inhabited by nomads, who did not have written history, not so many historical data on past earthquakes are available – regular written records started from the middle of the XIX Century only [Mushketov & Orlov 1893].

The first strong earthquake, which geological effects had been described in special publication was the 1885 Belovodsk one ($M \sim 7.0$) that severely affected northern foothills of the Kyrgyz Range [Ignatiev 1886]. Nothing was reported, however, about its effects southward, in the Sausamyr Valley and further to the south. Other strong events occurred about 100 km to the north-east from the region in question, where one of the strongest intra-continental seismic event – the $M 8.2$ Kemin earthquake caused extensive surface faulting and slope failure north from the Issyk-Kul Lake [Bogdanovich et. al. 1914, Kuchai 1969, Delvaux 2001]. One more strong earthquake – the $M 7.6$ Chatkal occurred in 1946 almost at the same distance to the west from our region [Leonov 1970, Kuchai 1971].

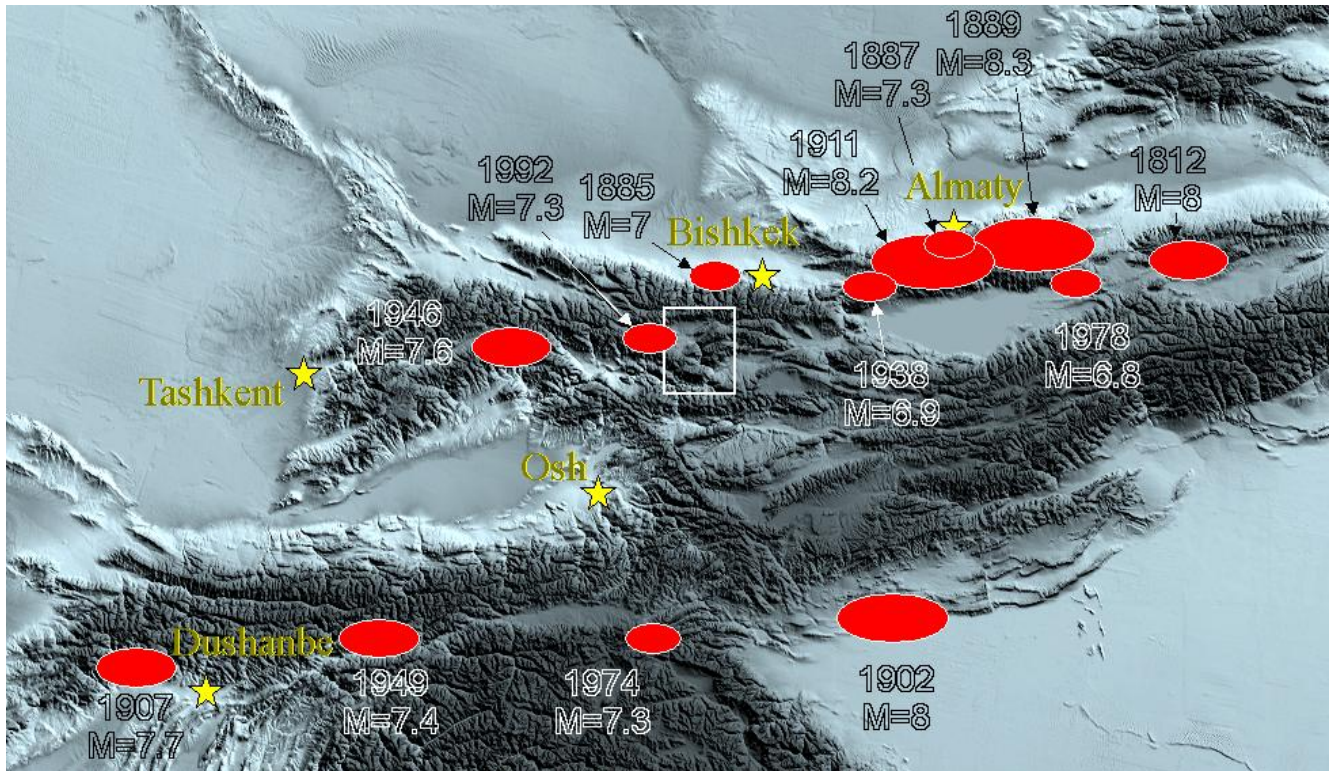


Figure 15. Strongest earthquakes of the Tien Shan region
Study area is outlined by the rectangle

No strong earthquakes have ever occurred in the historical period in the Kokomeren River basin until August 19, 1992, when the M7.3 Suusamyр earthquake shook the area. Earthquake was accompanied by surface rupture [Ghose, et al., 1997]. Surface faulting associated with this event was very expressive at the eastern part of the epicentral zone (42.21° N, 73.64° E) where three sub-parallel reverse faults ruptured the Suusamir River floodplain and channel, which resulted in river's diversion (Figure 16).



Figure 16. Surface rupture (reverse fault) of the M 7.3 Suusamyр earthquake
Above, photo made in August 25, 1992, few days after the earthquake.
Below – left part of the same scarp in 2006, 14 years later

These fault scarps are still very expressive, especially the northern one (Figure 17). Another 6-km long source fault fragment ruptured the surface about 25 km to the west while no evidences of surface faulting were found out in between (Bogachkin, et al., 1997).



Figure 17. 1992 fault scarp about 2.5 m high on the Suusamyр first river terrace
Boy staying at the footwall is about 1.7 m high

Fortunately this earthquake affected rarely populated area and, thus, caused about 50 casualties only. Most of victims were due to landslides in Neogene and Quaternary deposits at the southern feet of Suusamyр Range (Figure 18), 15-20 km south from the epicenter.

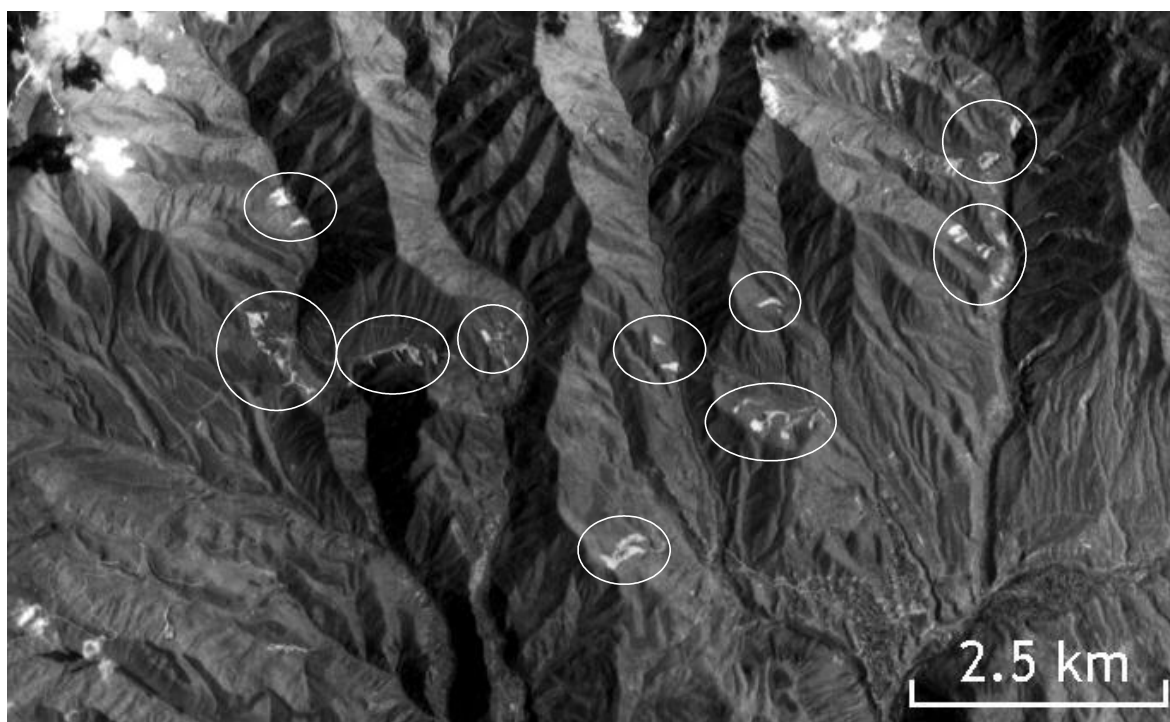


Figure 18. Landslides triggered by the Suusamyр earthquake (outlined) at the southern feet of the Suusamyр Range. Fragment of the KFA-1000 space image of obtained about 1 year after the 1992 Suusamyр earthquake

Several other landslides occurred at the Chet-Korumdy Ridge in the western part of Suusamyр depression [Havenith et al. 2006] (Figure 19) (No 27 on Figure 2). Due to Bishkek-Osh highway reconstruction most of them were partially reworked. It is interesting that these landslides strictly inherited pre-existing slope failures, which are clearly visible at some parts of the Chet-Korumdy Ridge, above and nearby from the 1992 landslide scars (Figure 20) and on the aerial and space photographs made before the earthquake (Figure 21-A). Some of them have been activated, while much larger potentially unstable section of the same slope remained intact (see right side of Figure 21-A and B).



Figure 19. Landslide on the southern slope of the Chet-Korumdy Ridge triggered by the Suusamyр earthquake
Photographed on August 25, 1992



Figure 20. Toppling at the central part of the Chet-Korumdy Ridge above the 1992 landslide scar
Photographed in 2006

Only one really large rockslide (more than 10 million cubic meters in volume) occurred during this event about 40 km west-south-west from the epicenter in the upper reaches of the Belaldy River valley, north from Toktogul reservoir at 42.06° N, 73.15° E (Figure 22). It dammed the stream and dam's breach one year later caused devastating debris flow that affected Belaldy and Torkent villages [Ghose, et al. 1997].

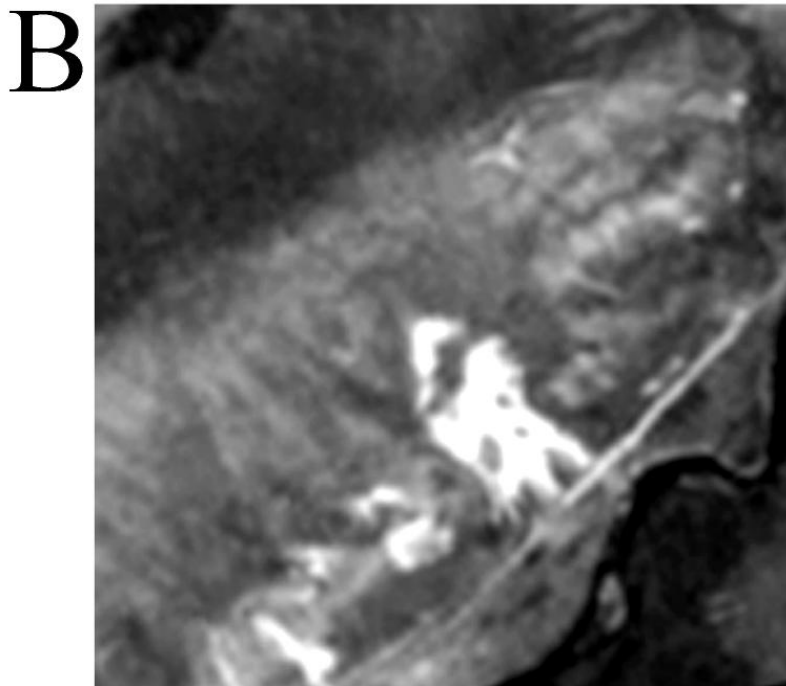
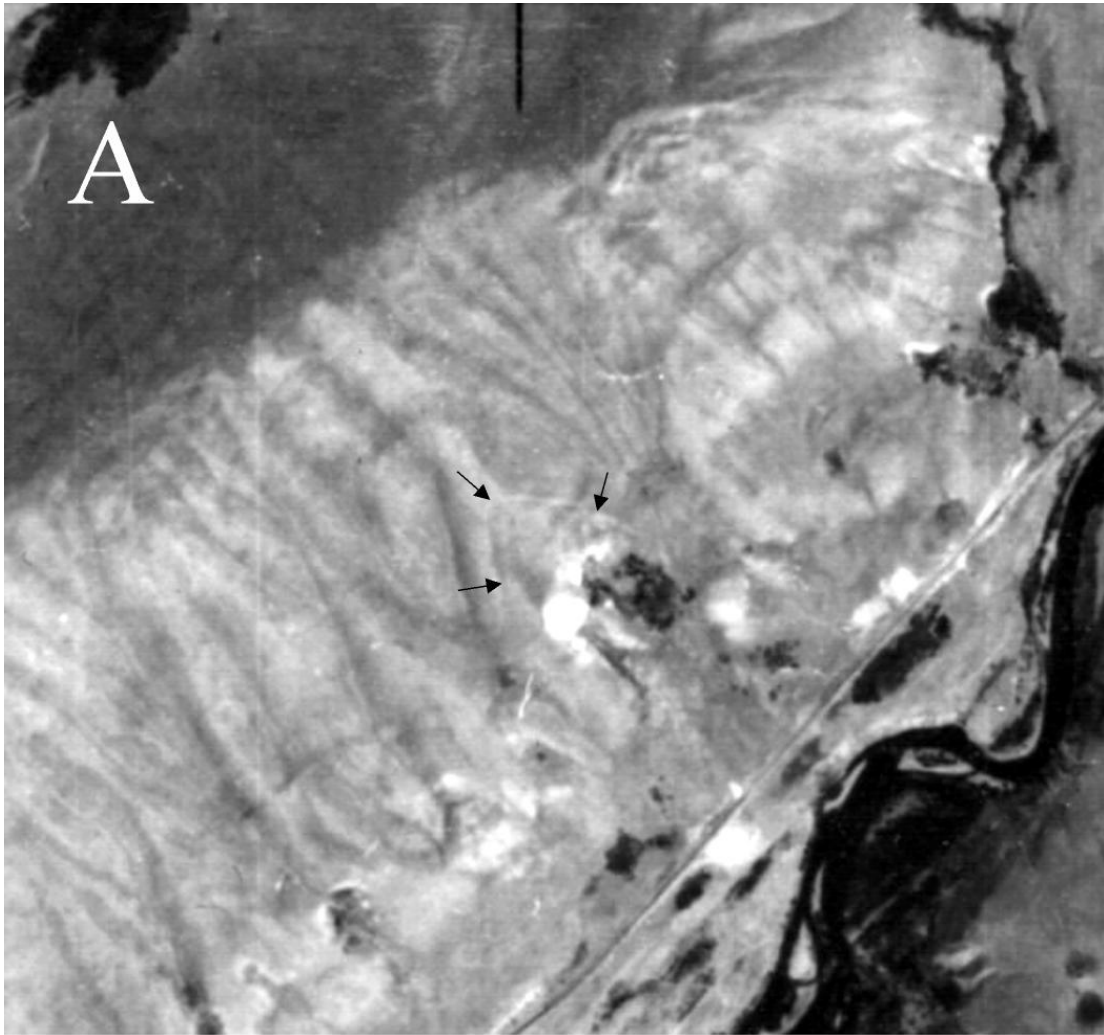


Figure 21. Comparison of zoomed space images of the same section of the Chet-Korumdy Ridge obtained before the Suusamyр earthquake (A – 2-m resolution) and one year later (B – 8 m resolution). Note presence of the arcuate fracture that formed the scar before the event (arrows on Figure A)

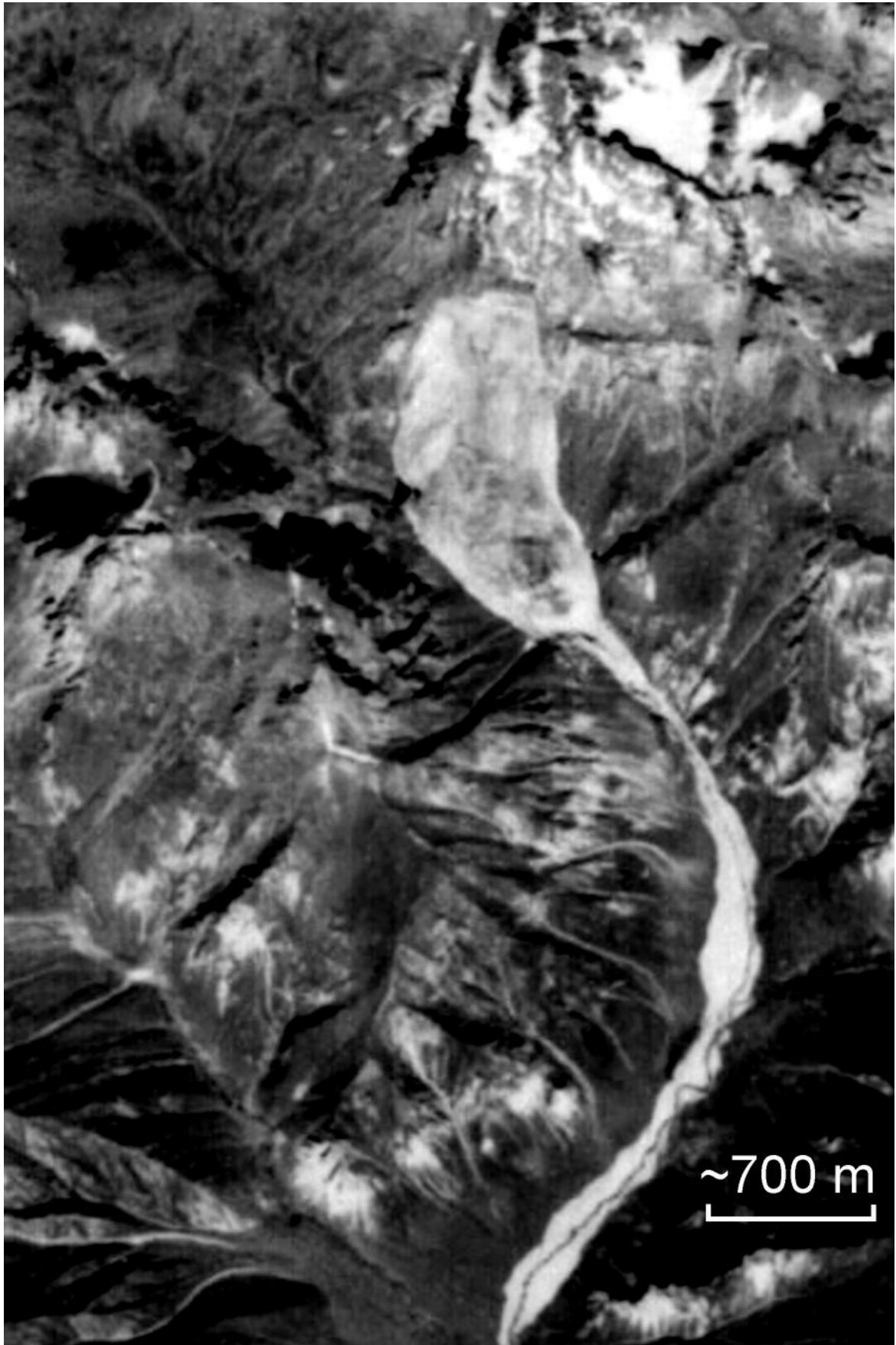


Figure 22. Rockslide in the upper reaches of the Belaldy creek caused by 1992 Suusamyр earthquake
River valley downstream was affected by the debris flow that occurred about one year later.
Zoomed fragment of the KFA-1000 space image

In the deep Kokomeren River valley the Suusamyр earthquake caused only minor rockfalls (Figure 23), most of which can be hardly identified now, 15 years after the event.



Figure 23. 1992 Earthquake induced rockfall on the right bank of the Kokomeren River valley
Photo was obtained just few days after the event

2.4 HYDROGEOLOGICAL CONDITIONS

It is well known that groundwater is one of the main factor governing slope stability. However, in most of case studies that will be described hereafter, its role seems to be not as important as in formation of landslides in nonlithified soils. Deep valleys with high slopes composed of fractured bedrock provide good drainage conditions. Poor rock massifs' saturation is facilitated by dry arid climate with average precipitation rate of about 450-800 mm/year (of course in the past, when most of rockslides occurred climate could differ from the modern one). We should also take into consideration that most of study area is located bellow snow-line, which, at present, is at the elevation of about 3800 m.a.s.l in this part of the Tien Shan. Practically there are no, if any, springs directly inside rockslide scars. However, such springs are typical at the distal parts of rockslide deposits. One can ask, what can be the source of this water? It seems that, apart from rain and snowmelt water that infiltrates into huge granular mass of rockslide debris and releases gradually, condensation in the porous upper parts of rockslide bodies composed of large angular boulders with free air circulation between them can be one more possible source of ground water that feed these springs.

3 ROCKSLIDE CASE STUDIES

Hereafter we describe most interesting rockslides and rock avalanches, which can be visited during the training course.

3.1 THE SNAKE-HEAD ROCK AVALANCHE

Interesting and in many respects still mysterious bedrock slope failure occurred in prehistoric times (most likely in Late Holocene) in the eastern part of the Suusamyр intermontane depression, in the upper reaches of a small unnamed gully on the right bank of the Karakol River valley (42.35° N, 74.34° E) (No 1 on Figure 2).

The initial failure of about $5 \times 10^6 - 7 \times 10^6$ m³ of Devonian sandstone converted into rock avalanche that traveled 2815 m (runout measured from the head-scarp crown towards rock avalanche tip) along narrow and gently inclined valley. After reaching alluvial fan, rock avalanche debris formed an elongated blade bounded by longitudinal levees with transverse levees and furrows between them (Figure 24).

This rock avalanche is just an expressive member of a large cluster of land- and rockslides developed at a limited area about 10 km from east to west and 3 km from north to south only (Figure 25). It includes both well-developed landslides and slopes with indications of ongoing deformations (Figure 26, Figure 27). Several similar clusters divided by the same-size gaps without prominent slope failures have been identified along the northern boundary of the Suusamyр depression [Strom, Abdrakhmatov 2004; Havenith et al. 2006]. These clusters coincide with recent surface ruptures (see Figure 8) that give grounds for the hypothesis of their origin due to strong earthquakes.

Initial rockslide at the site in question has very unusual asymmetric head-scarp (Figure 28) about 400-500 m long and only 300-350 m wide, so that horizontal "depth" of this "bite" exceeds its width (Figure 29). Destruction affected almost the entire hillside but rockslide mass moved more along the slope rather than towards its dip direction. We assume that it could be due to high southward-directed seismic acceleration that had caused rock massif failure.

Proximal part of rockslide several dozens of meters thick and about 800 m long rests at the scar's bottom and at rather wide upper reaches of the unnamed creek (see area A on Figure 24, Figure 28). It has an expressive wavy surface with several small closed depressions. This "compact" body extends up to rather sharp narrowing of the valley (Figure 30), which had formed an obstacle on the way of moving rockslide debris. But it did not halt completely. Rather small part of debris continued its motion and formed long runout rock avalanche. The latter had traveled nearly 2000 m along the creek's valley with mean angle of about 5° only. Rock avalanche debris fills the creek's bottom and its deposits have more or less planar surface (Figure 31). Though there is a minor stream at present, it did not produce any prominent erosion feature. Rock avalanche surface is turf-covered, boggy in some parts. Rare angular boulders can be seen through the grass. Several hundreds meters downstream, at the local widening of the creek's valley, small landslides on valley slopes had added some material to this rock avalanche (see Figure 24, area C). At the foot of the hilly area rock avalanche sharply turned to the right along the lowermost part of the pre-existing alluvial fan and finally formed an elongated palm-like body 650 m long, up to 150 m wide and, as it can be estimated, 4-6 m thick (Figure 32). It looks from above like a head of a snake, that is why we called the entire feature the Snake-head rock avalanche. Total volume of this distal part of rock avalanche can be roughly estimated as $\sim 3 \times 10^5$ m³. Volume of deposits that filled the narrow bottom of the creek is of the same order. Thus, only $\sim 10\%$ of the collapsed rock mass was involved in the avalanche-like motion.

The palm-like blade is bounded by the levees that rise up to 4-5 meters above the surrounding alluvial fan surface and 1-2 m above the internal part of rock avalanche deposits (Figure 33). The latter represents the system of levees and furrows, which strike transverse to the direction of rock avalanche motion (Figure 34). Such relief is completely different from that typical of the debris flow deposits and, at the same time is not typical of the most of "classical" rock avalanche deposits. In the outcrops along the small spring that has eroded the right edge of rock avalanche distal part one can see that it is composed of the intensively shattered debris (3-5-cm fragments in fine matrix) while surface of the blade is covered by angular boulders 20-30 and, rarely, 40-50 cm in size. Rather steep edges of the distal blade (see Figure 33) indicate that it was formed, most likely, by dry material. If it would move as a debris flow with high content of water, it would spread much wider forming a fan-shape body.

We hypothesize that an extreme mobility of this relatively small rock avalanche could be caused by the "bottle-neck effect" – transfer of the momentum of abruptly decelerating entire rock mass to its small portion that pass through the prominent narrowing (see Figure 30). It should be noted, however, that further investigations should be carried out to explain mechanism of the Snake-head rock avalanche formation from the very beginning of rock slope failure to the final halt of debris motion.

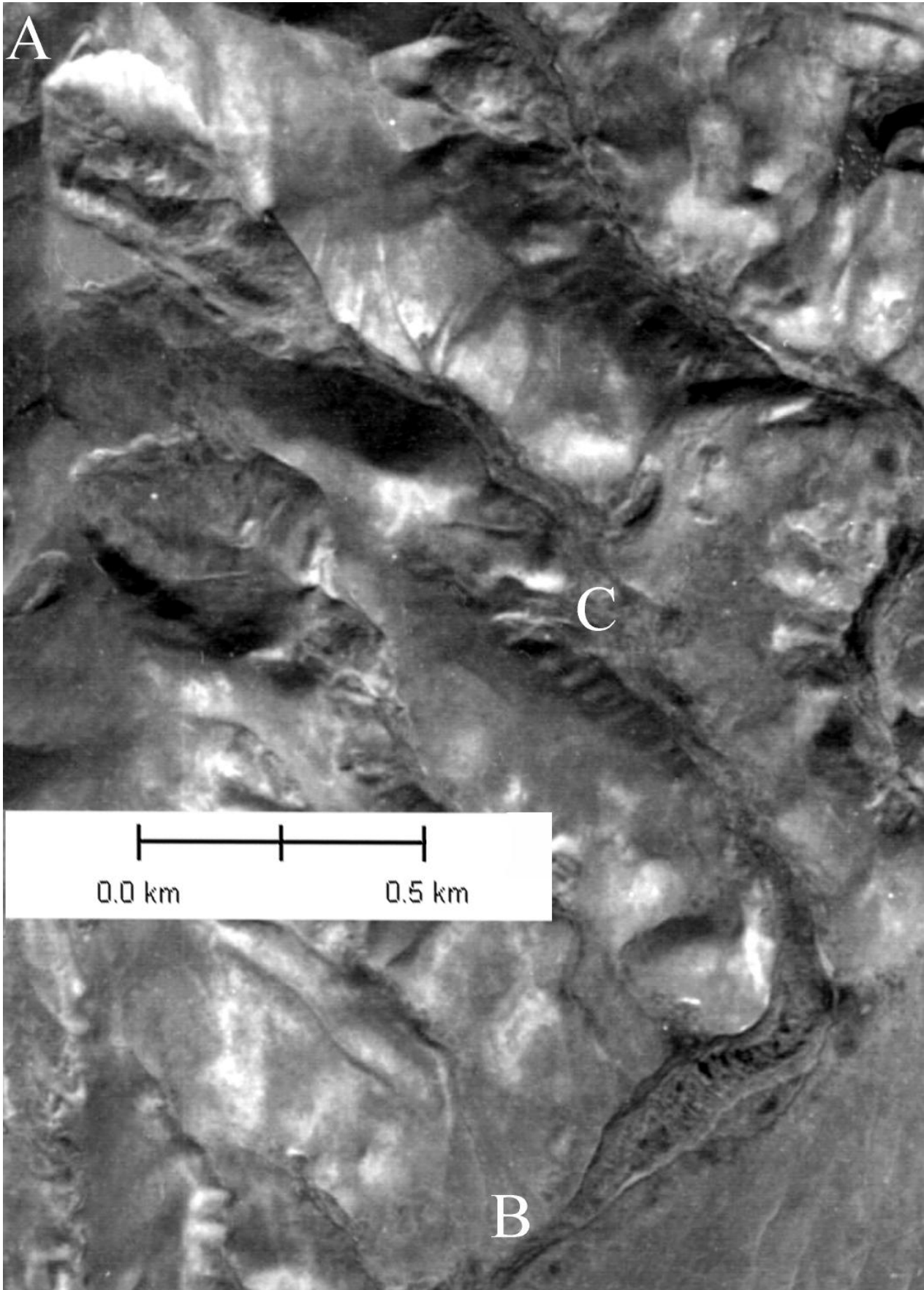


Figure 24. Long runout Snake-head rock avalanche

The initial massive rock slope failure at **A** was accompanied by rock avalanche that traveled along the narrow gorge about three kilometers up to **B**. **C** – part of the transitional zone where debris of additional landslides "fell into" the main rock avalanche

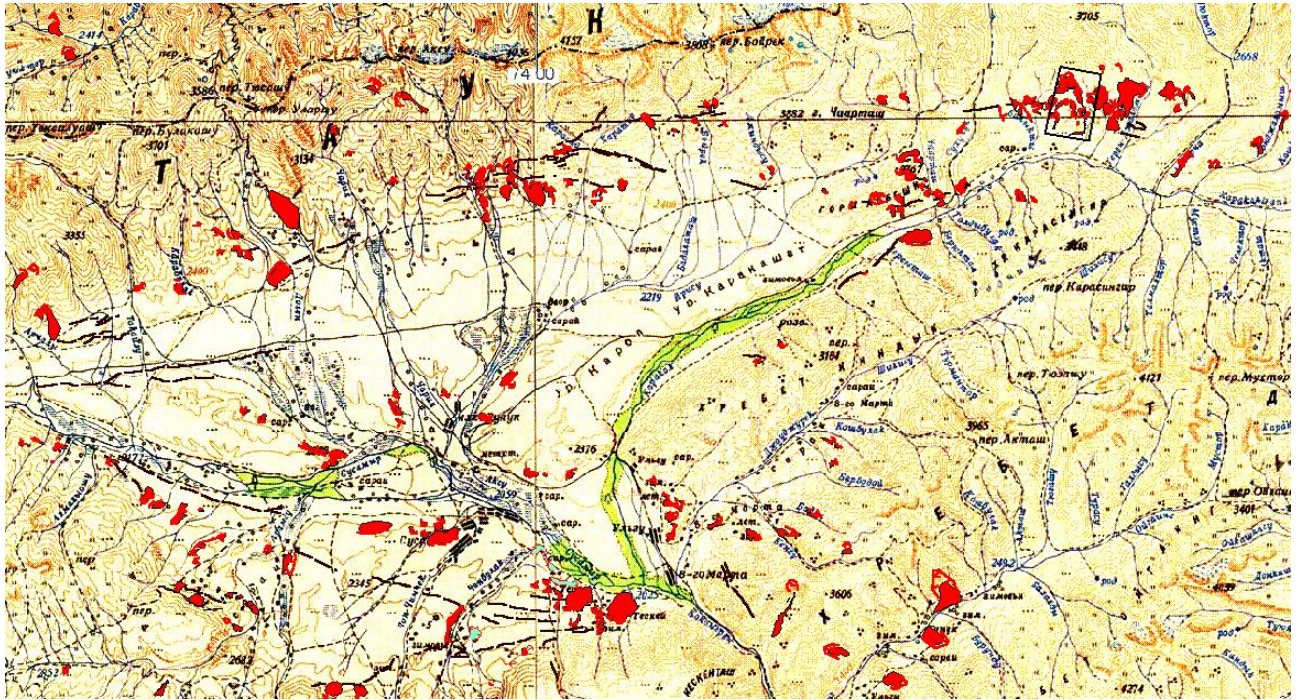


Figure 25. Spatial distribution of rockslides, landslides and recent faults of the Suusamyr intermontane depression
The Snake-head rock avalanche, shown on Figure 24 is marked by a rectangle



Figure 26. Gully slope totally affected by landslides
east from the Snake-head rock avalanche.



Figure 27. Landslides east from the Snake-head RA downstream from the site shown on Figure 26

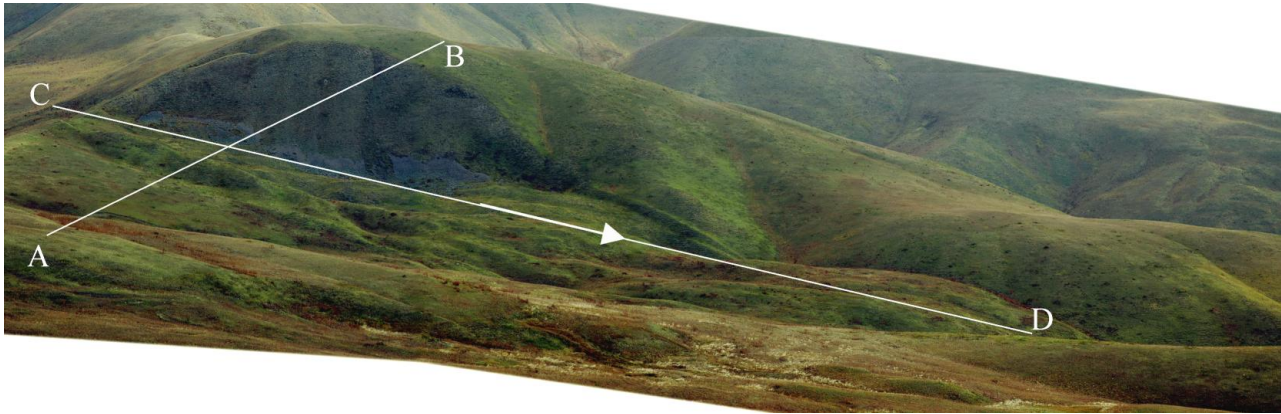


Figure 28. Head-scarp of the Snake-head rockslide and the proximal part of rock avalanche deposits
 Note quite asymmetric form of the head-scarp that destroyed the entire hillside, while rockslide mass moved right (arrow) more along the slope rather than towards its dip direction. Schematic cross-sections AB and CD are shown on Figure 29.

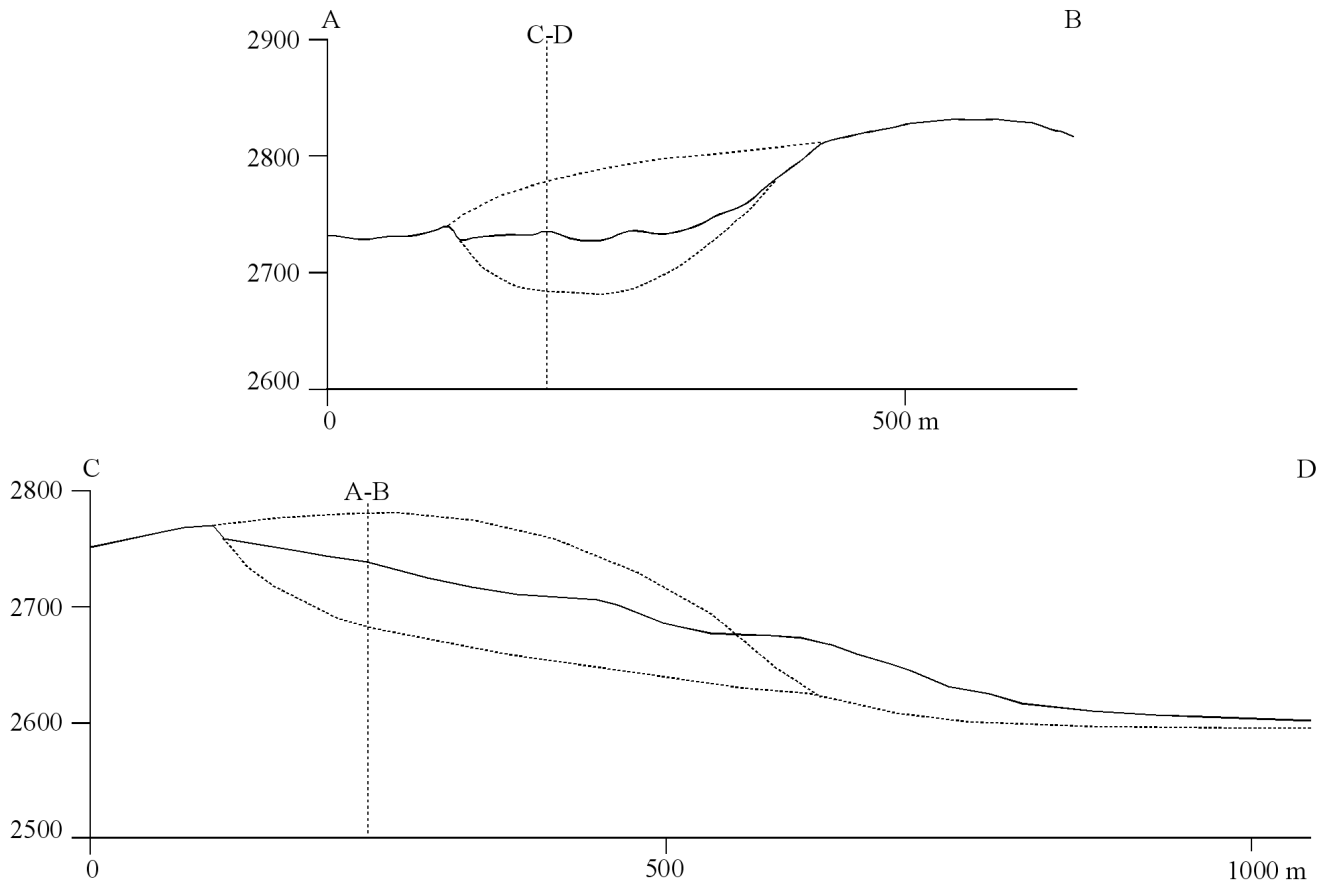


Figure 29. Schematic cross-sections of the Snake-head rockslide scar

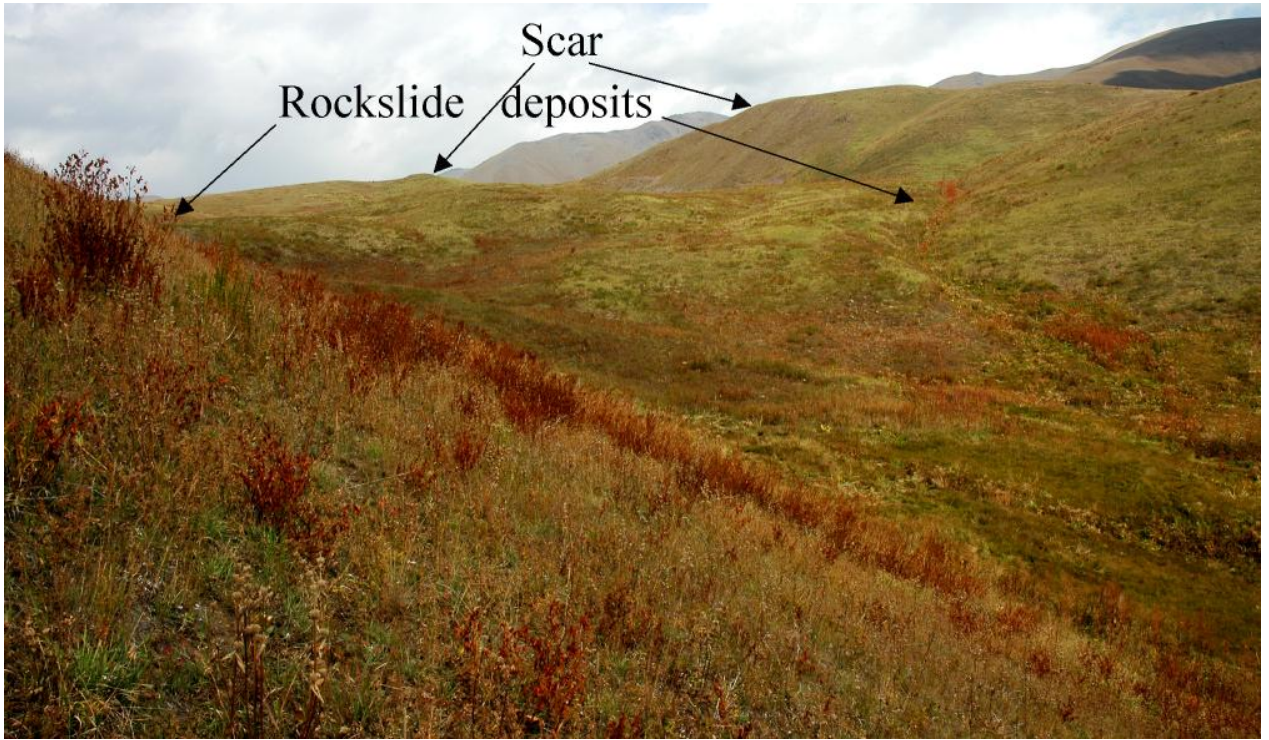


Figure 30. Distal end of the Snake-head rockslide compact part at the narrowing of the creek valley



Figure 31. Nearly horizontal surface of the Snake-head rock avalanche upper part immediately below its compact part



Figure 32. The Snake-head rock avalanche palm-like distal blade



Figure 33. Boundary levees of the Snake-head rock avalanche distal blade
Left-site (above) and right-side (below)



Figure 34. Transverse levees and furrows at the central part of the Snake-head rock avalanche distal blade
General view above and zoomed outlined section below

Several rockslides can be seen on the opposite (left) bank of the Karakol River valley (Figure 35). It is evident that rockslide bodies that can be identified on this photograph have different ages, thus indicating recurrent slope failures.

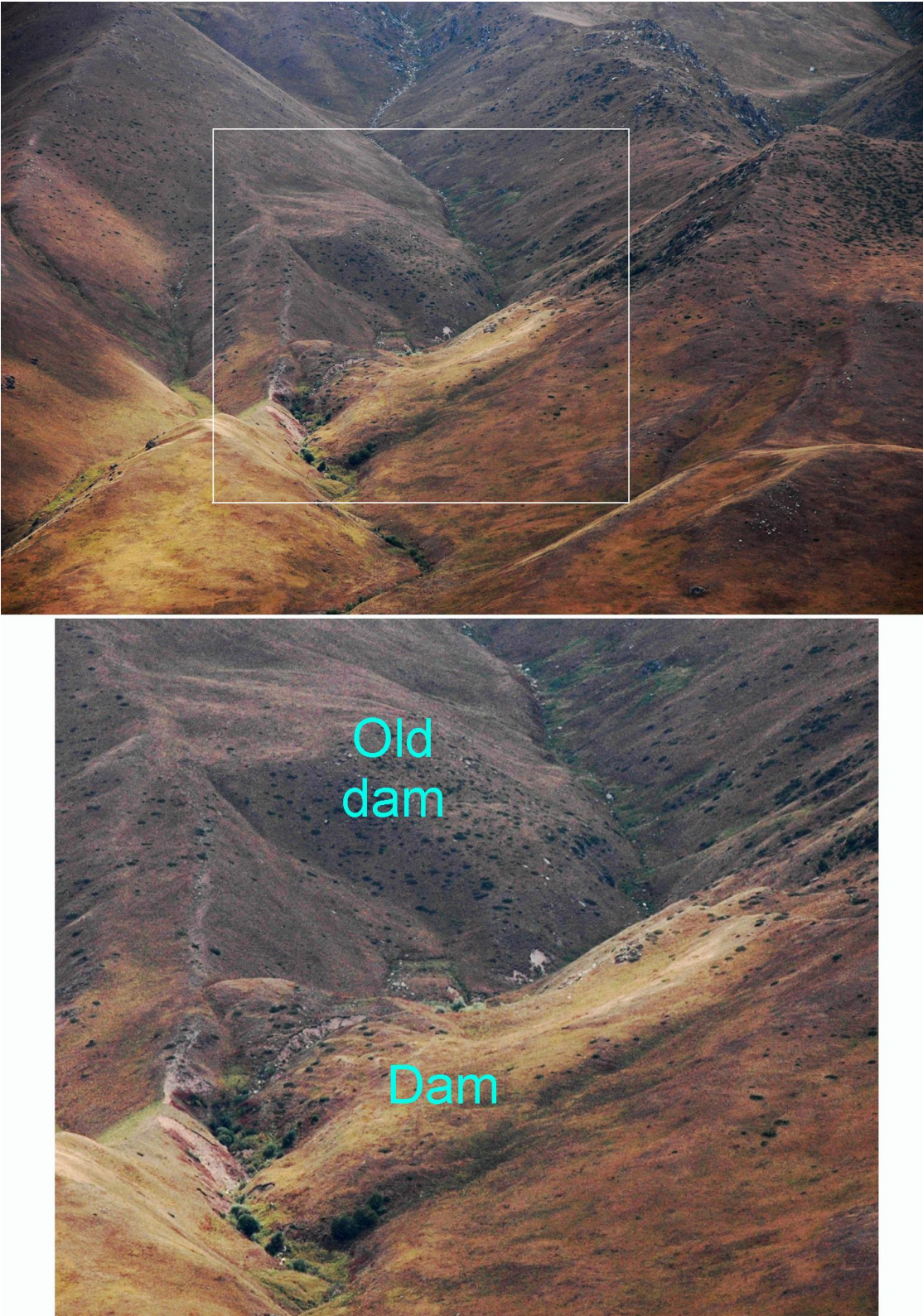


Figure 35. Recent and old (significantly eroded) rockslide dams in the gully at the left bank of the Karakol River valley opposite the Snake-head rock avalanche site

3.2 THE SEIT ROCK AVALANCHE

This impressive rock avalanche (No 2 on Figure 2) is located 5-6 km downstream from the Kojamkul village named after a hero who lived here in the beginning of the XX century and who brought a huge boulder to the grave of his friend that can be seen aside a road. It was partially destroyed by the 1992 Suusamyr earthquake.

The enormous heap of angular granite boulders and debris fills the small gully at the eastern flank of the Kokomerren River valley at 42.11° N, 74.14° E, while rock avalanche scar is seen far away on the main watershed slope (Figure 36).



Figure 36. Overview of the Seit primary rock avalanche
Practically all debris accumulates at its the distal part

It is a classical example of the "Primary" rock avalanche [Strom 1996, 2006], when practically all debris accumulates at its distal part (Figure 37, Figure 38). Rock avalanche seems to be rather recent – we assume that it occurred about several hundreds – 1 thousand years ago. This assumption is based on the fact that the deposits' distal tip fills the stream of the creek incised in the low terrace (Figure 39). Thick Archa (Central Asian juniper) trees growing on its surface are up to 320 years old (Figure 40) (Olga Maksimova, personal communication), which corresponds to the upper limit of the slope failure age; the latter can be also measured by the lichenometric method (Figure 41).

Rock avalanche was formed by the collapse of about 20 million cubic meters of granites in the upper reaches of the deep dry valley (Figure 42). Though upper part of the transitional zone is now almost debris-free, the initial thickness of moving debris can be reconstructed from the trimlines that remained on the slopes dozens meters above resultant deposits' surface (Figure 42 – Figure 44). We should note that similar phenomena indicating decrease of debris thickness during rock avalanche motion can be observed at several other rock avalanches, which will be described hereafter.

Rapid rock avalanche motion halted when it struck over the sharp bend of the slope composed partially of granite and partially of boulders in sandy-gravel fill, which, likely, represent the reworked glacial deposits (Figure 45). Frontal part of rock avalanche has an expressive wavy surface with longitudinal levees and furrows (see right part of Figure 43 and Figure 46), which orientation reflects the direction of debris motion. It seems that motion halted abruptly; otherwise angular boulder with X-like fractures (Figure 47) resulted from the adjacent boulders collision should separate in several blocks.

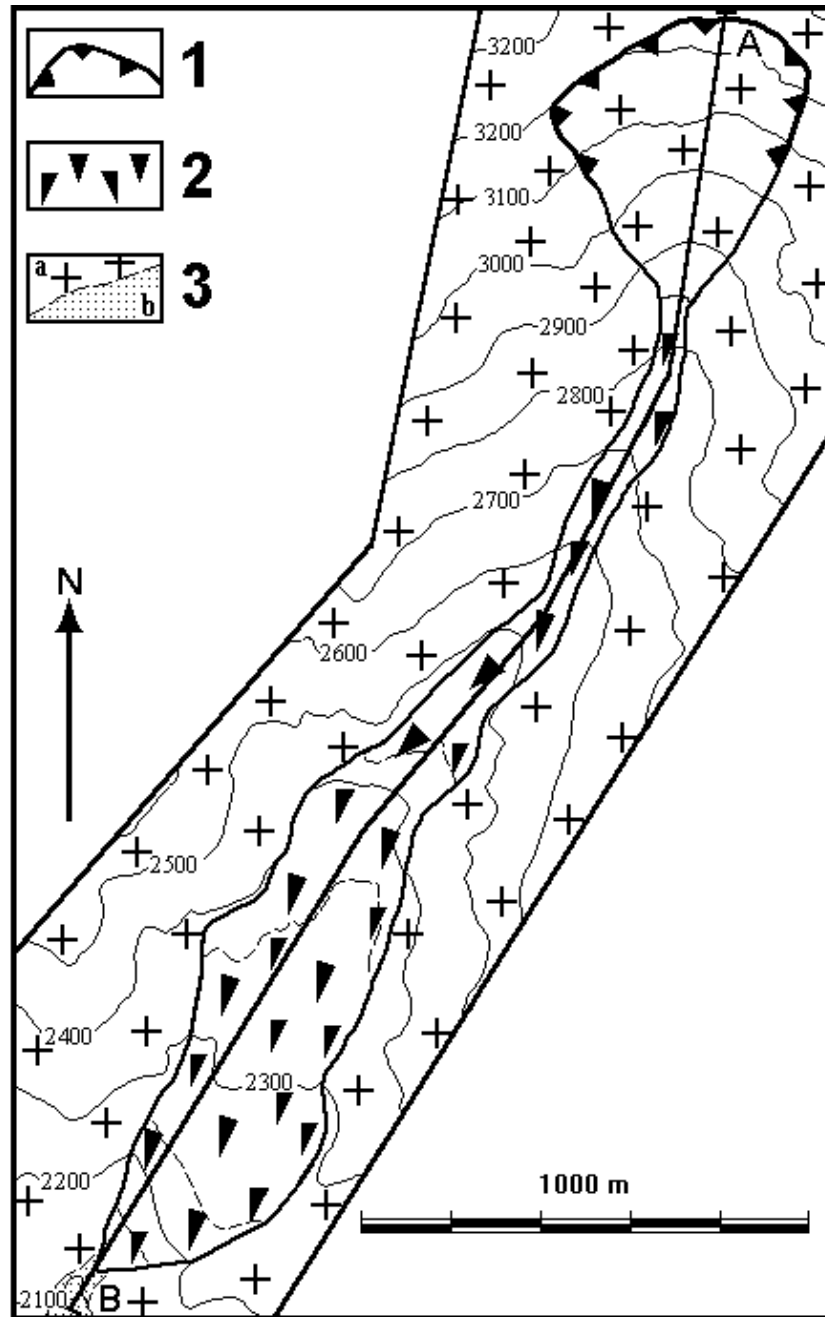


Figure 37. The schematic map of the Seit rock avalanche

1 – rock avalanche scar; 2 – rock avalanche debris; 3-a – bedrock granite; 3-b – pre-rock avalanche alluvial deposits

Uppermost part of rock avalanche deposits is composed of huge angular boulders (see Figure 47), while debris just below this carapace seems to be crushed at a much greater extent (see Figure 39). Locally molard-like hills up to 1.0-1.5 m high composed of rather large angular blocks are observed (Figure 48). Their origin is, however, questionable – it's quite possible that these 'hills' originated not due to ejection of the material from the internal part of debris, which should be finer than the surrounding debris, as it is typical of 'classical' molards [Cassie et al., 1988], but due to *in-situ* destruction of large fractured blocks.

The Seit rock avalanche is not the only one large-scale bedrock slope failure in this area. Just nearby there is a deep short gully with small remnant of debris inside it, which could be interpreted as a scar of much older (Pre-Seit) rockslide (No 3 on Figure 2) (Figure 45).

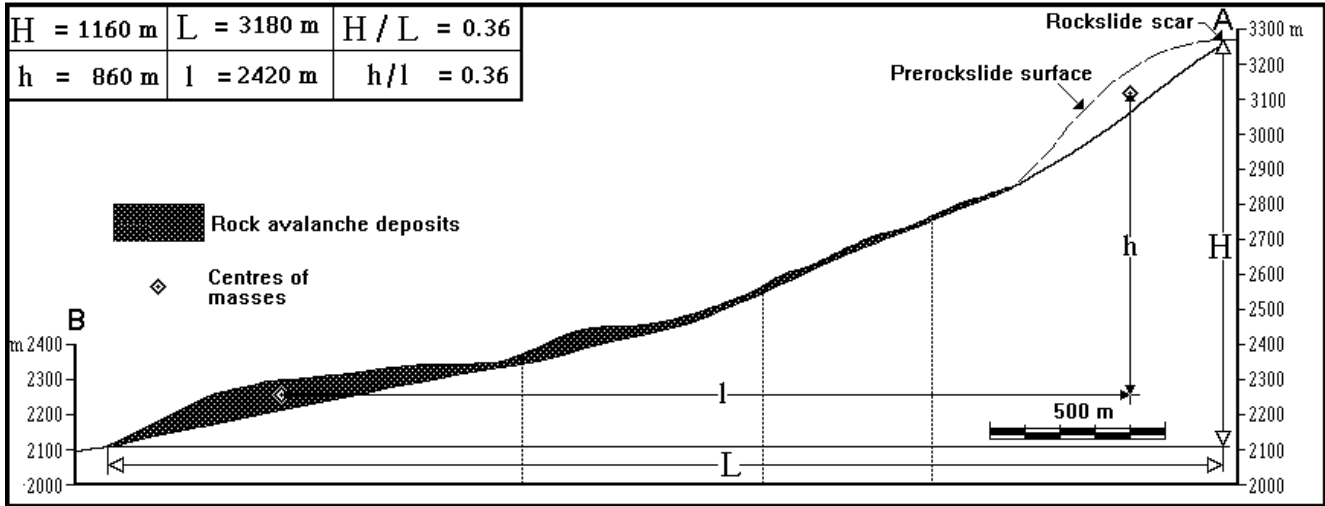


Figure 38. Longitudinal cross-section along the Seit rock avalanche



Figure 39. The Seit rock avalanche body fills the creek's channel



Figure 40. Drilling of the ~300 years old Archa tree growing on the Seit rock avalanche deposits



Figure 41. Various lichens on the boulder surface

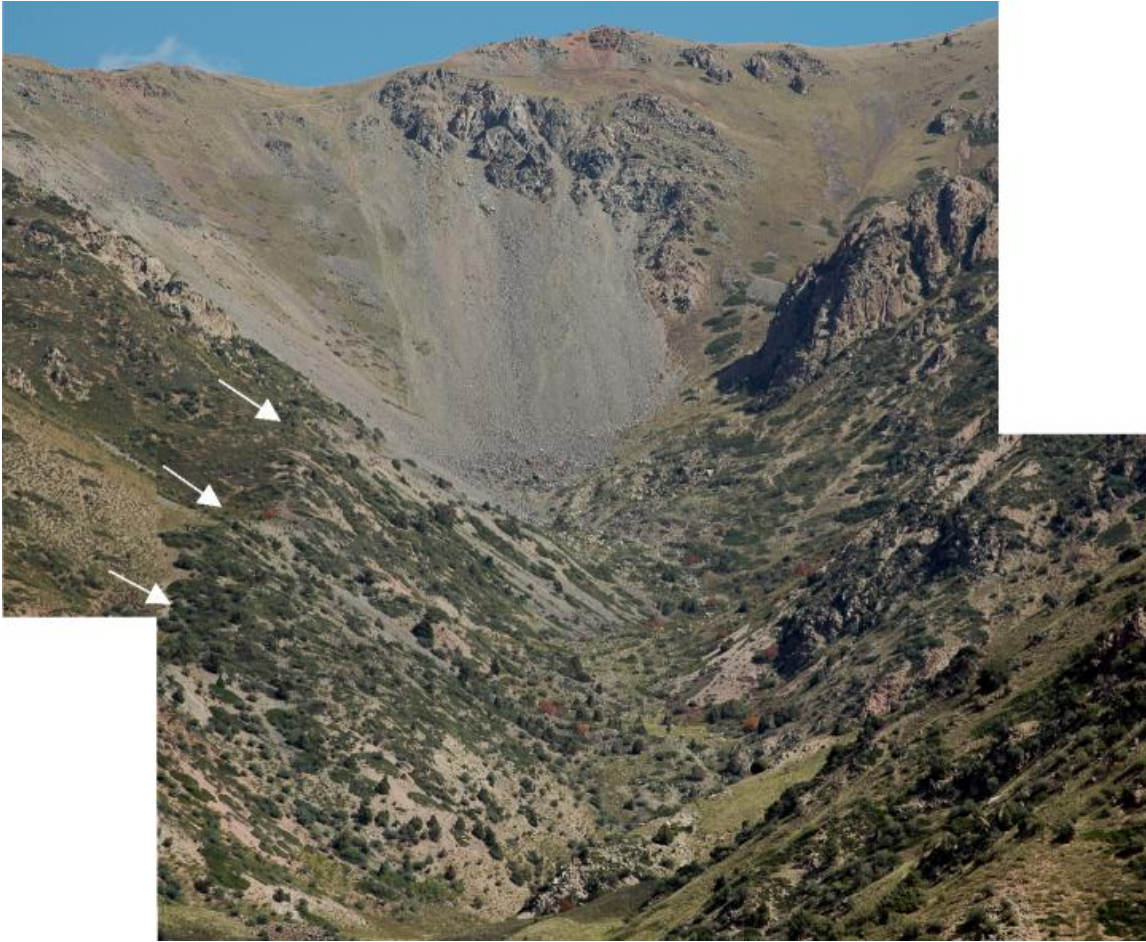


Figure 42. Scar and the transition zone of the Seit rock avalanche
 Note remnants of RA debris that form narrow bench (trimline) on the right bank of the valley about 50 m above its bottom (arrows), indicating the initial thickness of moving debris



Figure 43. Trimlines at the right side of the Seit rock avalanche path
 marking the thickness of moving debris



Figure 44. Lower part of the Seit rock avalanche transition zone
 Central part of RA deposits is 10-15 m lower than its border zones marked by trimlines (arrows). Dashed and solid white lines indicate the assumed initial and final thickness of moving debris at this section

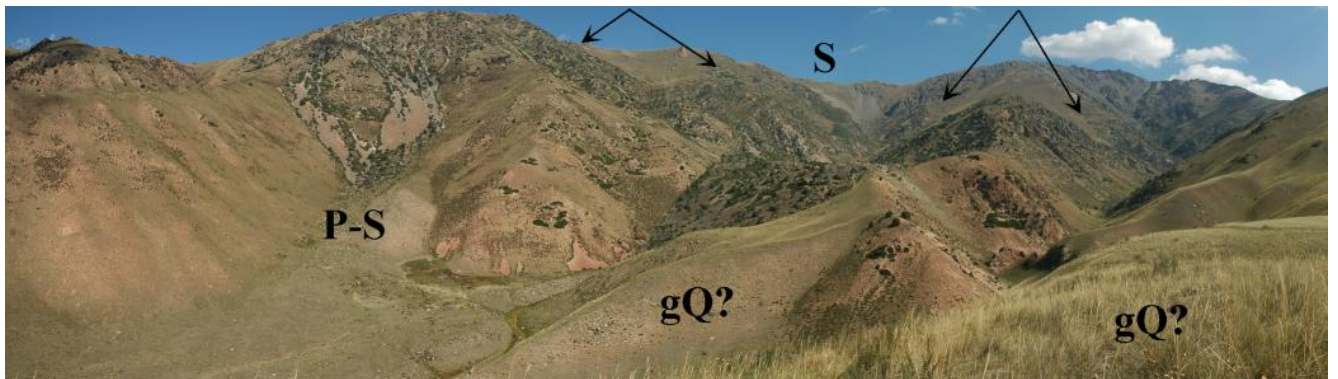


Figure 45. Overview of the Seit RA (S) and Pre-Seit rockslide scar (P-S)
 Arrows mark smooth remnants of older relief; gQ? – reworked glacial deposits (assumed)



Figure 46. Wavy surface of the Seit rock avalanche distal part



Figure 47. Angular fractured boulder that had been broken just before motion halted (otherwise its parts would be separated)



Figure 48. The molard-like hill on top of the Seit rock avalanche deposits

3.3 ROCKSLIDES IN THE OIGAING AND BURUNDU RIVER VALLEYS

Several rock slope failures had happened in the deep valleys of the Kokomeren left tributaries – the Oigaing and Burunsu Rivers. Rockslide about $30 \times 10^6 \text{ m}^3$ in volume descended from the right bank of the Oigaing River valley about 10 km upstream from its mouth (42.12° N , 74.24° E) (No 4 on Figure 2). Slope is composed of Palaeozoic granites and metasediments. 50–70 m thick rockslide body has been significantly eroded by the river and only its proximal part remains at the scar's foot. Its internal structure along with expressive rockslide scar 750 m high and up to 1000 m wide can be observed from the opposite bank of the Oigaing River (Figure 49).

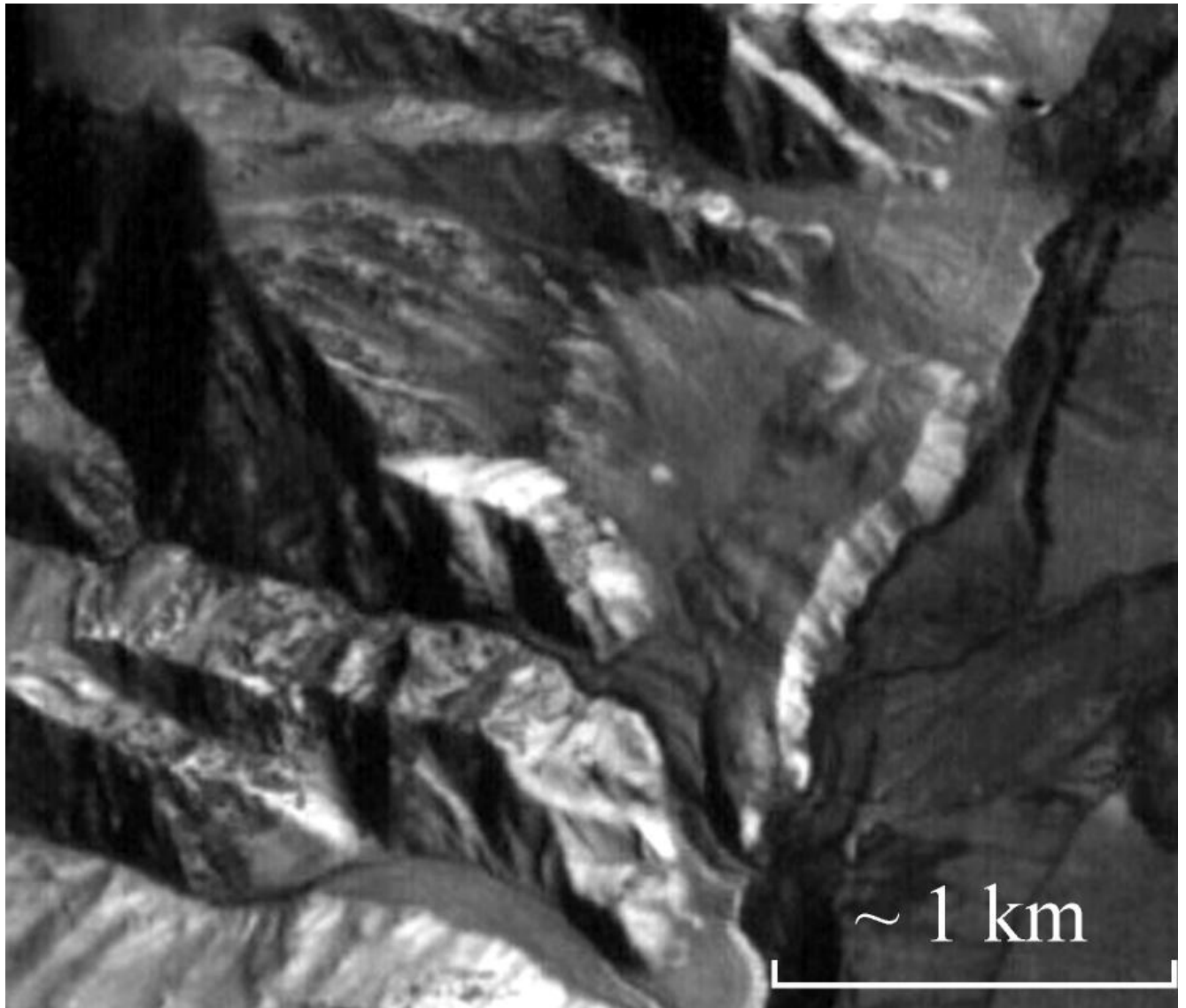


Figure 49. The Oigaing rockslide
Zoomed fragment of high resolution KFA-3000 space photograph

Much smaller bedrock landslide about 10^6 m^3 in volume only had dammed the Burundu creek – the small left tributary of the Kokomeren River that merges it 4 kilometers upstream from the Kyzyl-Oi village (No 5 on Figure 2). It had blocked the river at 41.99° N , 74.19° E , two kilometers upstream from its mouth by compact dam up to 100 m high with convex slopes. Dam's surface is composed of angular granite boulders. Angle of repose of its upstream slope is about 35° . Most of rockslide debris had accumulated at the scar's foot and Burundu River incised its new path with 15-20-m high waterfall through the right bank bedrock that indicates that pre-rockslide level has not been reached yet.

3.4 THE CHONGSU ROCK AVALANCHE

This rock slope failure about $20 \times 10^6 \text{ m}^3$ in volume descended at 41.99° N , 74.02° E from the ridge that bounds Kyzyl-Oi intermontane depression. It is located in the upper reaches of the Chongsu River (No 6 on Figure 2). Mountain range and depression are separated by neotectonic fault, which is visible in the outcrop just near the distal end of Chongsu rock avalanche (Figure 50, Figure 51). The collapsed spur in the upper reaches of the unnamed gorge as well as the entire ridge are composed mostly of granite.

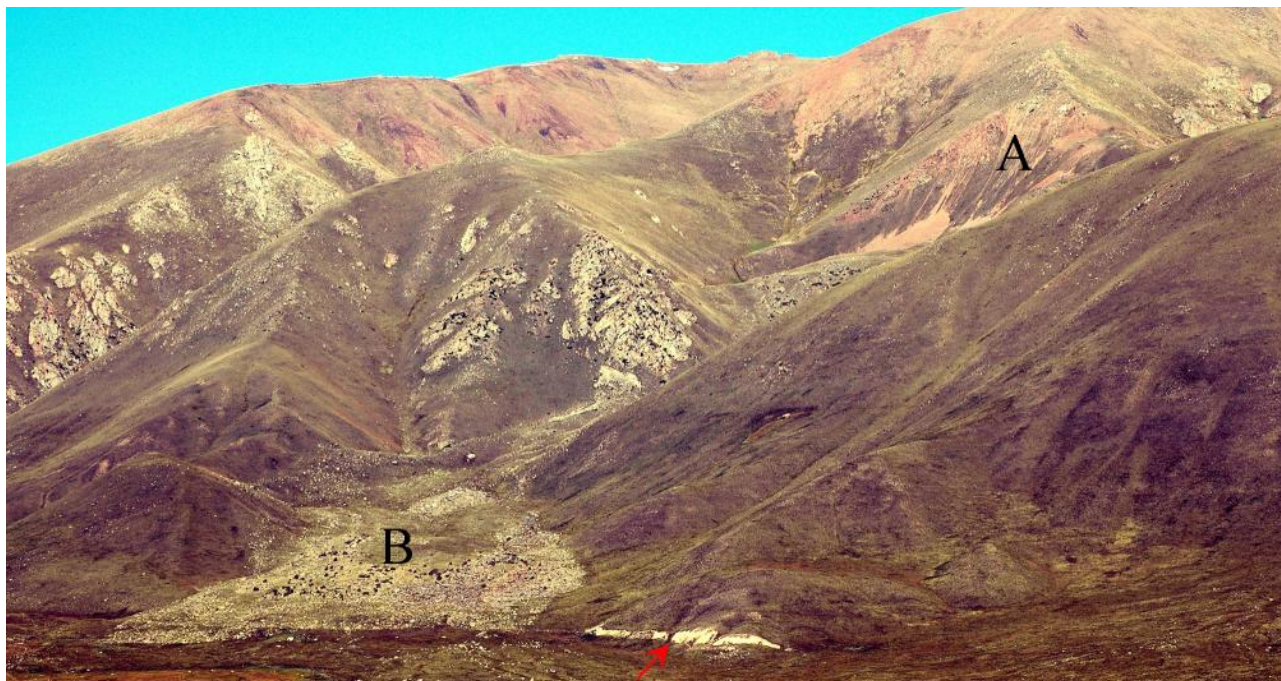


Figure 50. Overview of the Chongsu rock avalanche
A - headscarp, B - distal rock avalanche fan. Red arrow marks the outcrop of neotectonic reverse fault (Figure 51)

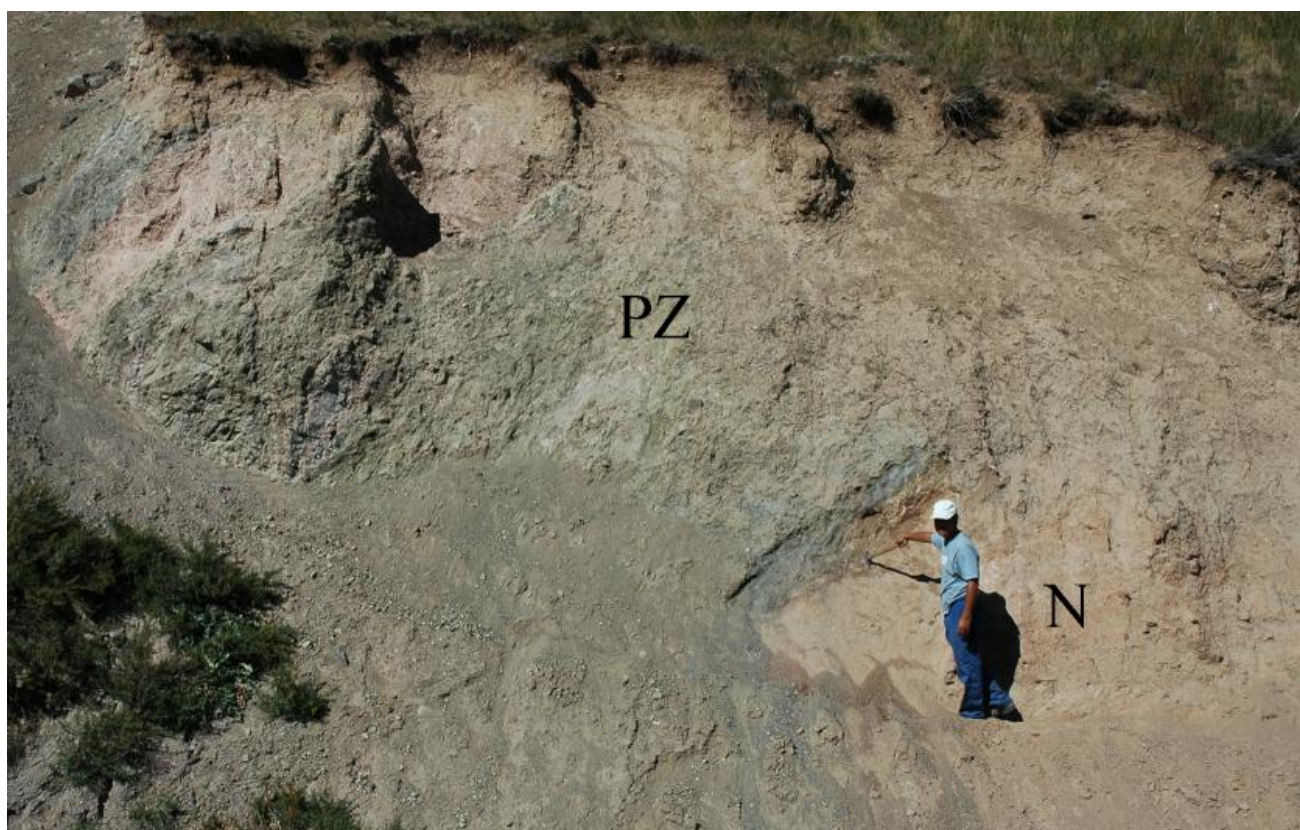


Figure 51. Neotectonic reverse fault
PZ – crushed Paleozoic rocks; N – Neogene deposits

This event is an excellent example of the so called "secondary" rock avalanche [Strom, 1996, 2006] which characteristic feature is the distinct division of the collapsed rock mass into two parts: compact body immediately at the foot of the failed slope and long runout rock avalanche that descended from the concave (secondary) scar on the frontal or downstream side of a compact body (Figure 52, Figure 53). In many cases volume of the secondary rock avalanche exceeds volume of the secondary scar. It excludes the possibility that secondary rock avalanche could collapse later, some time after initial slope failure. The abovementioned Snake-head rock avalanche represents another sub-type of the secondary rock avalanche, which characteristic feature is a "bottleneck" on the way of moving debris that divides the rockslide body into compact and avalanche-like parts.

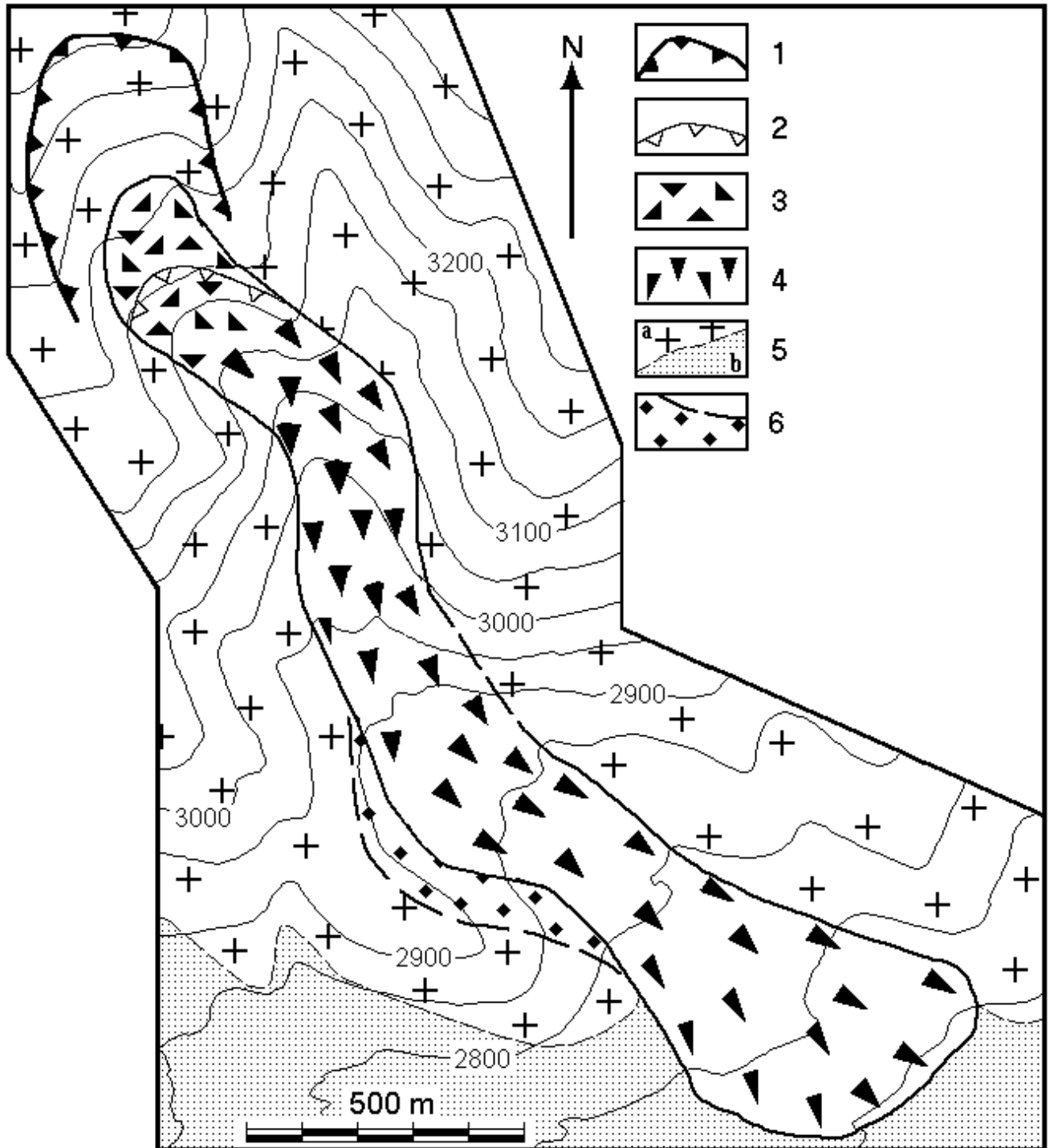


Figure 52. The schematic map of the Chongsu rock avalanche
 Legend: 1 – Main scar; 2 – Secondary scar; 3 – Rockslide deposits; 4 – Rock avalanche deposits, including those remaining on the slopes above resultant surface of the deposits; 5 – Bedrock (a) and Quaternary deposits (b); 6 – Remnants of rock avalanche splash above the main deposit surface

The Chongsu rock avalanche morphology provides a good chance to reconstruct process of debris motion and, thus, to make some assumptions on the mechanical processes that took part during rock avalanche emplacement.

Expressive trimlines on the valley slopes that had confined rock avalanche transition zone downstream from the secondary scar are visible much above the final rock avalanche surface (Figure 53 – Figure 55). They stretch parallel to it for a long distance – about 700 m on the left slope and up to 1 km on the right one. Since they are visible on both sides of the transitional zone it is unlikely that trimlines mark the inertia run-ups, when rockslide debris splashes either on one or on another slope like the Karmadon rock-ice avalanche [Nikitin, et al., 2006] or like the Pandemonium Creek rock avalanche [Evans, et al., 1989]. In this case we assume that trimlines indicate constancy of moving debris thickness up to its section shown on Figure 55 where trimline level sharply decreases so that it merge the resultant rock avalanche surface. It means that at some stage of motion thickness of moving debris decreases rapidly. Moreover, since the final level of debris within the proximal part of rock avalanche is much lower than initial one, it is obviously that most of material "flowed out" leaving the above benches only.

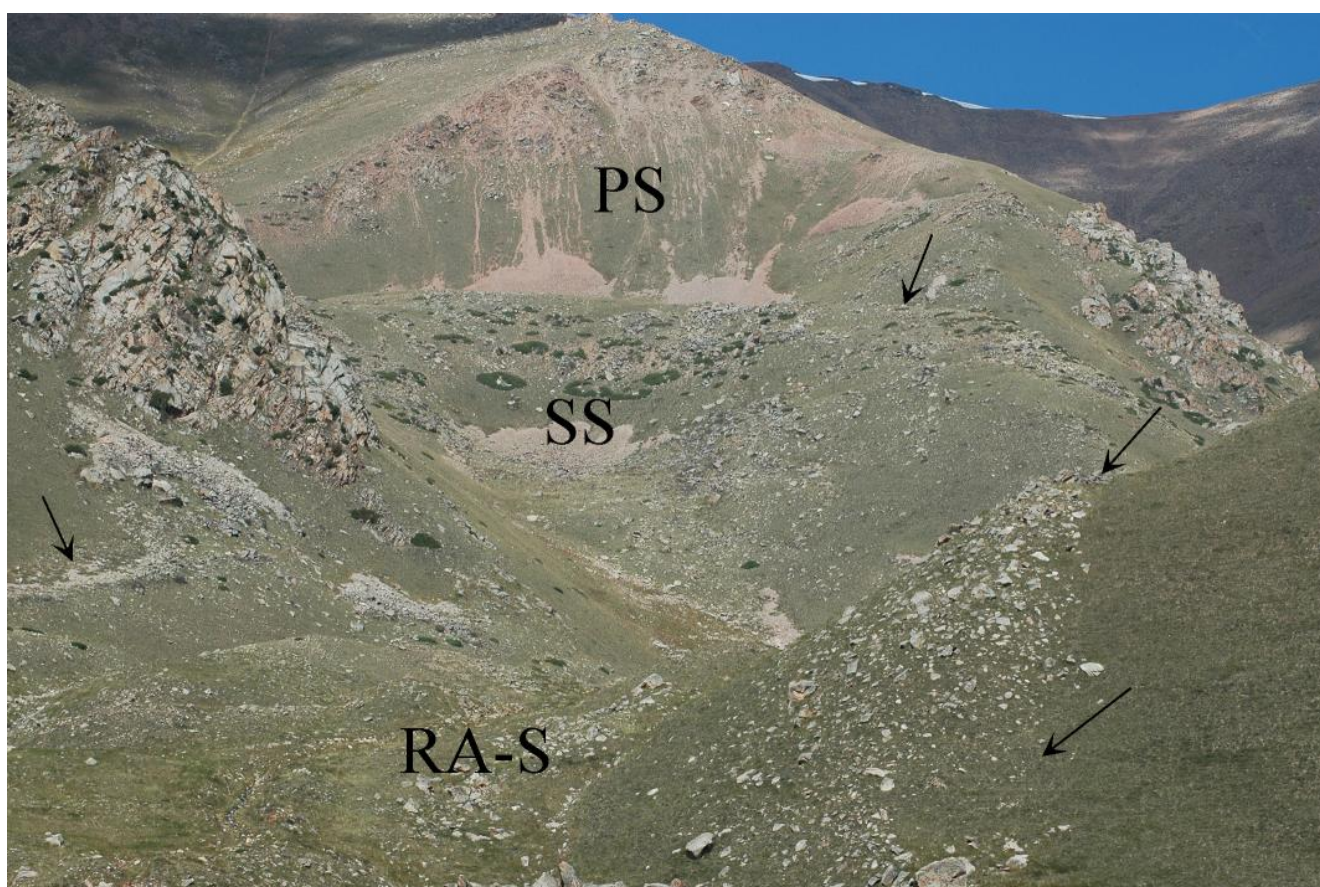


Figure 53. Primary (PS) and secondary (SS) circus-like scars of the Chongsu rock avalanche
Arrows mark the trimlines on the valley slopes much above than final rock avalanche surface (RA-S)

Besides, there is an apron of angular granite boulders on the right slope of the valley above the trimline represented by nearly horizontal bench (see Figure 54). This apron is very thin, "one boulder thick" in general, and rises up to 15 m above the bench. Moreover, few boulders rest on the slope outside the main apron (Figure 56), allowing assumption that they moved by the ballistic trajectory. Similar phenomena were observed at the Avalanche Lake rock avalanche in the Mackenzie Mountains in Canada [Evans, et al. 1994]. It can be hypothesized that boulders that had formed the apron itself had moved by the same way. Position of both thin continuous apron and separate angular boulders is not random – this splash of debris outside the main mass had occurred just at that section where moving debris had to turn on its way sharply.



Figure 54. Trimline on the right slope of the Chongsu rock avalanche transit zone
Arrows mark a narrow bench corresponding to the initial thickness of moving rock avalanche. Splash of debris above the trimline is visible at the left part of the photograph

"Downstream" from the point where left trimline level decreases it is visible that, unlike the Snake-head event, which completely filled the valley bottom up to some level (see Figure 31), this rock avalanche formed distinct mound about 5 m high (Figure 57). The distal part of the Chongsu rock avalanche created a fan-like body from 3-5 to 7-10 m thick composed of huge angular boulders. It has distinct lateral and frontal edges (Figure 58), which indicate that motion halted abruptly. It should be noted that we can see grain size composition of its debris from the surface only. No one outcrop exists where its internal structure is observable.

Frontal part of rock avalanche deposits overlays a small transverse levee composed of the same-size granite boulders, which, unlike those described above, are roughly rounded (Figure 59). Most likely it had been formed by pre-rockslide debris flow, which should be quite powerful, judging from boulders' size.

Few kilometers east from the Chongsu rock avalanche at 42.01° N, 74.05° E at the north-western boundary of the Kyzyl-Oi depression there is one more large rock slope failure (No 7 on Figure 2). Unlike the above Chongsu case this bedrock failure named Chongsu-2 did not transform into long runout rock avalanche. Its deposits formed a convex compact body (Figure 60). Failure had occurred few hundreds meters north from the surface rupture shown on left zoomed fragment of Figure 9. Such coincidence gives grounds for the assumption that both rockslides had occurred due to strong earthquake that produced this rupture as well. To prove (or disprove) this assumption we have to date both rockslides and rupture.



Figure 55. Abrupt decrease of the trimline level on the left slope of the Chongsu rock avalanche transit zone
It indicates change of rock avalanche initial thickness. Note constant trimline level "upstream"



Figure 56. Angular boulder (black arrow) outside the splash indicating the ballistic trajectory of debris now resting above the nearly horizontal bench (HB)



Figure 57. The Chongsu rock avalanche left boundary just "downstream" from the site shown on Figure 55
Person marked by the circle is about 1.6 m high



Figure 58. Lateral and frontal edges of the Chongsu rock avalanche indicating abrupt halt of its motion



Figure 59. The Chongsu rock avalanche front overlaying pre-rock avalanche debris flow (levee composed of roughly rounded boulders formed by – at the foreground)



Figure 60. The Chongsu-2 rockslide

3.5 THE SARYSU ROCK AVALANCHE

One more rock avalanche had occurred at the eastern part of the Kyzyl-Oi depression (41.96° N, 74.22° E) (No 8 on Figure 2). Huge block of metasediments descended from the same watershed as the gigantic Kokomeren rockslide, which will be described hereafter, but from its opposite – northern slope. The initial descend of this block was rather small ~200 m only (Figure 61), but it resulted in a 4.5-km long rock avalanche, which is a longest well-preserved rock avalanche within the entire study region. It traveled along the dry gully at an average angle of about 11°.

Rock avalanche body resting in the rather narrow valley has smooth, partially turf-covered surface with expressive trimlines rising 10-20 m above the main part of rock avalanche debris. Unlike

the Seit and the Chongsu rock avalanches where parallel trimlines follow both sides of the path, in this case remnants of debris above the resultant surface are visible, first, along the right side, and then along the left one (Figure 62), thus indicating rapid liquid-like motion of debris accompanied by its “shaking” from one “bank” to another.

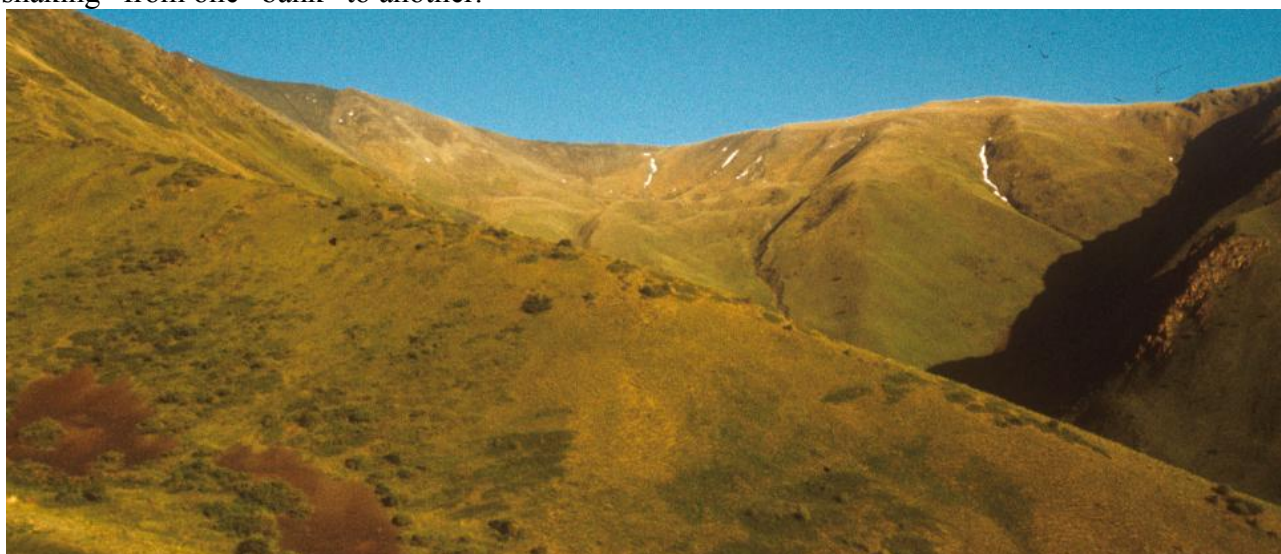


Figure 61. The Sarysu rock avalanche headscarp



Figure 62. Upper part of the Sarysu rock avalanche

Arrows mark trimlines left by moving debris first on the right side and then on the left side of the rock avalanche path

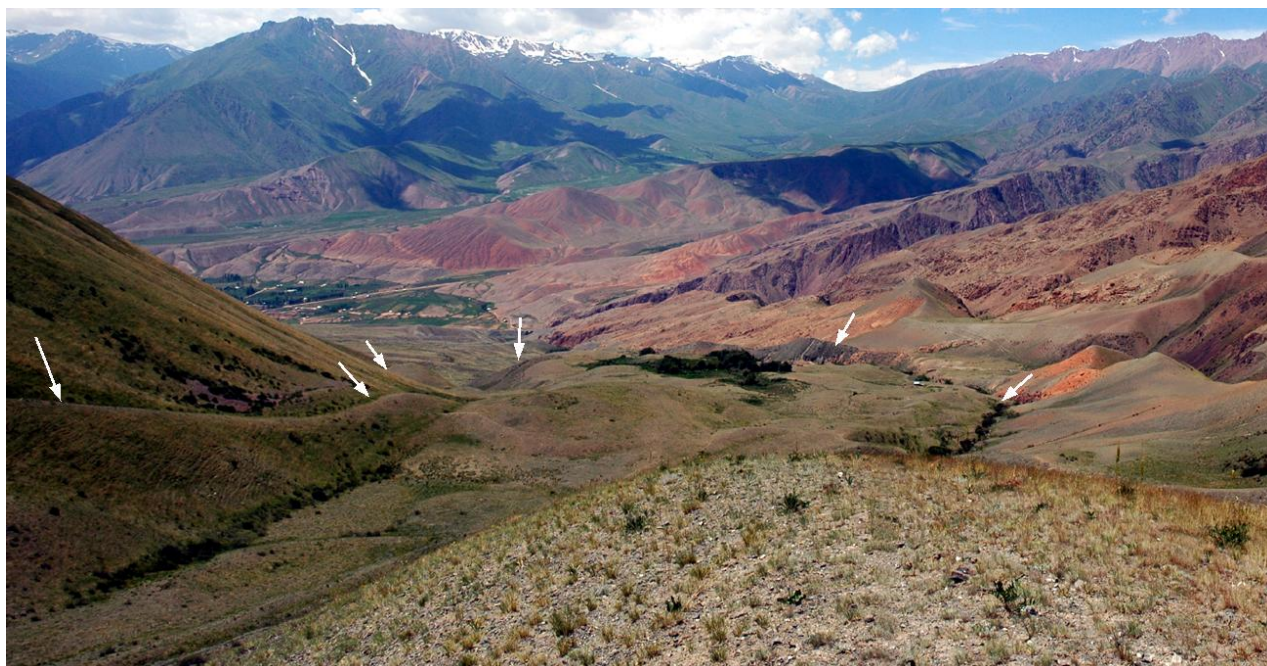


Figure 63. Lower part of the Sarysu rock avalanche path

Small arrows mark rock avalanche side boundaries and its distal limit.

"Downstream" the rock avalanche path the left trimline lowers and joins the "mainstream" (Figure 63), which follows down up to rock avalanche termination composed of macadam-size crushed debris (Figure 64).

Since no prominent "secondary scar" could be seen above the avalanche-like part of this feature it is likely that it originated due to the "bottle-neck effect" as at the Snake-head rock avalanche described above.



Figure 64. Distal end of the Sarysu rock avalanche

3.6 TOPPLING SITE

The phenomenon directly related to the rockslide formation can be observed at the southern boundary of the Kyzyl-Oi depression at 41.94° N, 74.095° E (No 9 on Figure 2). Here the northern slope of a 500-600 m high ridge (Figure 65) composed of Paleozoic metasediments with distinct bedding planes steeply dipping south (inside the slope) (Figure 66) is crossed by numerous upslope-facing scarps up to several meters high (Figure 67, Figure 68). According to the first impression the entire rock massif is sliding southward.

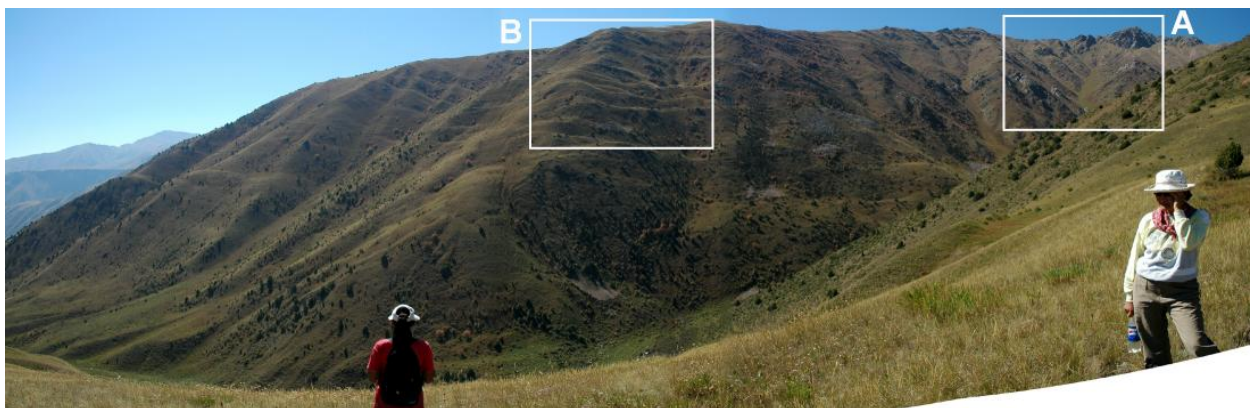


Figure 65 . Upslope-facing scarps at the upper part of the slope
Ridge bounding the Kyzyl-Oi depression from the south. Rectangles mark areas shown on Figure 66 (A) and Figure 67 (B)

However, such impression is false. In fact these upslope-facing scarps indicate that almost the entire northern slope of this ridge undergoes gradual creep deformation (Figure 69) associated with downslope bending of bed heads (Figure 70). This process is known as toppling [Varnes 1978].

According to Nichol et al. "*Slow, ductile toppling of rock masses commonly creates large-scale mountain slope deformations. In some cases, toppling can initiate a brittle catastrophic rockslide. A theoretical and field-based study has been aimed at distinguishing these two alternative modes of toppling. The results indicated two distinct types of behavior: ductile, self-stabilizing flexural toppling in weak rock with a single dominant joint set; and brittle, catastrophic block toppling in strong rock containing persistent, down-slope oriented or horizontal cross-joints. The two mechanisms exhibit very different patterns of pre-failure stress*" [Nichol, et al. 2002]. However, intensive seismic shaking can cause rapid slope failure even at the sites featuring first type of the above two mechanisms. It

could happen, in particular, at the site shown on Figure 70, which collapsed during the 1992 Suusamyр earthquake. Similar processes at the Chet-Korumdu Ridge composed of the Neogene semi-lithified sediments still go on as can be seen on Figure 20.



Figure 66. Structure of rock massif shown on Figure 65
Bedding planes steeply dip in the massif



Figure 67. Upslope-facing scarps at the most affected part of the slope, shown on Figure 65



Figure 68. Side view on the toppling site
Note interception of the talus

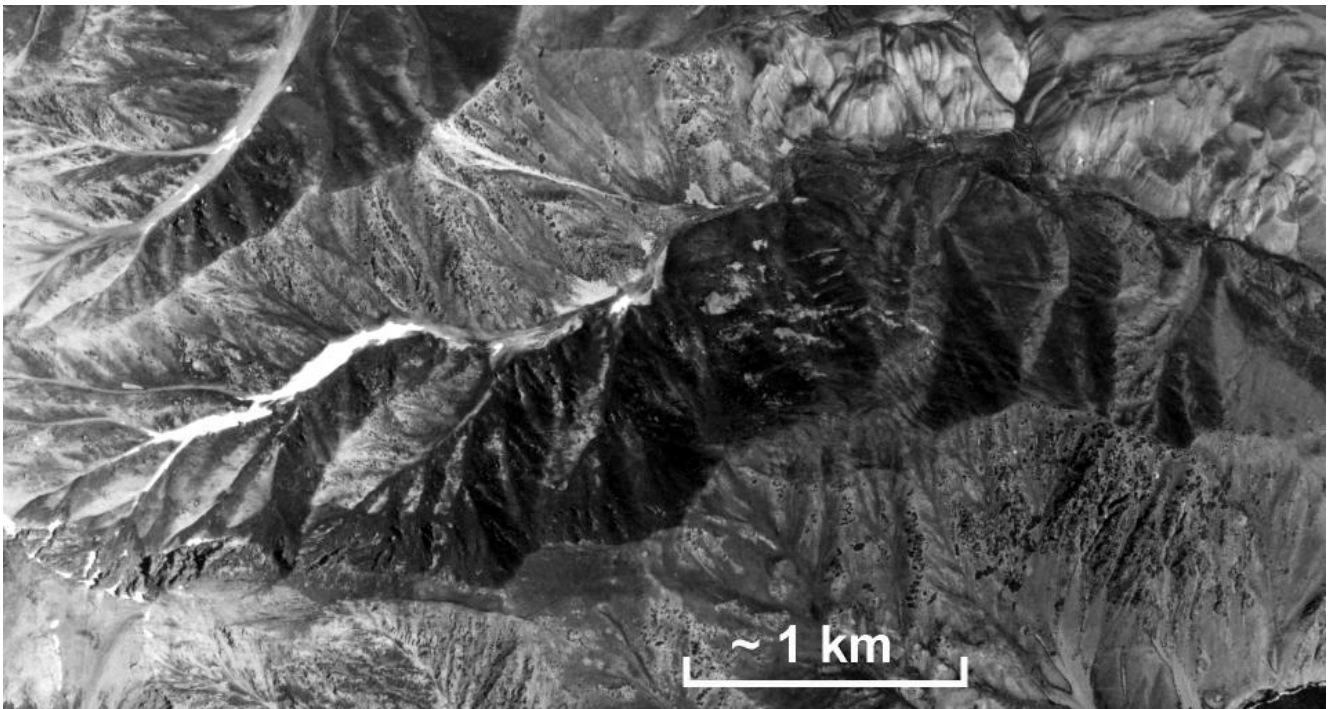


Figure 69. Aerial photograph of the ridge undergoing toppling deformations
Deposits of several minor rockslides can be seen in the gully at the foot of the most affected part of the slope

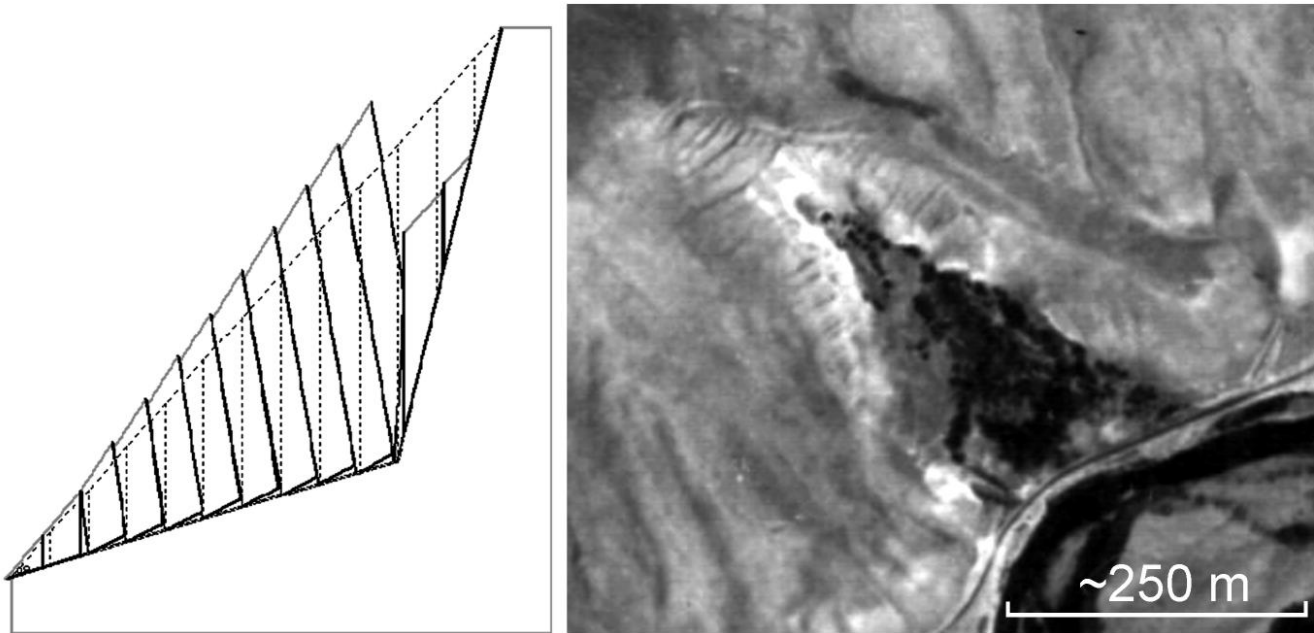


Figure 70. General scheme of toppling and example of such phenomenon that had taken place on the southern slope of Chet-Korumdu Ridge composed of Neogene sediments. Part of the slope affected by toppling had failed in 1992 during the Suusamyр earthquake along with other landslides shown on Figure 19. This image was obtained several years prior to the earthquake

3.7 THE KASHKASU ROCKSLIDE AND THE UPPER TUURAKAING ROCK AVALANCHES

Several rockslides and rock avalanches could be found in the deep valleys that fell into Kokomeren River from the right, downstream from the Kyzyl-Oi depression (Figure 71).

An expressive rockslide 5-10 millions cubic meters in volume collapsed from the ~700 m high steep slope and blocked the Kashkasu River at 41.91° N, 74.17° E (No 10 on Figure 2). This dam still exists while the small dammed lake had been filled by sediments. Now there is a small forested meadow surrounded by cliffs (Figure 72). This rock slope failure formed a compact body, which downstream part is much wider than the upstream one and has distinct convex shape with nearly planar surface and steep frontal slope (Figure 73, Figure 74).

As it can be seen on Figure 73, the sliding surface of this rockslide appeared on the slope much above its foot, so that descending rock mass had to fell onto its bottom nearly at a right angle. It could result into squeezing of the rockslide frontal part by the overtaking material that originally rested at the upper part of the source zone (Figure 75). Just this squeezed debris could form the lower widened part of rockslide dam. This type of rockslide was classified as "spread" [Strom, 1996] or, better, "jumping" rock avalanche. The same mechanism is typical also for the Northern Kara-Kungey rock avalanche that will be described later on.

Besides the surface outflow used by the small stream and marked by dark-green bushes visible on Figure 73, there is a spring marked by white arrow, that release groundwater filtering through the upper narrower part of the dam. No springs are visible on the lower part of the dam.

At least two more rock avalanches can be found in the central part of the adjacent Tuurakaing River basin (Figure 76) at 41.88° N, 72.21° E and 41.89° N, 74.19° E. This small river has an enormous fan composed of huge, roughly rounded granite and gneiss boulders that differs significantly from much smaller fans of other tributaries of the Kokomeren River that have the same-order catchments. Glaciers, that have existed at the upper reaches of this river, never extended towards its mouth, at least in the Holocene, while freshness and expressiveness of the alluvial fan indicates that it was formed rather recently.

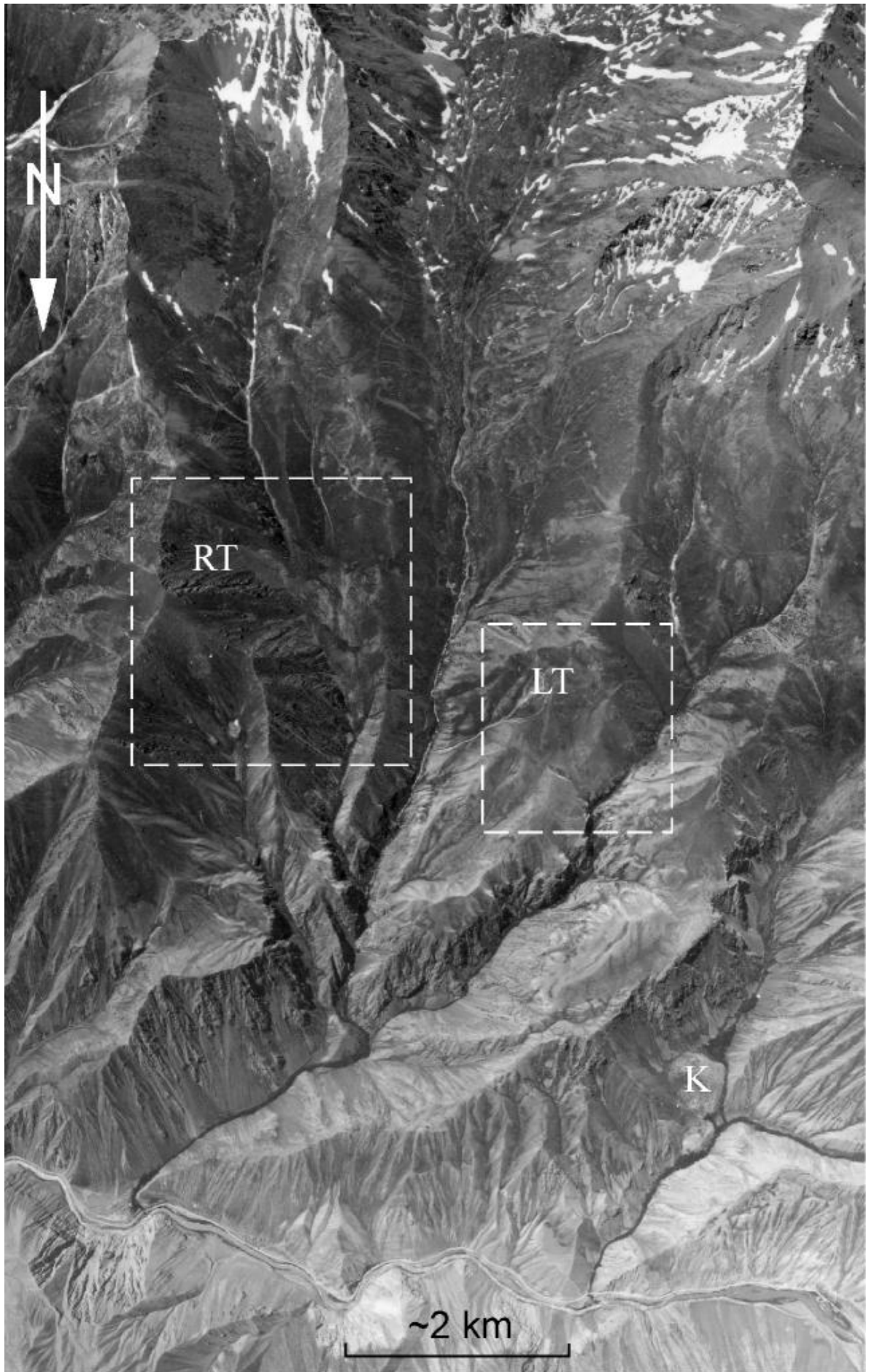


Figure 71. Aerial photograph of the Tuurakaing River basin and of the lower part of the Kashkasu River basin
LT – the Left Tuurakaing rock avalanche; RT – the Right Tuurakaing rock avalanche; K – the Kashkasu rockslide.
Outlined areas are shown on Figure 76



Figure 72. The Kaskasu rockslide dam and a planar surface of the infilled dammed lake



Figure 73. Kaskasu rockslide dam

The planar surface visible in front of the dam is the top of rockslide body lower part (see Figure 74).
White arrow marks springs that filter through the upper part of the dam



Figure 74. Lower widened part of the Kashkasu rockslide dam
Take notice of its convex shape. View from the path that crosses the upper part of the dam (see Figure 73)

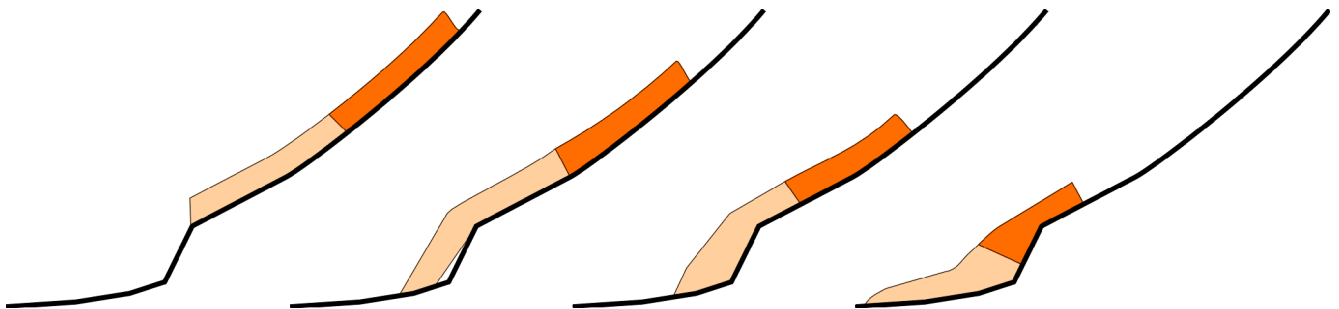


Figure 75. Schematic model of a "Jumping" rock avalanche formation

3.8 THE KOKOMEREN ROCKSLIDE

One of the most interesting features in the entire Kokomeran River basin is the gigantic Kokomeran rockslide 1.0 km³ in volume approximately (Figure 78 – Figure 80). It caved in Pleistocene from the left bank of Kokomeran River at 41.93° N, 74.23° E (No 12 on Figure 2). Tremendous amount of rock debris collapsed onto the wide river terrace about 100 m above the riverbed that had existed at the time of failure (more than 150 m above the present riverbed) (see Figure 79), crossed it and filled the river channel, which is about 50 m above the present-day riverbed.

3.8.1 Rockslide description

Thickness of rockslide deposits resting on this terrace is up to 400 m. River channel that existed at that time had been blocked as well. After this event river had cut the blockage through and incised its channel about 50 m deeper. Locally, it had eroded a new gorge that bypassed the blocked channel (Figure 81). At present the rockslide deposits base can be found on the right bank of Kokomeran River at a level of about 1700-1710 m.a.s.l., while the top of deposits that had filled this concurrent river channel is at ~1900 m.a.s.l. Lacustrine deposits upstream could be found at a level up to 1880-1890

m.a.s.l. Thus, we can expect that blockage's efficient height was at least 200 m (Hartvich, et al. 2008). The main part of the deposits that rest on the left-bank terrace is hardly attainable. However, remnant of its frontal part on the right bank of the Kokomeren River is just above the road at 41.92° N, 74.20° E and its internal structure and grain-size composition could be studied in details.

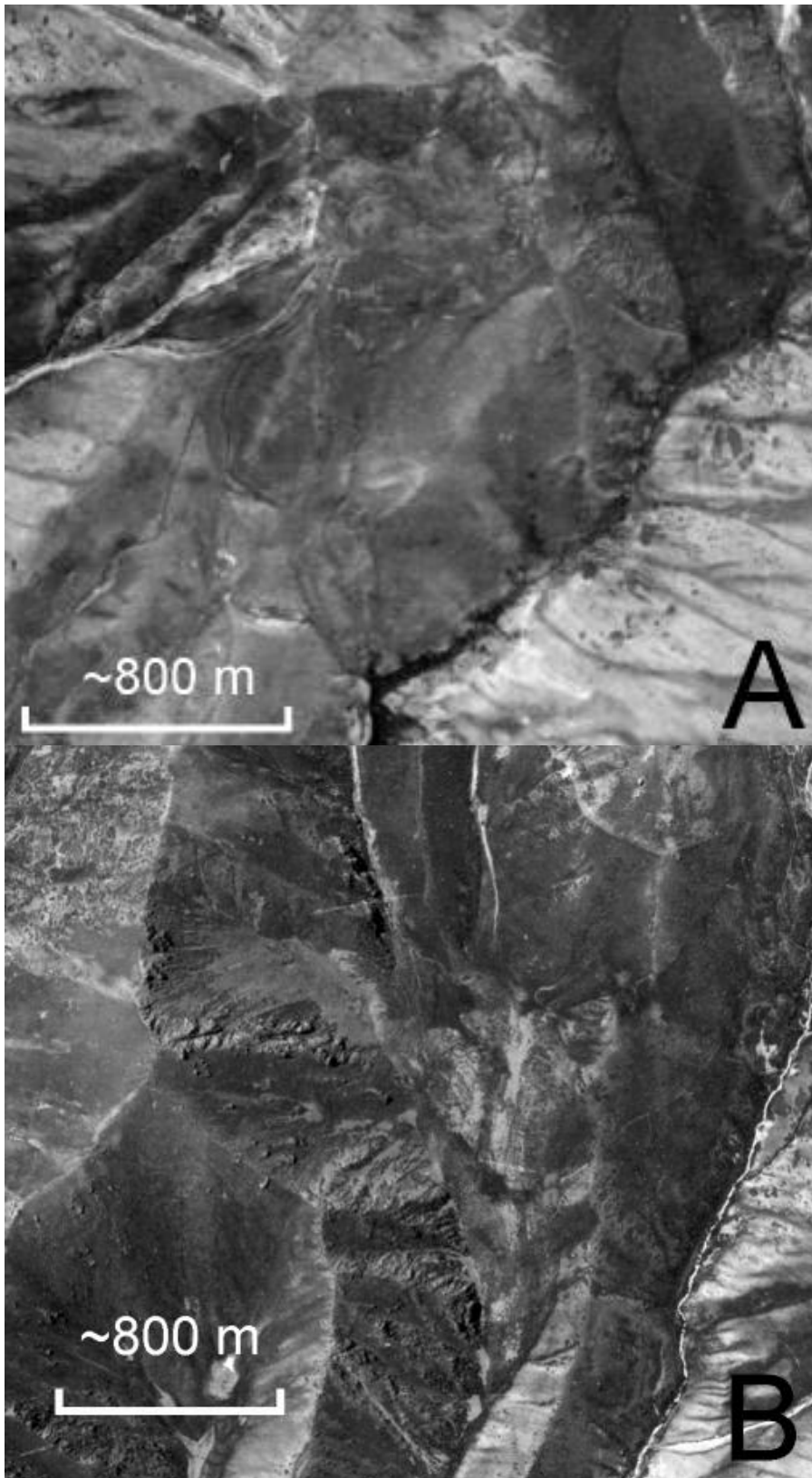


Figure 76. Left (A) and Right (B) Tuurakaing rock avalanche
Zoomed fragments of aerial photographs



Figure 77. Debris flow deposits of the Upper Pleistocene – Holocene (?) age overlying Upper Pleistocene alluvium at the upstream part of the Tuurakaing River fan

1600-m high rockslide scar is composed of alteration of various multicolored types of metasediments and igneous rocks – dark-gray metasediments, reddish granite, alternating red granite and dark-gray sandstone sheets, possibly with some fault zones (Figure 82). Both the lower part of the slope and left bank terrace basement are composed of reddish granite (see Figure 80).

The emplacement mechanism, which model is presented on Figure 83, could be reconstructed due to expressive variability of rock types involved in this rockslides (Figure 84) allowing the comparison of their original and final (after rockslide) position.

Two major zones may be distinguished in the main part of this natural dam (see Figure 84). The upper one about 200-250 m in thickness is composed of blocks and large massifs of fractured reddish granite, overlaid, in its turn, by the gray "layer" of metasediments' blocks and big fragments (Figure 85, upper part). The lower one, up to 150-200 m in thickness, consists of heavily shattered rocks, divided into some "layers" of granite and metasediment fragments (Figure 85, lower part). It is clearly visible that these "layers" are inclined 20 to 30° inside the slope – towards the scar base (Figure 86). Small amount of large angular boulders present in the lower part as well, but anyway, extent of rock crushing here is much higher than in the upper part (Figure 87). The succession of the "layers" corresponds to the bedrock alternation in the slide scar, so that the structure typical of bedrock outcrops (see Figure 82) retains in the rockslide deposits (see Figure 85, Figure 86). It gives evidence that this part of sliding masses, up to 150-200-m thick, moved as a single whole, without mixing and we assume that intensive shattering typical of the lower part of rockslide body took place during the emplacement.

Practically the same succession of the lithologies could be found out in the right-bank frontal part of the rockslide body that filled old river channel (see Figure 81). Its basal unit composed of intensively shattered granite overlays bouldery alluvium (Figure 88). This "former" granite looks like a compact, homogeneous mass, but it crumbles in the water completely. Its separate particles represent angular quartz and feldspar grain fragments usually with conchoidal surface texture. The smallest particles are mainly the quartz scales.

The grain size composition of shattered granite sampled from this unit corresponds to fine sand (!) with specific gravity of 2.67 - 2.68 g/cm³ (Table 1). The method of sample preparation practically has no impact on the grain size composition due to the lack of the clay minerals. The latter indicates that such grain size composition is the result of the mechanical crushing but not of the subsequent

weathering. Being compacted in the laboratory to the relative density 1.90 g/cm³ it has filtration coefficient 0.05 m/day only. Thus, we can say that this material is practically impermeable.

Above this completely shattered granite we can see the succession of crushed granites and metasediments that remain unmixed (Figure 89) though underwent intensive crushing and was displaced for more than 2 km from the source zone.

Table 1. Grain size composition of shattered granite from the basal unit of the Kokomeren blockage right-bank part

spec. gravity	*prep. method	Fractions (mm)											
		1.0-0.5	0.5-0.25	0.25-0.1	0.1-0.05	0.05-0.01	0.01-0.005	0.005-0.002	0.002-0.001	<0.001			
		Content (%)											
Sample 1/91	2.67	A	11.9	27.9	27.6	8.4	17.1	2.7	2.4	0.4	1.6		
		B	6.9	31.6	27.6	10.5	14.1	3.7	0.4	1.6	3.6		
Sample 2/91	2.68	A	6.4	28.7	25.2	11.2	21.8	3.7	–	1.4	1.6		
		B	7.8	24	22.5	15.3	17.1	4.6	1.4	2.5	4.8		

*Methods of sample preparation: A – to specify microaggregation content (shaking in the water); B – to specify grain content of maximum dispergation (boiling in the water with natrium pyrophosphate)

Frontal part of this unit has a direct contact with bouldery alluvial (reworked moraine?) deposits that compose the lower part of the valley slope. Crushed debris immediately near this contact is intensively cemented (Figure 90) and is composed, locally, of meter-size mixture of crashed granite and metasediments with distinct boundaries between these lithologies (Figure 91). We assume that this part of rockslide debris originated from the apical zone of granite intrusion where small granite veins had intruded the host massive.

Typical crushed material of the granite-metasediments alteration can be seen on Figure 92. Results of grain-size analysis of material sampled from these outcrops are presented in Table 2.

Table 2. Grain size composition of crushed granite and metasediments' alteration of the Kokomeren blockage right-bank part

	Fractions (mm)														
	>80.0	80.0-40.0	40.0-20.0	20.0-10.0	10.0-5.0	5.0-2.0	2.0-1.0	1.0-0.5	0.5-0.25	0.25-0.1	0.1-0.05	0.05-0.01	0.01-0.005	0.005-0.002	<0,002
	Content (%)														
Sample 1/2005	1.8	1.1	3.35	5.9	14.35	19.6	17.0	5.5	13.2	8.3	3.55	4.1	0.8	0.3	1.2
Sample 2/2005	2.9	8.0	12.4	14.3	15.0	16.7	12.2	1.1	4.35	2.7	2.0	3.7	1.75	1.3	1.6

Sample 1/2005 – 44.7 kg of crushed granite; Sample 2/2005 – 42.7 kg of crushed metasediments; spec. gravity = 2.66 g/cm³

These samples' analysis was performed in three steps – field sieving and extraction of <5-mm fraction; dry sieving and extraction of <1-mm fraction and further laboratory sieving with washing and areometric analysis. Table 2 presents combined results of these three stages.

This material forms large part of the right-bank rockslide deposits (Figure 93). Inclination of separate "layers" within the lower part of the right-bank body increases up to 30 - 40° (see cross-sections on Figure 84. It is overlaid by "layers" composed of much coarser angular boulders with very small, if any, amount of fines. Similar to the comminuted debris these units do not feature any mixing – just above the comminuted material there are granite angular boulders (Figure 94), overlaid, in turn, by layers of metasediments, which extent of comminution strongly depends on the lithology. Anyhow, they are generally much coarser than those from the lower part of the body.



Figure 78. Aerial photograph of the Kokomeren rockslide



Figure 79. Dissected body of the Kokomeren rockslide
View from the Tuurakaing fan. 1 – granite basement; 2 – river terrace alluvium; 3 – rockslide deposits



Figure 80. The Kokomeren rockslide overview
 Arrow in the right lower corner marks active fault that will be described later and shown in detail on Figure 98

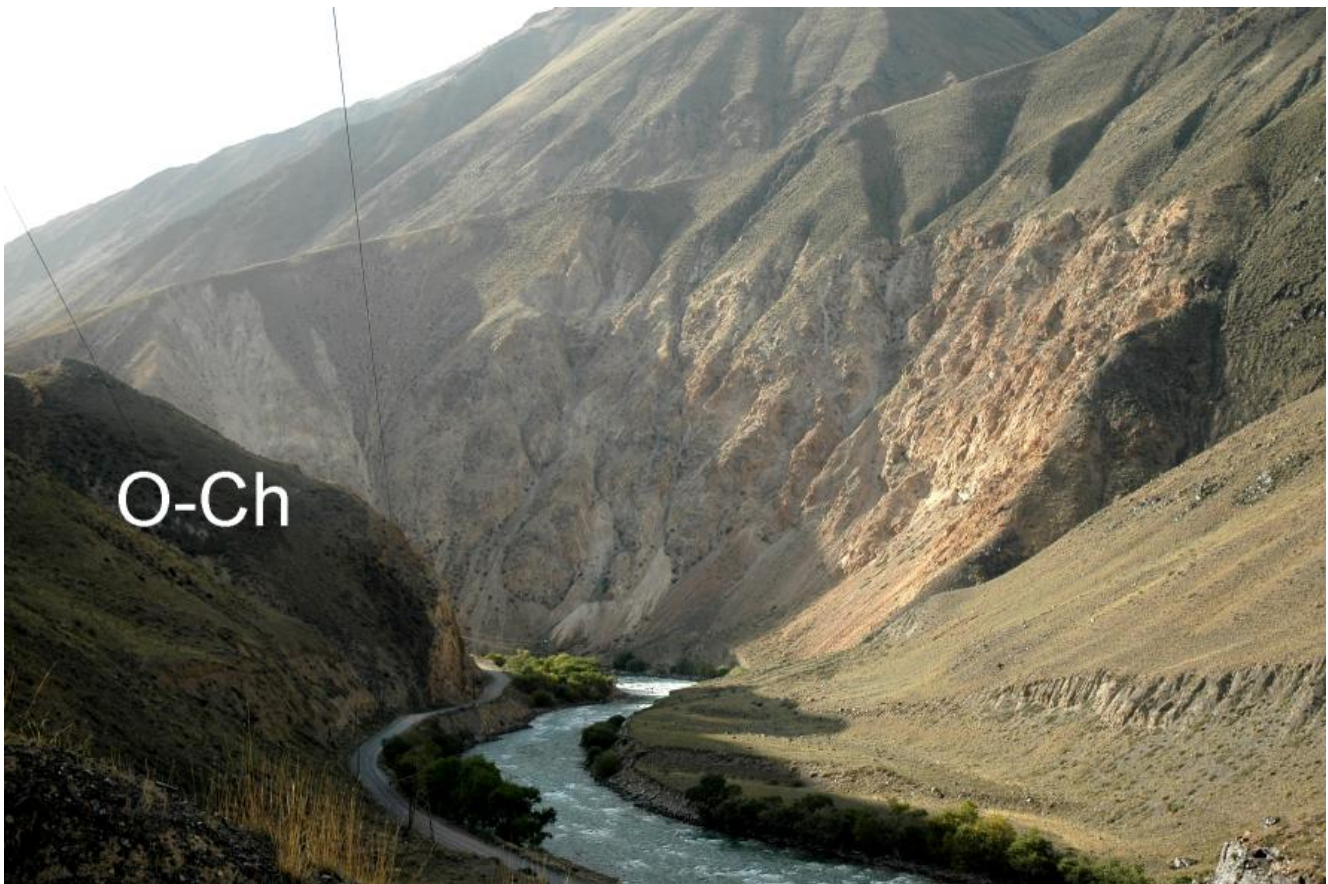


Figure 81. New gorge of the Kokomeren River that had been eroded after the blockage
 O-Ch – old river channel filled by frontal part of the rockslide body

The boundary between the blocky and shattered zones is abrupt, without any transitional zone that may be interpreted as the evidence of sharp change of deformational conditions in the superficial and internal parts of the moving rockslide.



Figure 82. Alternating bedrock succession in the Kokomeren rockslide source zone
White arrows mark eastern boundary of the rockslide scar

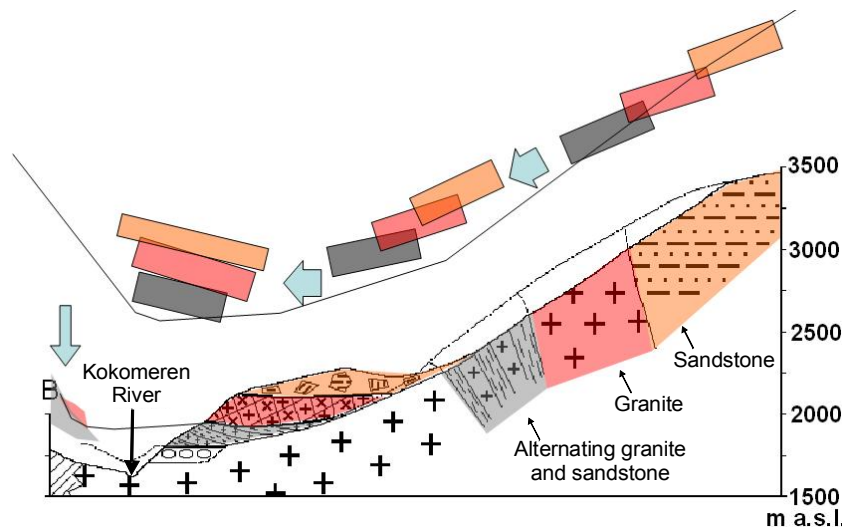


Figure 83. Reconstruction of the Kokomeren rockslide emplacement mechanism
(after Hartvich, et. al. 2008)

3.8.2 The Kokomeren rockslide 'satellites'

Gigantic bedrock slope failure that formed the Kokomeren rockslide was accompanied by much smaller rockslide about 2 km upstream (41.92° N, 74.19° E) (No 11 on Figure 2) that descended from the left bank of Kokomeren River valley just opposite the Kashkasu River mouth (Figure 95). Remnants of its deposits can be found on the Rivers' right bank where large amount of angular boulders of the same material that forms upper part of the scar area rests on the terrace-like surface several dozens meters above the riverbed. We named this feature the Kashkasu-mouth rockslide.

The geomorphic position of this rockslide deposits on the slope of the Kokomeren River valley is very similar to the position of the right-bank part of the Kokomeren rockslide body, thus, it is likely that both failures had occurred simultaneously.

One more rockslide (No 13 on Figure 2, Figure 96) had blocked the small gully east from the Kokomeren rockslide at 41.92° N, 74.25° E (see also Figure 80). Since it forms rather well-preserved dam it can be assumed that this slope failure is much younger than the main gigantic slope failure. It can be hypothesized that this rockslide was caused by strong earthquake associated with surface faulting subsequent to that one, which caused the giant Kokomeren rockslide failure. Evidences of such recurrent faulting were described in section 2.2 and will be described hereafter.

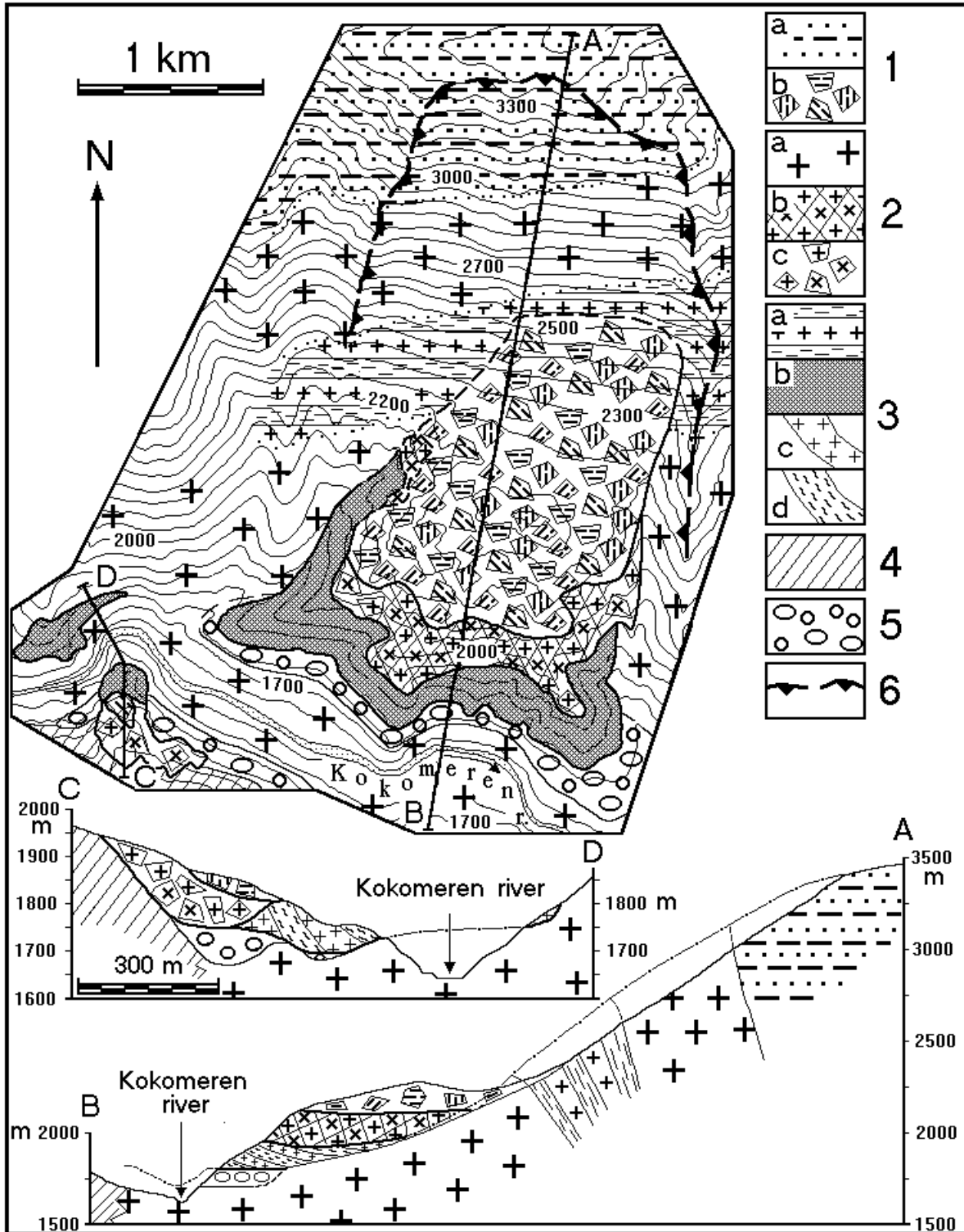


Figure 84. The schematic map and cross-sections of the Kokomeren rockslide blockage

Legend: 1a - Sandstone, 1b - Sandstone fragments in rockslide deposits; 2a - Granite, 2b, c - Granite in rockslide deposits, forming a huge massif (b) and crushed into blocks (c); 3a - Alternating granite and sandstone, 3b-d - Shattered granite and sandstone in rockslide deposits (b - on the map, c,d - on the cross-sections, where c - shattered granite, d - Shattered sandstone); 4 - Limestone, schist and diabase alternation; 5 - Alluvium; 6 - Rockslide scar



Figure 85. Vertical cross-section of the left-bank part of the Kokomeren rockslide body
Its characteristic features are preservation of the unmixed lithological units and presence of coarse debris in the upper part of the cross-section and of the intensively comminuted material in its lower part



Figure 86. Lower part of the Kokomeren rockslide body resting on the high left-bank terrace
Notice the inside-slope inclination of multicolored debris units



Figure 87. Shattered granite debris at the lower part of the Kokomeren rockslide body
Notice the succession of finer and coarser units



Figure 88. Pleistocene channel alluvium of the Kokomeren River overlaid by shattered granite of the Kokomeren rockslide right-bank part basal unit



Figure 89. Alternating "layers" of crushed rockslide debris on the right bank of the Kokomeren River
Crushed metasediments (gray) and granites (pink) that form unmixed units being displaced more than 2 kilometers from the source zone



Figure 90. Contact of the cemented rockslide breccia and bouldery alluvium of the Kokomeren River valley right bank



Figure 91. Meter-size succession of crushed but unmixed granites and metasediments that forms the cemented breccia at the frontal edge of the right-bank part of the Kokomeren rockslide



Figure 92. Typical grain-size composition of crushed granite (above) and metasediments (below) of the Kokomeren rockslide right-bank body lower part

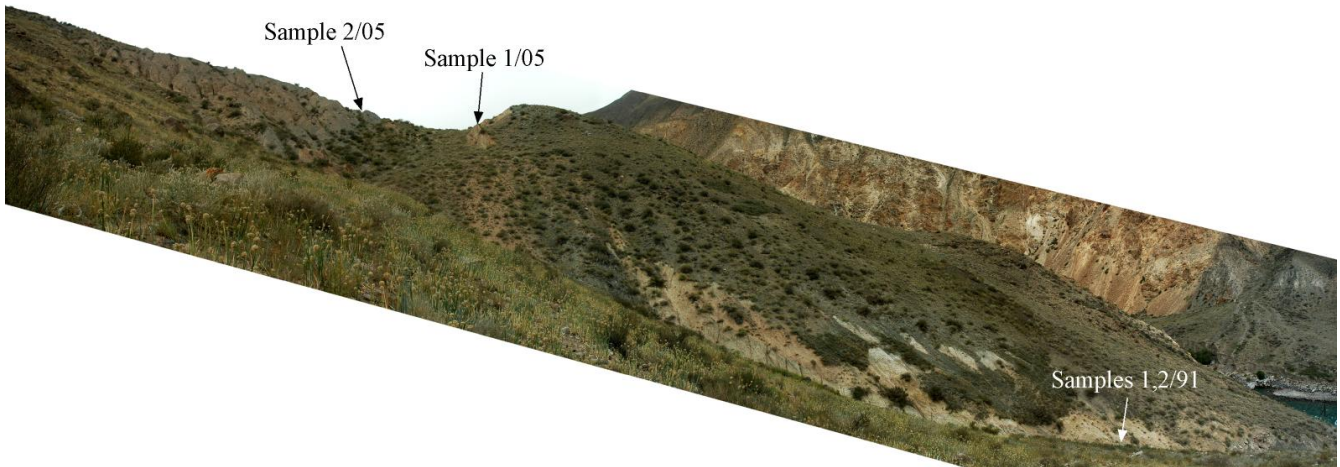


Figure 93. Overview of the shattered zone of the Kokomerren rockslide right-bank part
Arrows show where samples for grain-size composition were taken in 1991 (Table 1) and 2005 (Table 2)



Figure 94. Angular granite boulders on the top of the Kokomerren rockslide right-bank part

3.8.3 Active fault at the Kokomerren rockslide site

About 1.5 km downstream from the eastern end of the Kokomerren rockslide (41.91° N, 74.25° E) an expressive recent fault can be seen at the left bank of the Kokomerren River (Figure 97 - Figure 99). It is a north-north-west trending reverse fault with western side up that displace the Holocene terrace (see Figure 99) and overlying bedded silt sediments most likely of lacustrine origin.

As far as thickness of bouldery alluvium in the hanging wall is about $\frac{2}{3}$ of that in the footwall, while lacustrine silt thickness is constant within the entire outcrop it can be concluded that offsets had occurred at least twice – during alluvium accumulation and after silt caprock deposition. Piece of bedrock among boulders in the lower part of alluvium in the footwall (outlined on Figure 99) could fell from the tip of the uplifted block during first event. Though it was difficult to measure offsets precisely across the Kokomerren River, it is obvious that cumulative vertical separation is about 5-6 m and second event displaced caprock for about 2 m.



Figure 95. Strongly eroded rockslide scar opposite the Kashkasu River mouth



Figure 96. Partially eroded rockslide dam in the creek east from the Kokomeren rockslide
Collapsed slope is composed of Paleozoic granites. Part of the Kokomeren rockslide body can be seen at the upper left corner of the image

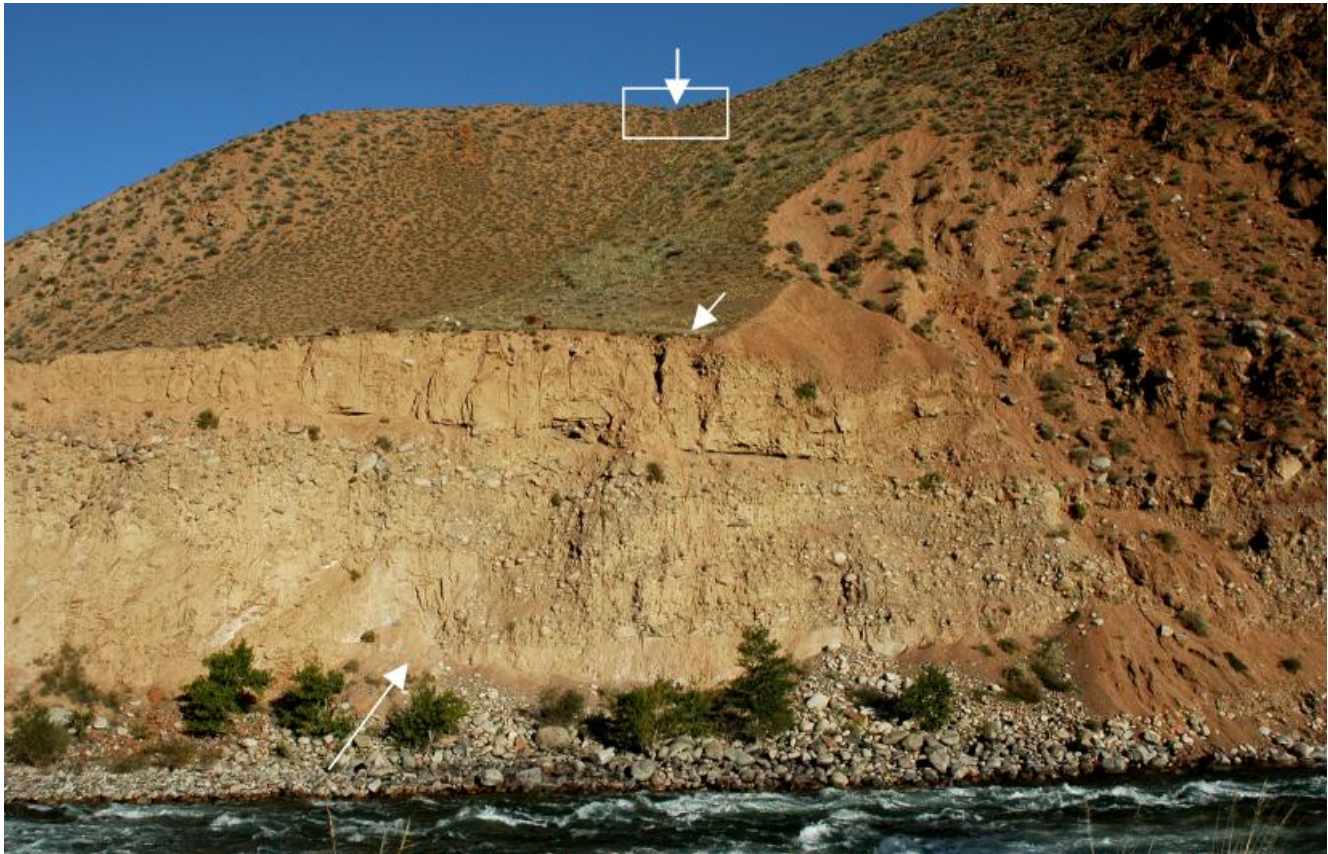


Figure 97. Recent fault rupturing left bank river terraces downstream from the Kokomeren rockslide
 Inclined arrows mark rupture surface at the low terrace; vertical arrow shows the position of this fault where it crosses remnant of high terrace (see zoomed outlined area on Figure 98)

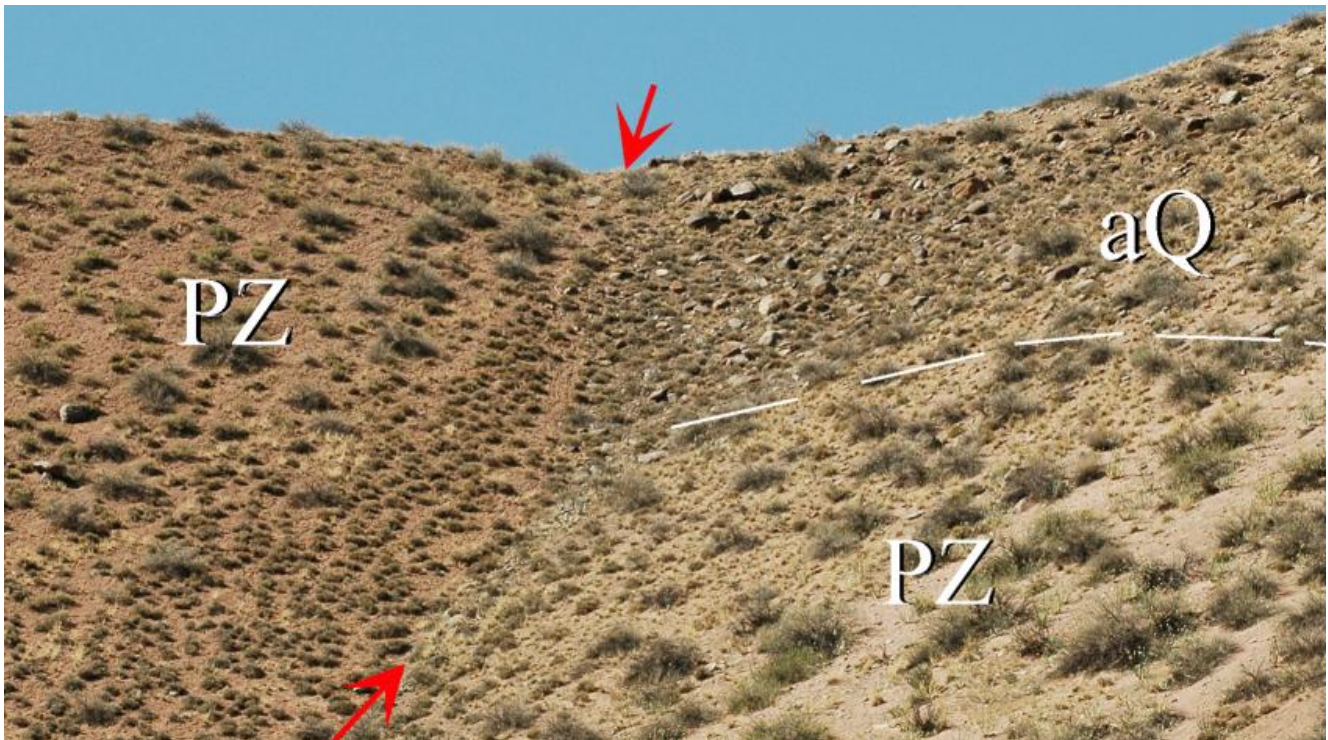


Figure 98. Displaced alluvium of high (Pleistocene) river terrace
 Alluvium base at the footwall is marked by dashed line. Red arrows mark active fault



Figure 99. Detail of recent reverse fault shown on Figure 97
Piece of bedrock among the alluvium is marked out

Both events should be younger than failure of the Kokomerren rockslide, since at that time Kokomerren riverbed was much higher than the displaced 12-15 m high terrace, which did not exist at

that time. However, displaced alluvium of high river terrace (approximately the same that underlay left-bank part of the Kokomeren rockslide) indicates earlier offsets. Amount of its separation (see Figure 98) is much bigger than that of the low terrace.

North-western continuation of this fault stretches directly towards the foot of the Kokomeren rockslide scar and we assume that one of rupturing episodes on this fault, most likely associated with strong earthquake, could trigger or even cause this gigantic slope failure [Strom, Stepanchikova, 2008].

In the opposite direction, at the right bank of the Kokomeren River, this recent fault can be observed at an eroded smooth slope just above the road (Figure 100). Unfortunately, it is the only one outcrop on the right bank of the valley where it could be found out up to now. The remaining part of the slope composed of the heavily weathered granite is covered by the matted outwash.

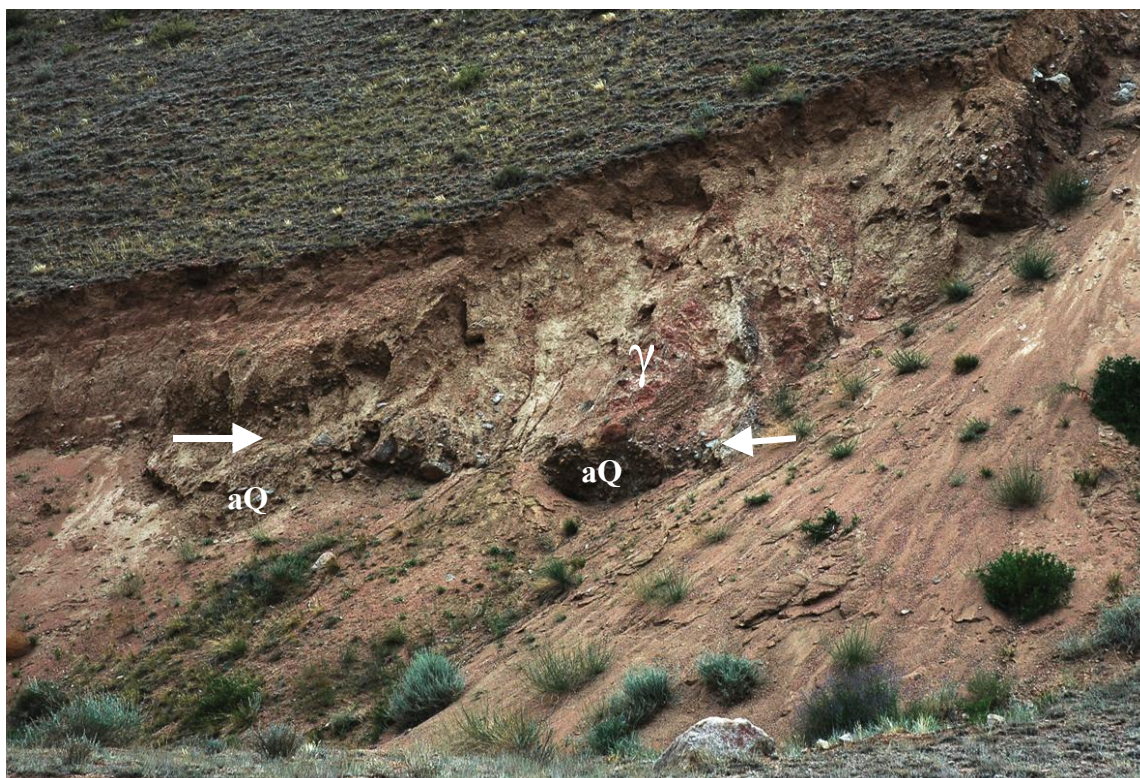


Figure 100. Crushed granite (γ) overthrusting the alluvium (**aQ**) at a right bank of the Kokomeren River. Assumed fault plain is marked by white arrows

3.8.4 Evidence of inundation and subsequent breach

At least 200-m high Kokomeren rockslide dam caused inundation of large part of the Kokomeren River valley and formed a lake that had stretched for more than 15 km upstream. Its volume can be roughly estimated as 10^9 m³. Powerful Kokomeren, which present-day mean annual discharge is $2,5 \times 10^9$ m³/year [State Water Inventory 1987] should infill it less than in one year. However, even being overtopped, the rockslide dam had existed for a rather long time. Due to combination of geological and geomorphic features at the blockage site the new gorge was cut through the bedrock (see Figure 81) that should slow down the process of dams breach significantly [Hartvich, et al. 2008]. It resulted in accumulation of large quantity of lacustrine sediments, represented mainly as thin-bedded silt sediments that can be observed in the numerous outcrops upstream (Figure 101 – Figure 105).

Practically all of them are not higher than 100 m above the present-day riverbed level. This indicate that the dammed lake was not filled by sediments completely, unlike, for example, the lake in

the middle part of the Naryn River basin dammed by the gigantic ($\sim 10 \text{ km}^3$) Beshkiol landslide [Korup, et al. 2006].

Total amount of lacustrine sediments accumulated in the dammed Kokomeren River valley can be roughly estimated as 10^8 m^3 ($\sim 1/10$ of the lake volume). It allows accessing the longevity of river damming [Korup, et. al., 2006]. According to the State Water Inventory [1987], present-day mean sediment yield of the Kokomeren is 140,000 tons/year that roughly corresponds to $7 \times 10^4 \text{ m}^3/\text{year}$. Assuming same rate of sedimentation at the end of Pleistocene when river damming took place we obtain time necessary to accumulate above-mentioned amount of sediments, which is about 1500 years. Palinological analysis of two samples collected from sandy and clayey layers at the outcrop shown on Figure 11 indicate that dam formation took place most likely in Late Pleistocene, during warm and rather wet epoch. This, in turn, allows assumption that both river discharge and sedimentary yield at the period of river damming was bigger than at present and, thus, the longevity of the Kokomeren Lake should be shorter, likely not more than few centuries.

Assuming that thin grading of lacustrine sediments (see Figure 10, Figure 102, inset in Figure 105) corresponds to the seasonal variations of washout, thus allowing to count years when these strata had accumulated, this estimate seems to be reasonable.



Figure 101. Lacustrine sediments overly bouldery alluvial deposits
Deposition of thick unit of fines at such a deep and narrow valley is possible in the lake conditions only

It allows estimating the incision rate of the stream that had eroded the ~100 m deep bypass gorge through the left-bank bedrock (see Figure 81).

The first outcrop of lake sediments (moving upstream from the dam) can be seen on the left bank of the valley just upstream from the Kashkasu River mouth (41.929° N, 74.18° E) where thin-bedded silt overly thin bouldery alluvium representing stream facies (see Figure 101). It is obviously that such a thick stratum of fines could not accumulate in the deep narrow gorge with rapids. Abrupt change of the lithology (silt overlaying large boulders) also indicate sharp change of sedimentation conditions. However, this outcrop located close to the dam, likely, represents the final stage of lake infilling, since initial sedimentation occurred at the upstream part of the natural reservoir as it take place in the Toktogul Reservoir, for example (Figure 106).

The widest development of lacustrine sediments can be observed in the Kyzyl-Oi depression, on the right bank of the Kokomerren between the Chongsu and Kobiuksu River mouths (see Figure 10, Figure 11) and on its left bank opposite the Kyzyl-Oi village (41.96° N, 74.17° E) (see Figure 103) where almost one half of the 100-m high terrace-like surface is composed of bedded silt mixed with talus that had been brought from the adjacent slope (see Figure 102).



Figure 102. Fine bedded lacustrine sediments overlying alluvium
Detail of the outcrop shown on Figure 103



Figure 103. Overview of the left bank of Kokomerren River opposite the Kyzyl-Oi village
Outcrop is composed of lacustrine silt resting over the "normal" alluvial sediments

Lithology of the basal units of lacustrine sediments visible at the outcrops along the road cut south from the Kyzyl-Oi village allows reconstruction of the Kikomerren Lake early history. Typical alluvium (pebbles with sandy fill) is overlaid by ~1.5 m thick unit composed of angular macadam-size debris of metasediments that could be brought here from the left bank of the Kokomerren River only, with red silty matrix that originated from the Neogene red beds of the Kyzyl-Oi depression. This unit, in turn, is overlaid by 'classical' lake sediments – well-bedded silt layers with sandy interbeds and rare pebbles (see Figure 104). Boundaries between these units are sharp indicating abrupt changes in the sedimentation conditions. It can be assumed, that black debris with silty matrix with relatively thick and alternating layers was accumulated when rising water disturbed talus of the right bank and silt of the left bank, which mixed being deposited over the floodplain (?) alluvium. It is possible that large amount of debris could collapse from adjacent slopes due to strong seismic shaking [Strom, Stepanchikova, 2008]. If so, this unit corresponds to the unit 2 shown on Figure 10. Later on, when water level rose rapidly, sedimentation conditions changed and lacustrine thin-bedded silt started accumulating.



Figure 104. Basal units of the lacustrine succession on the right bank of the Kokomeren River south from the Kyzyl-Oi village

Near the outcrop shown on Figure 10 one can see inclusions of coarse bouldery material in the lower part of lacustrine deposits. We interpret them as deposits of debris flows that entered the dammed lake, likely due to the breach of temporary blockages that could be caused by local slope failures in the western part of the Kyzyl-Oi depression.

The outermost site where fine lacustrine sediments can be observed is in the road cut opposite the Burundu River Mouth about 13 km far from the Kokomeren blockage (see Figure 105). Here, at 42° N, 74.16° E, thin-bedded silt is overlaid by slope scree. Further upstream, in the narrow gorge with slopes completely covered by talus, no similar sediments have been found.



Figure 105. Lacustrine deposits with bouldery inclusions opposite the Burundu River mouth, overlain by alluvium and talus



Figure 106. Lake-head deltas of rivers flowing into the Toktogul reservoir

Unlike expressive evidences of upstream inundation caused by Kokomeren rockslide, data on the mechanism and rate of this dam breach are limited. Presence of coarse bouldery sediments all over the river valley complicates outburst flood deposits identification. It can be hypothesized, nevertheless, that huge bouldery deposits that are widely developed at western termination of the Djumgal depression, where Kokomeren River enters it, could be deposited by powerful outburst flood.

However, presence of younger blockages in the gorge downstream from the Kokomeren Dam site does not allow concluding with confidence, which dam breach could be responsible for their deposition.

3.9 THE DISPLACED PENEPLAIN ROCKSLIDE

The Kokomeren rockslide is not the only one large-scale Pleistocene rock slope failure in the upper part of the Kokomeren River basin. One more Pre-Holocene event had occurred at its right bank at 41.90° N, 74.25° E (No 15 on Figure 2). This rockslide had been significantly reworked by subsequent erosion (Figure 107), so that it could be hardly identified on space and aerial images (DP on Figure 108) and DEMs. Nevertheless, geomorphic and structural analyses indicate that huge mass of gneiss had descended from the right slope of the valley and had blocked the Kokomeren River valley completely.

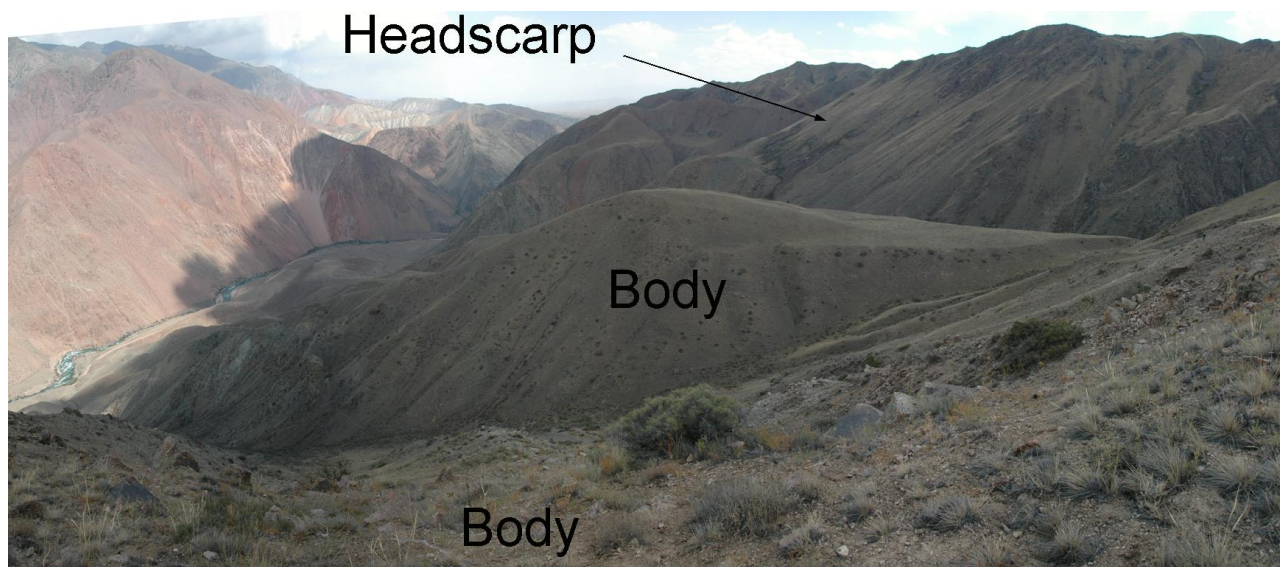


Figure 107. Deeply eroded body of the Displaced Peneplain rockslide
View from the uppermost part of the deposits (*brandung?*)

Remnants of its proximal part marked by fragments of the displaced Pre-Neogen planation surface still remain on the right bank of the unnamed gully (Figure 109). The 300-m high slope covered by scree further upstream represents its sliding surface. That is why we called this feature the "Displaced Peneplain" rockslide.

The "Displaced Peneplain" rockslide formed the body about 2 km² in plan view and up to 300 m thick. Its volume could be roughly estimated as 400-500×10⁶ m³. Its distal part rests on the slope of the right bank of the Kokomeren River valley much above the proximal one forming something like a *brandung* (Figure 110).

Unlike the above-mentioned Kokomeren rockslide, which internal structure could be studied and reconstructed in details, the "Displaced Peneplain" rockslide body, though being strongly reworked by erosion, has not so many good outcrops where one could observe its composition. Locally there are evidence of angular gneiss boulders on top of the body (see Figure 110, Figure 111). Some outcrops at the north-eastern part of the body are composed of heavily shattered "stratified" debris (Figure 112). However, since rockslide source zone is composed of more or less uniform lithology – mainly gneiss, and is masked by scree at a high extent, we could not reconstruct the original position of units that can be identified within the rockslide body.

As noted above the "Displaced Peneplain" rockslide had blocked the Kokomeren River valley. The newly formed gorge bypassed the blockage at its distal boundary through the bedrock of the River's left bank. The smooth hill composed of red heavily weathered granite that stretches along the right bank of the present-day Kokomeren River (Figure 113) represents the remnant of the original left bank of the valley. The river had cut a new channel, while the abandoned river channel can be seen aside the road 10-15 m above the present-day water edge (Figure 114). Large boulders resting just

above the road represent the stream facies of the alluvium that had been buried by much finer material, likely washed out from the adjacent slopes and distal part of the rockslide body.

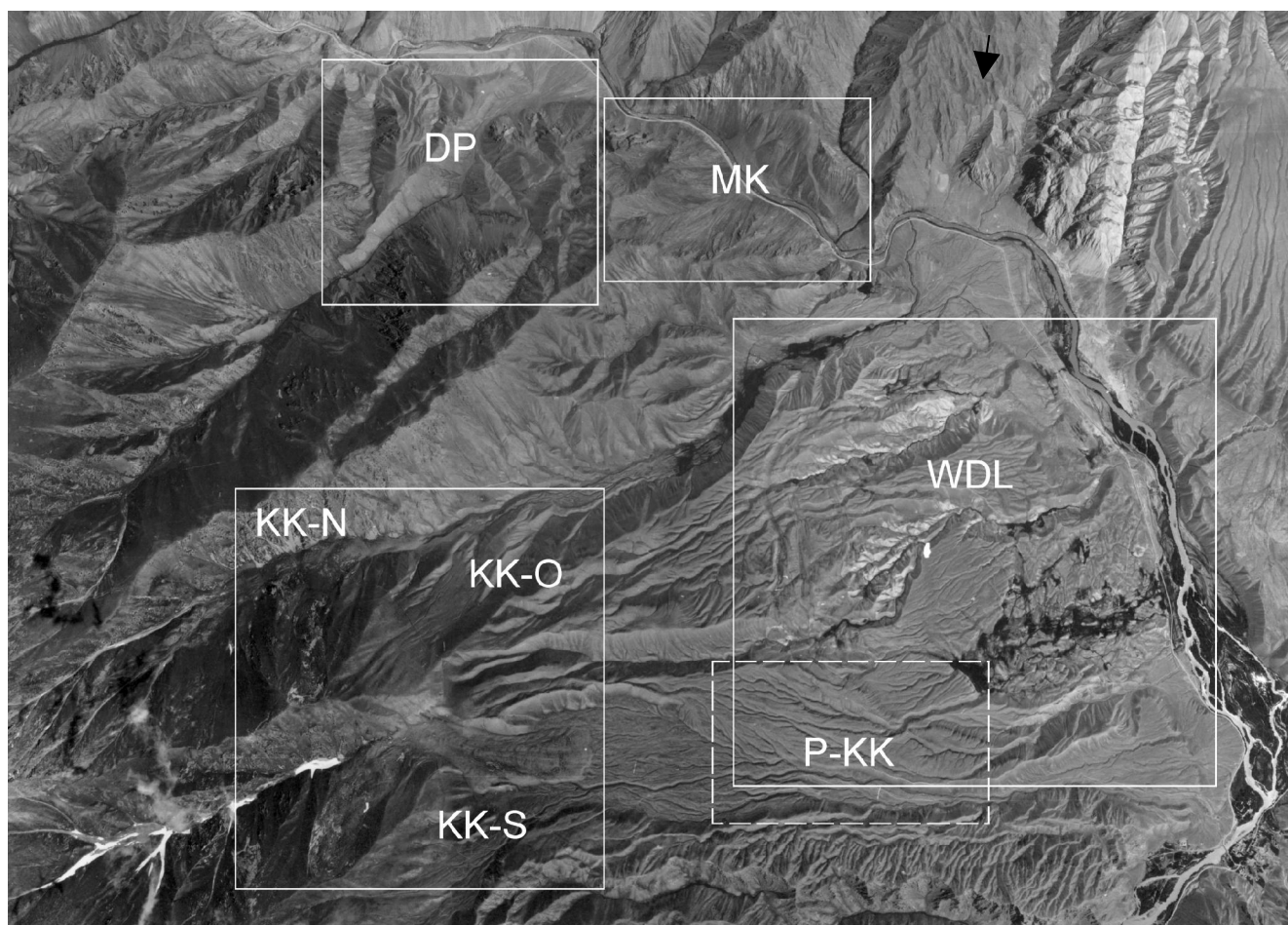


Figure 108. Landslides, rockslides and rock avalanches at the western termination of the Djungal intermountain depression and the surrounding ranges

DP – Displaced Peneplain RS, MK – Mini-Köfels RS, KK-N – Northern Karakungey RA, KK-S – Southern Karakungey RA, KK-O – Old Karakungey RA, P-KK – area where deposits of the assumed Pleistocene Pre-Karakungey RA has been found, WDL – Western Djungal landslide about 10 km² in Neogene and Quaternary deposits



Figure 109. Headscarp of the Displaced Peneplain rockslide
Remnants of displaced Pre-Neogen peneplain are marked by arrows



Figure 110. The Displaced Peneplain rockslide body.
Gully that dissects it had been eroded after rockslide emplacement.
Black arrow marks the uppermost part of the rockslide deposits (*Brandung?*)



Figure 111. Crushed gneiss of the Displaced Peneplain rockslide body upper part resting over red granite (lower right corner of the photograph)

As compared with the Kokomeren rockslide, which frontal part had filled the stream that was about 40 m above the present level (see Figure 81 and Figure 88), this channel should be much younger and, thus, the "Displaced Peneplain" rockslide must be younger than the Kokomeren one. Since both of them had occurred quite close to an active faults described in section 3.8.3, it could be proposed that both failures were triggered by the recurrent movements along this fault and, thus, the "Displaced Peneplain" rockslide must be considered as seismically triggered phenomenon, similar to the Kokomeren rockslide [Strom, Stepanchikova, 2008].

It can be confirmed by the evidence of the river damming that occurred after the Kokomeren Rockslide dam breach. At least two river damming episodes could be identified at the part of the Kokomeren River valley that had had been eroded through the Kokomeren dam. The older one corresponds to lacustrine silt layer overlaid by stream alluvium that outcrops in the road cut at 41.918° N, 74.216° E (Figure 115). The younger episode led to formation of the second silt-rich succession that overly the above mentioned stream alluvium. It can be seen on the same bank about 50 m higher at 41.921° N, 74.211° E (Figure 116). Lacustrine sediments are divided by typical mountain river alluvium corresponding to the period of unconfined stream evolution.



Figure 112. Outcrop where the "stratified" internal structure of the rockslide body is visible



Figure 113. Fragment of the left bank of the abandoned stream of the Kokomeren River

Arrow marks the outcrop shown on Figure 114



Figure 114. The upstream part of the abandoned pre-Kokomeren valley filled by alluvium



Figure 115. Lacustrine silt sediments overlaid by stream alluvium
Road cut at the Kokomeren River right bank at 41.918 N, 74.216 E

It is evident that accumulation of thick stratum of fine well-bedded sediments in the narrow gorge without well-developed floodplain is not possible in the "normal" stream conditions. Thus they are good indications of lacustrine conditions, which are possible due to river damming only. Besides

the "Displaced Peneplain" event, which, likely, caused the formation of a lacustrine unit, river damming could be associated either with the Mini-Kölfels rockslide described in the next section of the Guidebook or by catastrophic debris flows that formed a huge fan at the Tuurakaing Creek mouth (see Figure 77).

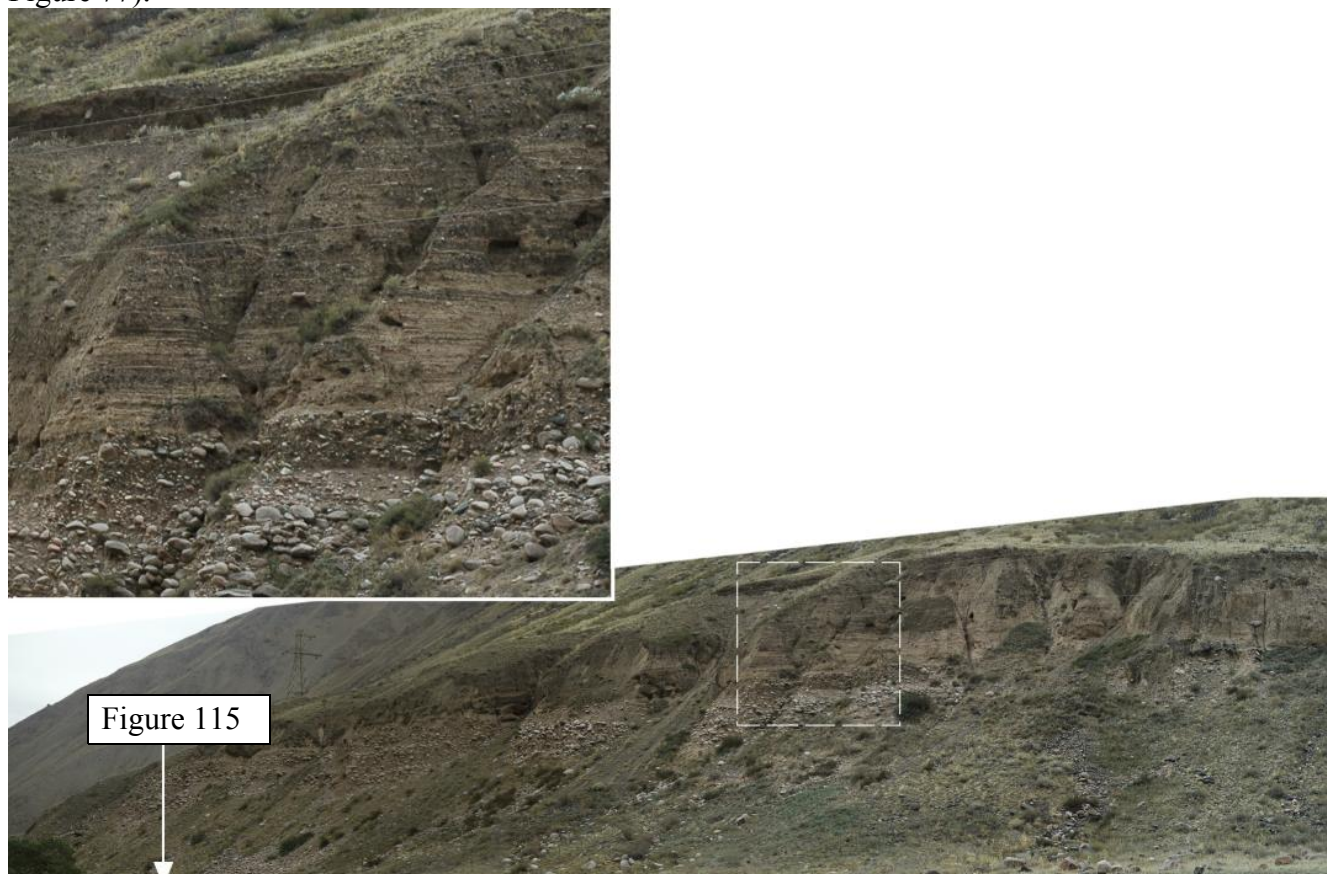


Figure 116. Fine thin-layered sediments overlying stream alluvium at 41.921 N, 74.211 E

3.10 THE MINI-KÖFELS ROCKSLIDE

About 1 km upstream from the point where the Kokomeren River enters the Djungal intermontane depression at 41.906 N, 74.28° E one can see a rockslide (No 17 on Figure 2) representing a minor model of the famous 1.5-2 km³ Köfels rockslide [Erismann 1979]. Heap of the reddish-coloured granite and gray-brownish gneiss debris that descended from the right slope of the valley rests on the left bank of the Kokomeren River composed of gray Palaeozoic terrigenous deposits (Figure 117).

As in the Köfels' case, frontal part of this "Mini-Kölfels" rockslide filled the prominent lowering at the opposite bank of the valley (Figure 118). It is a typical "primary" rock avalanche which distal part raised much above its proximal part, where the dam had been cut through later on. However, unlike the Seit rock avalanche, which is also classified as the "primary" type, the "Mini-Kölfels" event had occurred in confined conditions – in the rather narrow deep valley. Nevertheless, lengthwise debris distribution is the same – most of the collapsed material moved ahead without any prominent accumulation at its proximal part.

On the right bank of the river, immediately above the motorway, one can see intensively crushed rockslide debris overlaying alluvium of the low terrace (Figure 119).

Rockslide had formed a dam about several dozens meters high, which height can be reconstructed from the elevation of the bench on the left bank of the river (see Figure 117). However, it had been overtopped shortly after the event, since the lake had been formed in the narrow gorge, and breached soon at its proximal part by the powerful Kokomeren River.

Though no lacustrine sediments have been found close to the dam, it was hypothesized (see above) that lacustrine sediments about 4.5 km upstream could be accumulated in the temporary lake dammed by the Mini-Kölfels rockslide. It is known that reservoirs' infilling starts from its upstream part where streams' velocity sharply decreases (see Figure 106). Thus, even in short-living temporary lakes lacustrine sediments would accumulate far from the dam, rather than just near it where the lake was much deeper.



Figure 117. Upstream view of the Mini-Kölfels rockslide deposits resting on the Kokomeren River valley left bank. Dashed white line show possible dam crest level



Figure 118. Central and downstream parts of the Mini-Kölfels rockslide body. Smooth hill left from the bedrock summit is the distal part of rockslide that filled the abandoned valley



Figure 119. Comminuted rockslide debris (crushed granite) overlying alluvium of the Kokomeren River right bank terrace about 5 m high

3.11 THE KARAKUNGEY ROCK AVALANCHES

Western termination of the Djungal intermontane depression had been the scene of numerous landslides and rock avalanches that took place repeatedly in Late Pleistocene and Holocene. Two gullies (Northern and Southern Karakungey) dissect the range that rises above the Djungal depression termination, and both of them are dammed by rockslides. Slope failures had occurred on the slopes of similar height (~500 m) and steepness, both composed of the granite and facing north and north-east (see Figure 108, Figure 120).

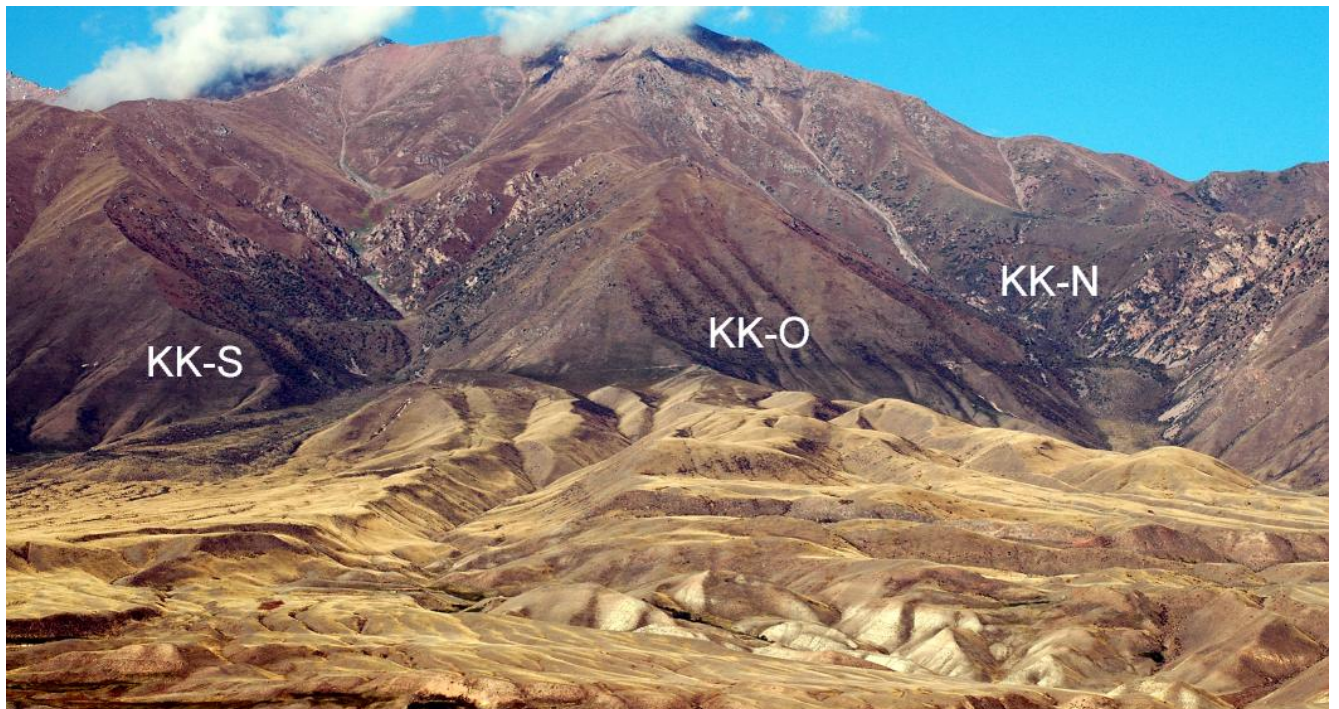


Figure 120. The Karakungey rockslides and rock avalanches at the western frame of the Djungal depression
 KK-S – the Southern Karakungey RA, KK-N – the Northern Karakungey RA, KK-O – Scar of the Old Karakungey RS

The southern rock avalanche at 41.86° N, 74.25° E (No 19 on Figure 2) is about $20 \times 10^6 \text{ m}^3$ in volume, while the northern one at 41.87° N, 74.24° E is about $10 \times 10^6 \text{ m}^3$ only (No 18 on Figure 2, Figure 121). It is likely that both failures had occurred simultaneously due to strong earthquake, though no one of these features have been dated by any quantitative method. Tree ring dating gives age of about 250 years, which corresponds to the upper age limit. It is evident that in fact they are older, but how much older is still questionable. One more significantly eroded scar can be identified between these gullies on the east-facing front slope (see Figure 120, KK-O). Corresponding deposits have been significantly reworked and could be hardly distinguished among bouldery alluvial fans that form the uppermost part of the depression fill. Such peculiarities show that this failure should be much older than well-expressed Karakungey rock avalanches.

Besides above-mentioned bedrock landslides that can be identified in the first place geomorphologically, there are some evidences of one more past rock avalanche (No 20 on Figure 2) that can be derived from the analysis of Quaternary deposits only, and will be described hereafter. We consider it as a much older and larger predecessor of the Southern Karakungey rock avalanche (P-KK on Figure 108).

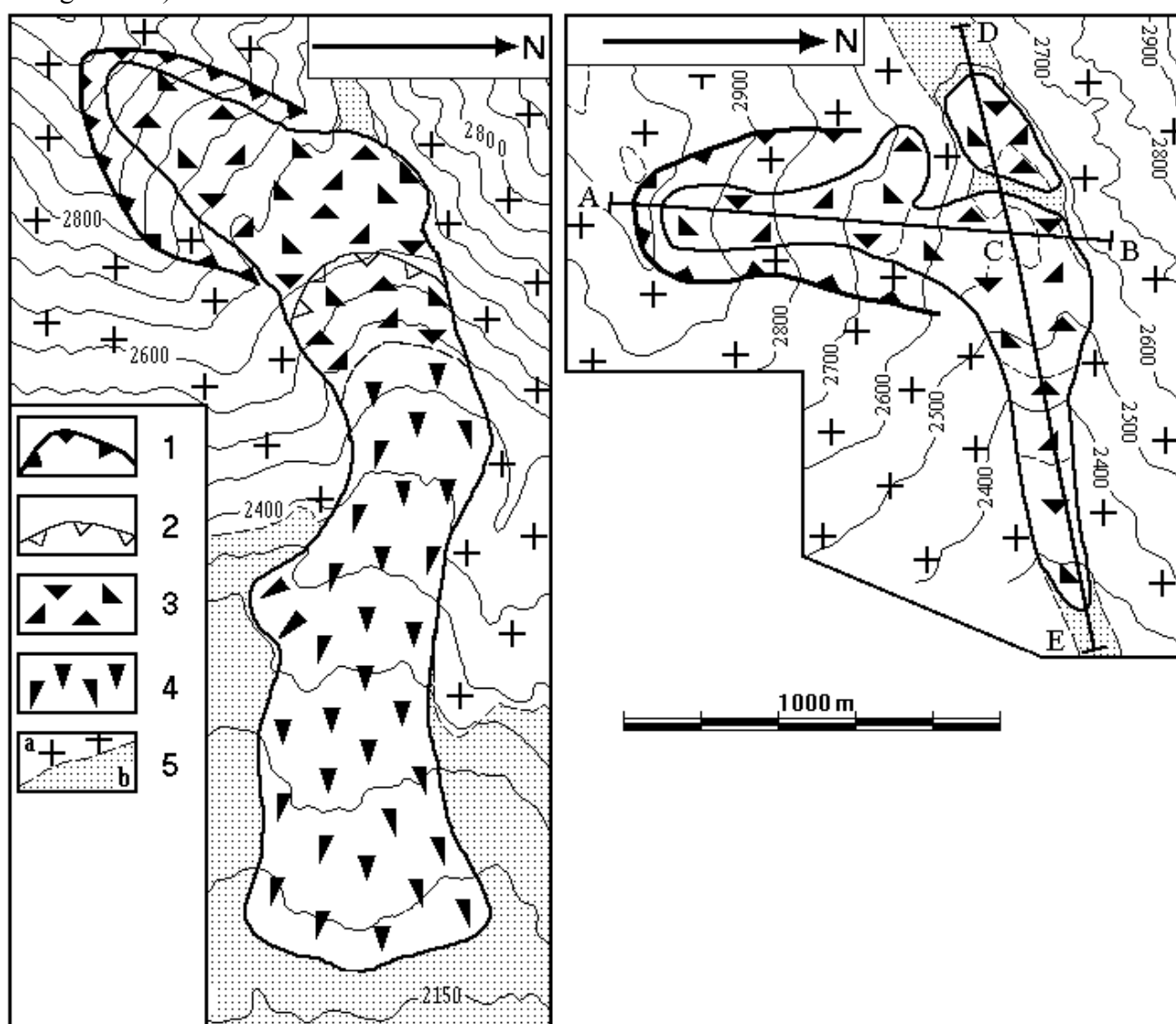


Figure 121. The schematic map of the Northern Karakungey rockslide (right) and Southern Karakungey rockslide (left)
 Legend: 1 – Main scar; 2 – Secondary scar; 3 – Rockslide deposits; 4 – Rock avalanche deposits of the secondary rock avalanche; 5 – Bedrock (a) and Quaternary deposits (b)

Southern Karakungey rock avalanche is a classical example of the secondary type of long runout bedrock slope failure, along with the Chongsu one described above. It formed a compact dam just at the scar foot that block the valley and has an expressive *brandung* raising 10-15 m above the dams'

crest, and concave secondary scar on its downstream slope (Figure 122, Figure 123). The collapsing rock mass hit the opposite slope at a rather sharp angle (about 40°) and deflected down-valley (Figure 124). Rock avalanche that originated after this collision was 2000 m long, 300-600 m wide and 15-20 m thick (Figure 125). Distinct secondary scar highlights the boundary between the compact and long runout parts of rockslide deposits (see Figure 122). Since the latter is more voluminous than the compact one, it could not descend from the dam with a significant delay (nominal volume of the secondary scar seems to be much less than the rock avalanche volume), thus secondary scar just marks the transfer from the first stage of emplacement to the second one. On its way rock avalanche had left trimlines more expressive at the true left slope (see Figure 125).



Figure 122. Southern Karakungey rockslide
Headscarp is visible on the background, while compact blockage with an expressive *brandung* (Br) and the secondary scar at the blockage's downstream slope – on the foreground



Figure 123. Headscarp and sharp upstream edge of the Southern Karakungey rockslide body
View from the brandung

Rock avalanche has a curved stripe of huge angular boulders (see Figure 124, Figure 126) while its axial part and boundary slopes contain large quantity of fines that differs this rock avalanche from the above-mentioned Seit and the Chongsu cases significantly. We assume that it could be somehow associated with a blow-in of fines from the adjacent wide Djungal depression.



Figure 124. View on the Southern Karakungey rockslide from its headscarp
Br – the brandung; *RA tip* marks the distal limit of the rock avalanche body



Figure 125. The frontal view on the Southern Karakungey rockslide and 1.5-km long secondary rock avalanche. Arrows mark the bench composed of rockslide debris that reflects the initial rock avalanche thickness during its motion

Unlike Southern Karakungey rock avalanche with distinct concave secondary scar, Northern Karakungey looks quite different. It also has a compact body at the foot of the rockslide scar but with convex slopes, including that above elongated avalanche-like part (Figure 127). The peculiarity of this bedrock slope failure is that its sliding surface came out on the slope not directly at its base, like in the previously described case, but about 50 m above (Figure 128). The same phenomenon was observed at the Kaskasu rockslide (see Figure 73) that is also characterized by the significant widening of the lower part of the dam. Jumping from this 'shelf' the descending rock mass of the Northern Karakungey rockslide divided into two parts – the bigger one converted into rock avalanche, while the smaller one formed separate heap of debris upstream from the main dam (Figure 129, Figure 130).

As it can be seen on Figure 127, rock avalanche followed along the creek's channel and snuggled up to the true left bank of the valley. It did not spread over the entire valley bottom as Southern Karakungey and Chongsu rock avalanches. We hypothesize that such difference reflects some differences in mechanisms of their mobility.

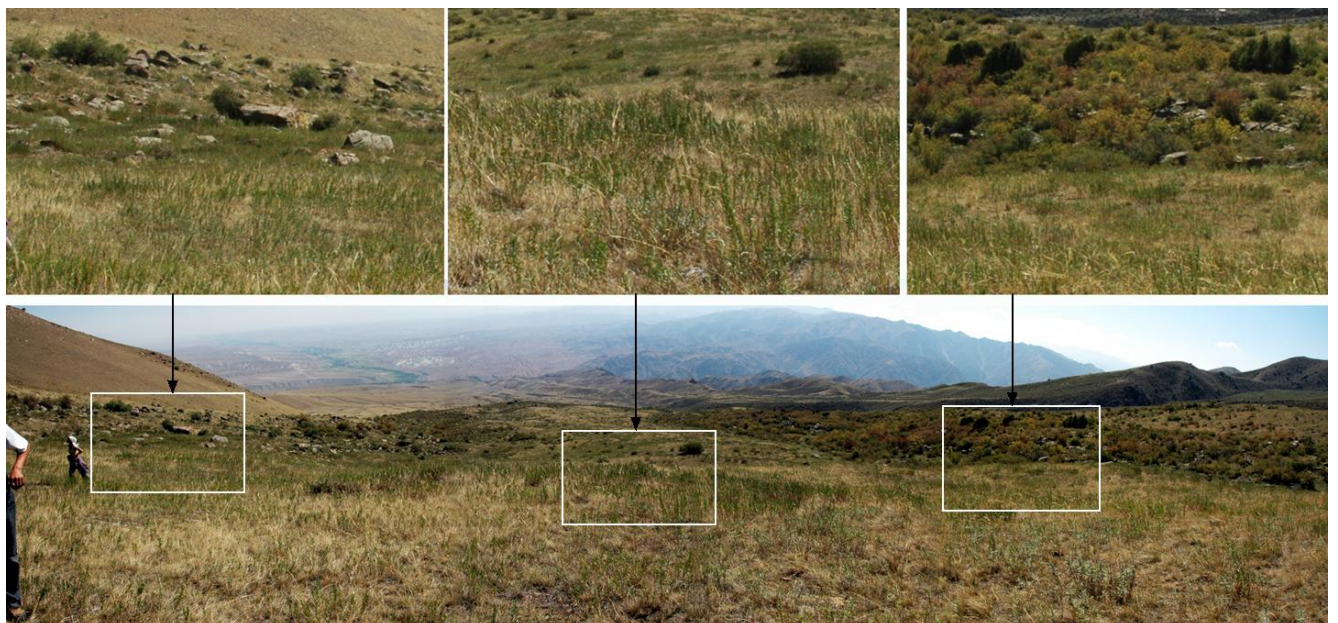


Figure 126. Surface of the Southern Karakungey rock avalanche (view "downstream"). Levees composed of angular granite boulders are shown on the left and right insets while smooth matter axial zone – on the central inset



Figure 127. Northern Karakungey rock avalanche
 Compact blockage with convex slopes at the background and rock avalanche termination at the foreground.
 Note that rock avalanche body fills the valley only partially

One more interesting feature can be observed east from the Southern Karakungey rock avalanche, about 4.5 km far from the foot of the rocky slope at 41.86° N, 74.3° E (see Figure 108). Here the small ridge that forms the left bank of South Karakungey Creek valley has an unusual dual structure. Its base as well as the entire ridge further to the east is composed of rounded granite boulders with sandy-gravel fill. It is typical debris flow (may be glaciofluvial) deposits that compose most of Quaternary sediments at the Djungal depression western termination. They could accumulate during Pleistocene glaciers retreat. But upper part of the ridge in question is composed of angular, not rounded boulders (Figure 131), quite atypical of deposits that had been brought for such a long distance from its source zone – the upper reaches of the South Karakungey Creek dissecting the adjacent range. Same succession is observed at adjacent outcrops as well at a distance of about 1.5 km in toto. We assume that this unit represents remnant of old rock avalanche deposits that had descended somewhere from the upper reaches of Southern Karakungey Creek, thus being much bigger than South Karakungey rock avalanche described above. Though it is difficult to locate its source zone, runout distance of this Pleistocene event (Pre-Karakungey rock avalanche – No 20 on Figure 2) should be about 7 km if not longer.

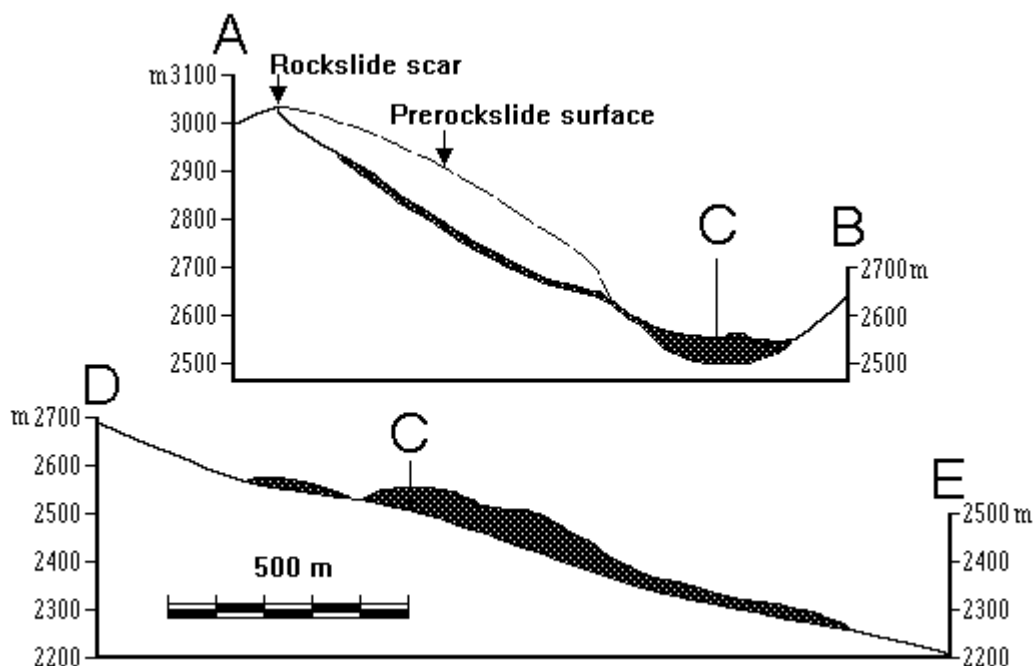


Figure 128. Schematic cross-sections of the Northern Karakungey rockslide
(see Figure 121)



Figure 129. Upstream separate part of the Northern Karakungey blockage
View upstream from the main body



Figure 130. View from upstream on the separate part of the Northern Karakungey rockslide and filled dammed lake

Unlikely that emplacement of such voluminous body composed of angular boulders could be due to any other process. Deposition area is too low and too far from the mountain range to be interpreted as end moraine. Thus, the proposed origin of this unit seems to be most logical. The fact that large-scale bedrock slope failures have occurred repeatedly at the same place proves the assumption of spatial clustering of such events [Strom, Abdrakhmatov 2004], which was mentioned before, when we described the Snake-head rock avalanche.

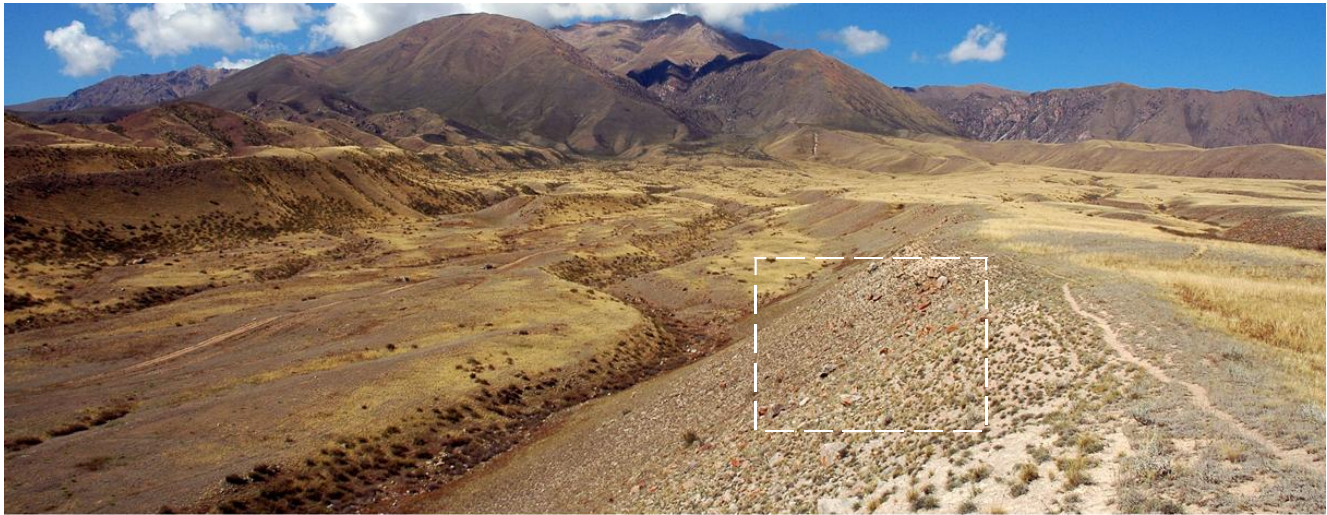


Figure 131. Angular boulders of the assumed Pleistocene Pre-Karakungey rock avalanche
Holocene Southern Karakungey rock avalanche at the background

3.12 THE MINGTEKE ROCK AVALANCHE

One more long runout rock avalanche (No 22 on Figure 2) had descended at 42.01° N, 74.34° E from the hanging wall of an active fault bounding the Djumgal depression from the north (see Figure 13). It is an expressive example of secondary rock avalanche that had traveled for about 4200 m. One can see an expressive trimline clearly visible on the left bank of the valley much higher than the final rock avalanche surface (Figure 132).

We consider this rock avalanche as one more example of secondary avalanches. It has a large amount of material accumulated at the foot of its headscarp, expressive flow-like avalanche portion that had dammed the Mingteke Creek and concave "secondary scar" that marks the boundary between compact proximal accumulation and highly mobile avalanche part.

3.13 LARGE LANDSLIDES IN THE NEOGENE-QUATERNARY SEDIMENTS

Besides the above rockslides and rock avalanches there are several large landslides within the study area that affect non-lithified Neogene and Quaternary deposits in the intermontane neotectonic depressions. Some of them are described hereafter briefly.

Huge rotational landslides in Neogene and Quaternary deposits that had affected areas about 3×2 km each are visible in the central part of the Djumgal depression opposite the Chaek village and south from it (Figure 133). The first one forms a tremendous amphitheater at 41.93° N, 74.57° E (Figure 134). Blocks inside the amphitheater are tilted due to rotation along the cylindrical sliding surface (Figure 135). Another landslide at 41.89° N, 74.52° E is significantly eroded and looks much older than the first one (Figure 136). These features are situated south from the recent anticline growing along the axis of the Djumgal intermontane depression (see Figure 133, Figure 134).

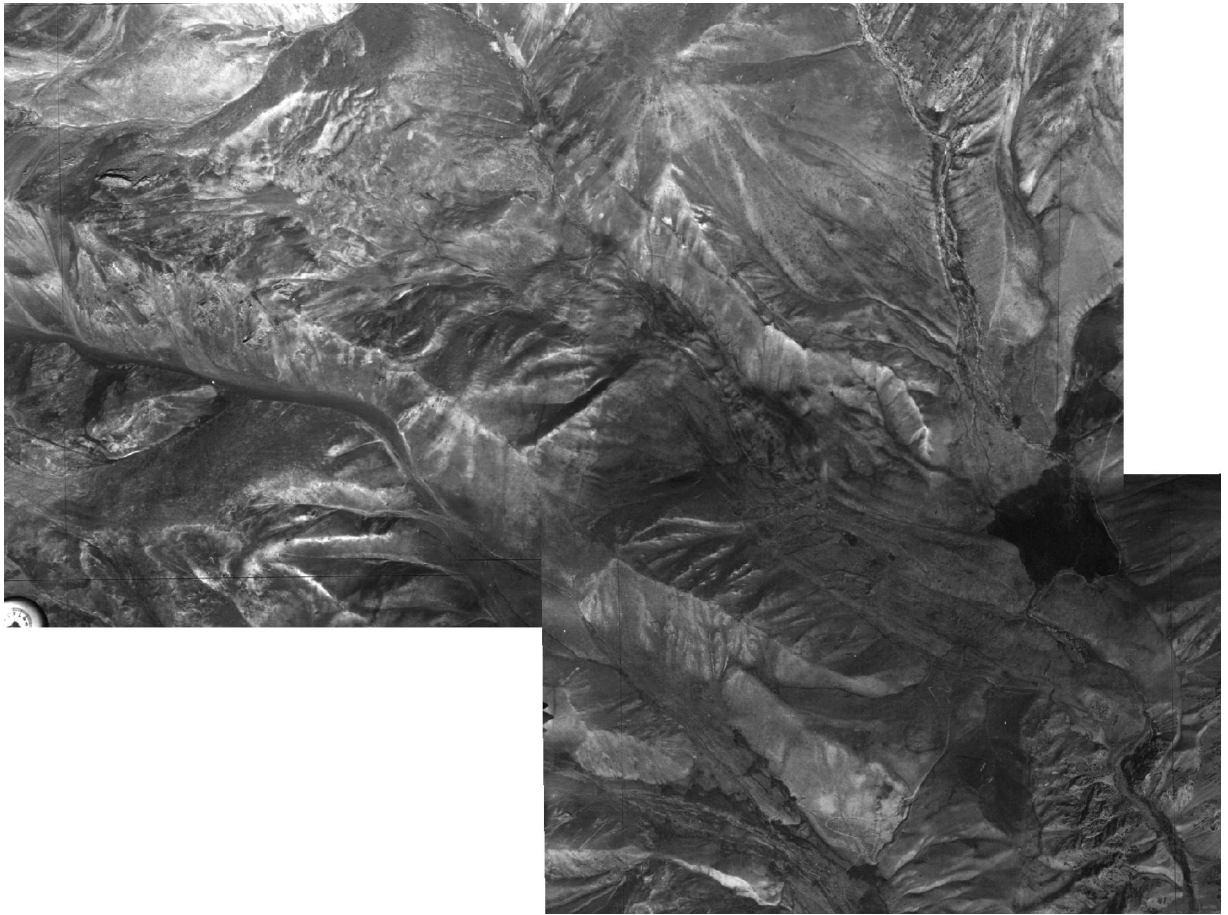


Figure 132. The Mingteke rock avalanche
Assemblage of aerial photographs

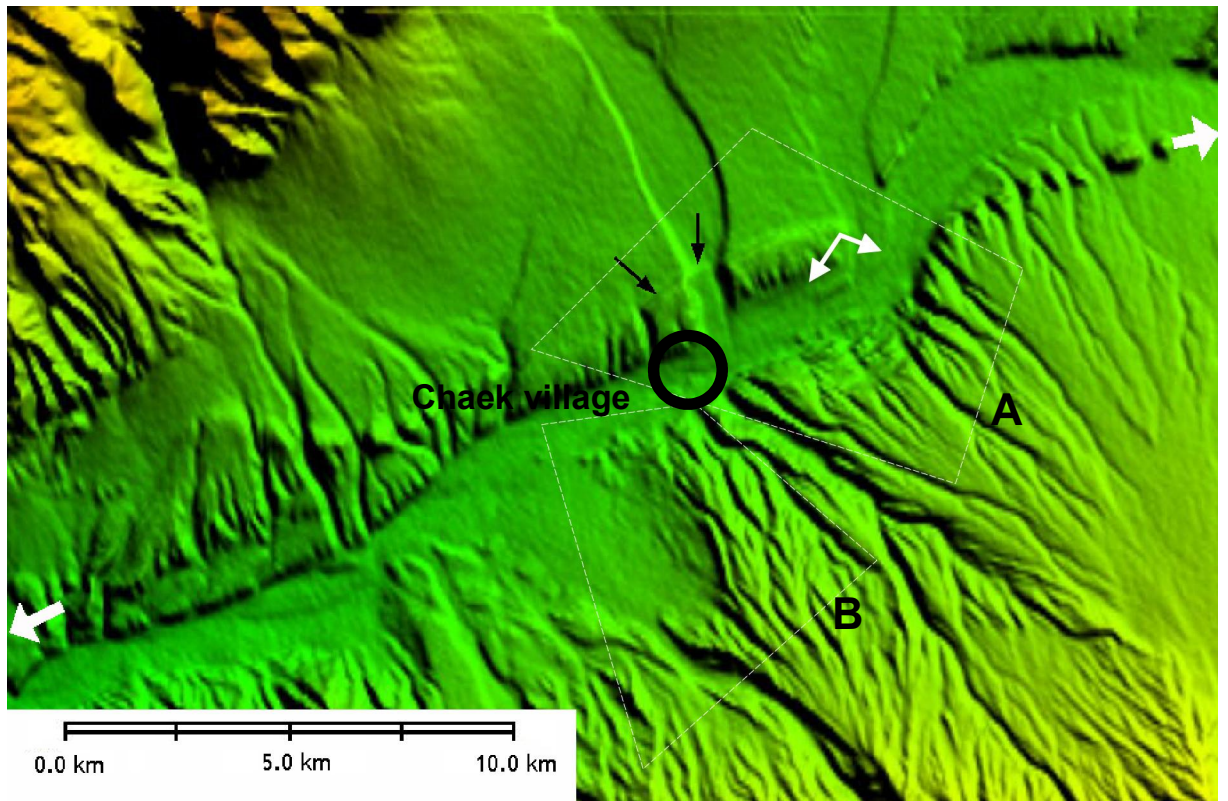


Figure 133. Huge rotational landslides in the N-Q deposits of the Djungal intermontane depression (3" SRTM DEM). Outlined areas are shown on Figure 134 (A) and Figure 136 (B). Large white arrows - recent anticline axis; small double-head white arrow - point of the panorama (Figure 135); black arrows mark recent offsets along the

northern limb of anticline which value at the higher level exceeds that at the more recent terrace indicating recurrent displacements

Its northern limb is, most likely, complicated by recent fault that displaces both the alluvial fan and low terrace in the valley that crosses the anticline (at 41.95° N, 74.53° E). Offset value outside the valley is bigger than on this terrace, while valley bottom is not displaced at all, thus proving the recurrent faulting. It can be hypothesized that landslides were triggered by earthquakes associated with these recurrent events.

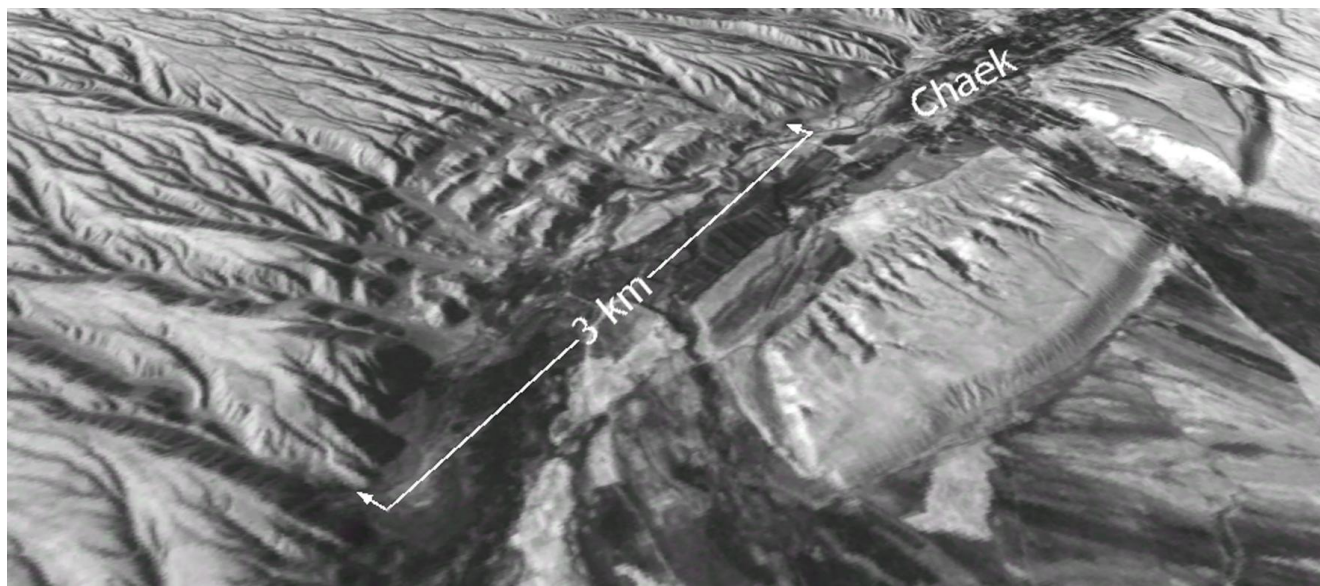


Figure 134. 3-D view of the area A, shown on Figure 133
Rotational Chaek landslide on the left bank of the river and recent anticline on its right bank



Figure 135. Panoramic view of the Chaek landslide

Another large landslide in the Djungal depression is located at its western centroclinal (41.87° N, 74.32° E). This Western-Djungal landslide (WDL on Figure 108, No 21 on Figure 2) had affected about 10 km^2 – almost the entire western termination of the depression on the right bank of the Kokomeren River valley composed of Neogene and Quaternary sediments. It is bounded by the horseshoe-like headscarp up to 50-70 m high. Depth of the sliding surface of this landslide is unknown. It can be assumed, however, that it comes out below the present-day Kokomeren riverbed. Most of its sliding surface, except the headscarp, should dip quite gently (Figure 137). At its southeastern part the uppermost layers have been completely removed, most likely by the intensive erosion of the area affected by superficial landslides. The entire landslide complex seems to be inactive at present. Unlike the Chaek rotational landslides, which bodies formed several tilted steps, the Western-Djungal landslide moved as a single block and can be classified as a landslide of the translational type.

One more complex landslide in the Neogene and Quaternary sediments is located at the southern part of the Suusamyry valley at 42.04° N, 73.88° E (No 23 on Figure 2), at a small depression separated from the main part of the intermountain depression by several hundreds meters high ridge.

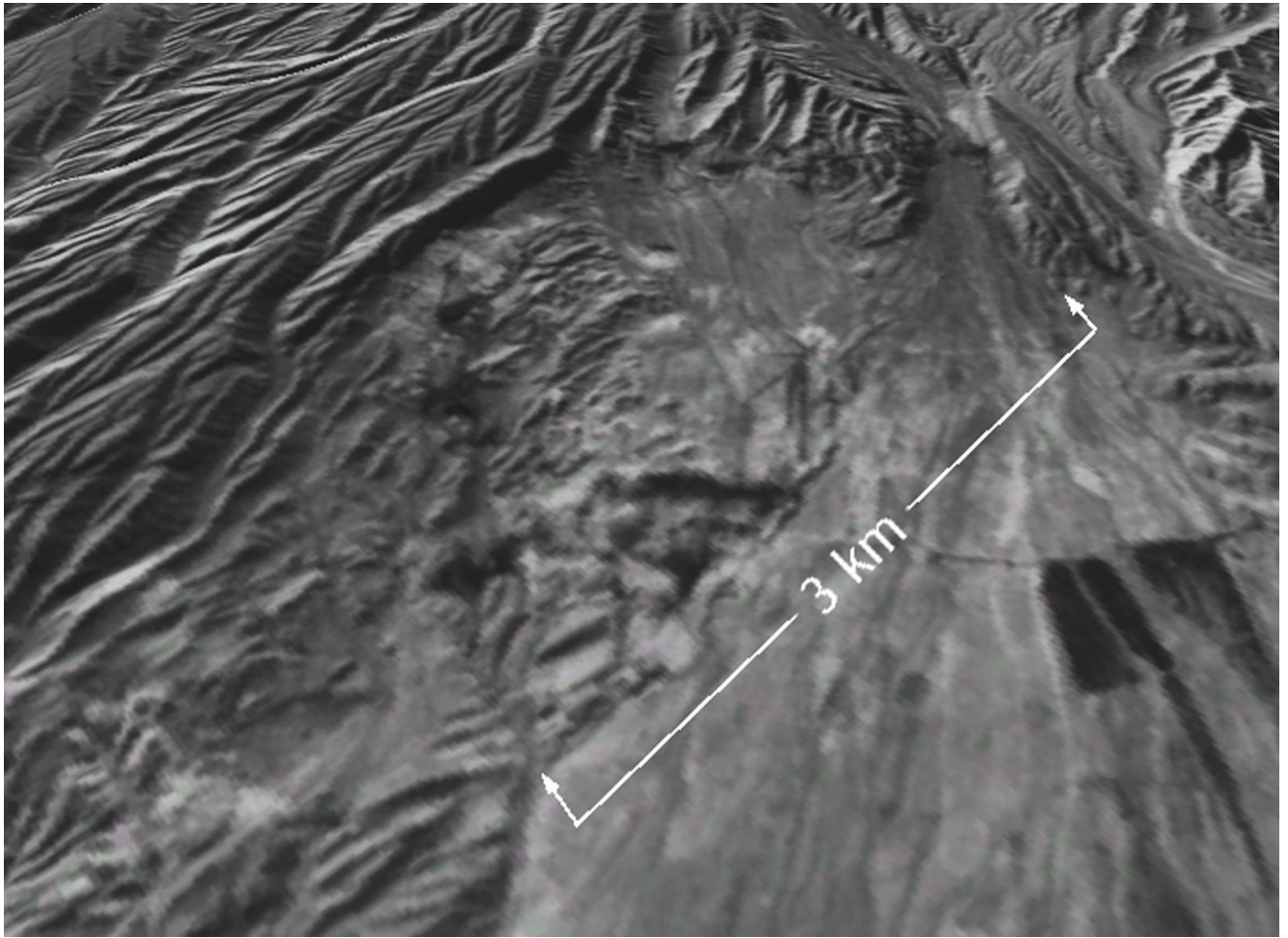


Figure 136. 3-D view of the area B, shown on Figure 133
 Significantly reworked rotational landslide South from the Chaek village. Large extent of erosion allows assumption that this feature is much older than the Chaek landslide

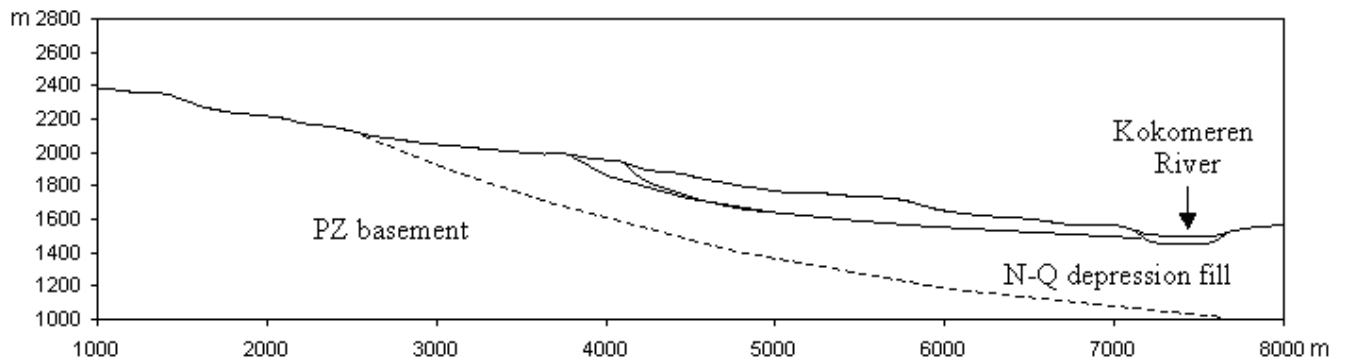


Figure 137. Hypothetical cross-section of the Western Djungal landslide

Landslide represents the lowering about 3×4 km in size bounded by the horseshoe-shaped headscarp up to 50 m high (Figure 138). Its relief has been significantly reworked by erosion, but most likely it could be classified as some combination of the rotational landslide and lateral spread.



Figure 138. Combined 3D DEM and KFA-1000 space image of the landslide in the southern part of the Suusamyry valley

3.14 CALDERA-LIKE COLLAPSE AT THE NARYN RIVER BASIN DOWNSTREAM FROM THE KOKOMEREN RIVER MOUTH

Rockslides and landslides described above do not exhaust all examples of these natural phenomena that can be found out in the Kokomeren River basin and in the adjacent part of the Naryn River basin.

Numerous large rockslides were found out in the Kokomeren River valley downstream from the Aral village, especially when it enters the Minkush-Kokomeren intermontane depression – one of the most active neotectonic structures of the Central Tien Shan [Sadybakasov 1972, Chedia 1986]. This zone extends for more than 125 km along the Naryn, Lower Kokomeren and Minkush River valleys from the Ketmen-Tiube intermontane depression at the West up to the Sonkul intermontane depression at the East [Strom, 1982, Belousov, et al., 1994].

Besides landslides, rockslides, sackungs and surface ruptures there are two really unique geomorphic features – caldera-like cavities at the right bank watersheds of the Naryn River valley where hundreds millions and billions cubic meters of rocks "disappear" in the range interiors [Strom 2000, Strom, Groshev, 2009]. One of them is located in the central part of the Santash Ridge that forms the right bank of the Naryn river valley in the upper reaches of the Kyzylkiol creek (41.81° N, 73.74° E) [Orlov, 1980; Strom, 1982]. It is a roughly rhomboid cavity (Figure 139) about 3×2 km in size with 250 to 700 m high steep slopes and relatively flat southward inclined bottom. Its south-eastern edge is cut through by the Kyzylkiol creek gorge, which upper reaches eroded the cavity's bottom at a depth of about 300 m (Figure 140).

The Santash ridge is build of the igneous and metamorphic Proterozoic and Palaeozoic rocks overlaid by Carbon red beds developed at its northern slope only (Figure 141). Though these red beds contain some gypsum layers, it seems that no rocks are subjected to karst in the ridge's interior. In the Kyzylkiol gorge, where it cuts the south-eastern cavity's edge (point "A" on Figure 139), only lowermost 20-25 m of slopes are "painted" by red mud left by debris flows that originated from the

cavity. Slopes above this level are covered by the gray-colored scree of local igneous and metamorphic rocks. It indicates, that the cavity southern edge breakage caused by the stream back erosion, took place recently, may be hundreds years ago. Earlier the cavity about 3 km³ in volume was a locked feature. It should be noted that in Kyrgyz language “Kyzylkiol” means “Red Lake” (may be there was really a lake in the past?). After the Kyzylkiol stream back erosion dissected it, the southern part of the cavity’s bottom was eroded (see Figure 140). Torn topographic features at the northern part of the cavity wall indicate its catastrophic origin (Figure 142).

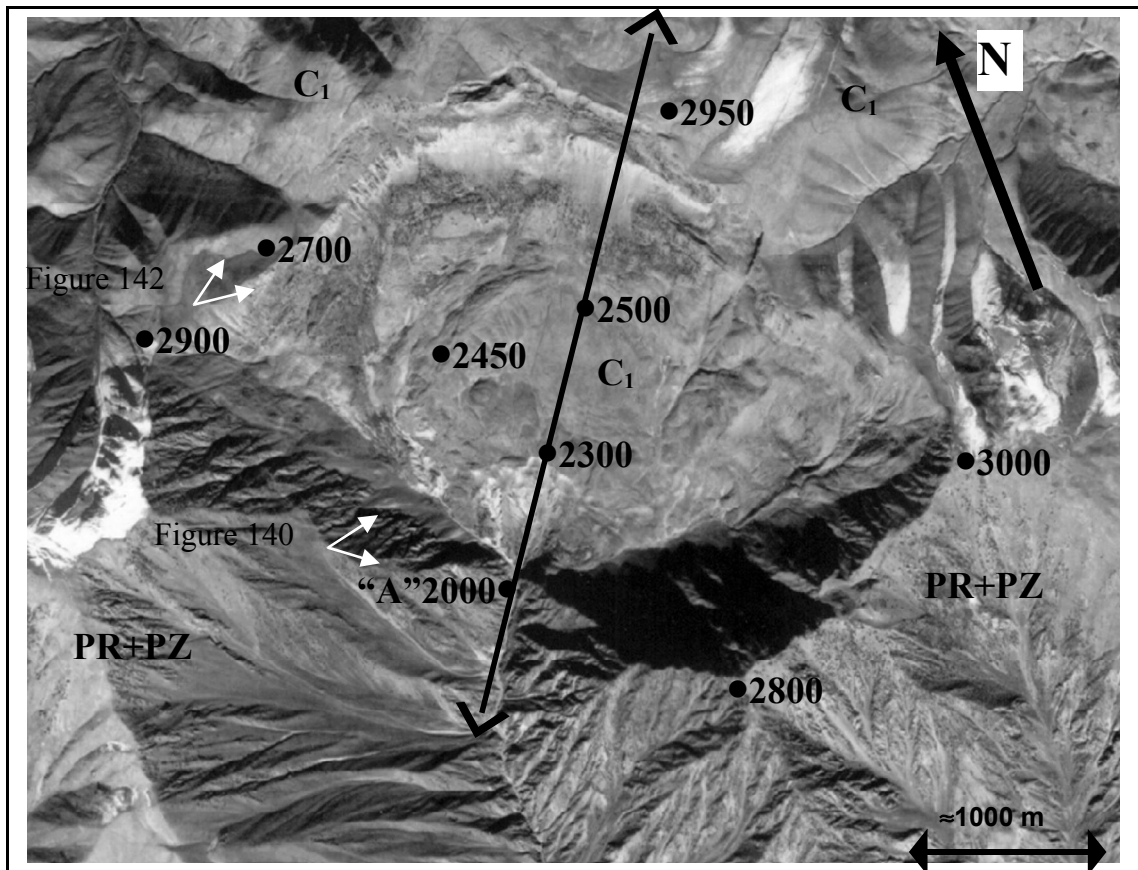




Figure 139. The Kyzylkiol caldera-like collapse

Fragment of high resolution KFA-3000 space photograph. Numbers – height of the specified points (•) above sea level;  cross-section (Figure 141)  – sites from which photographs were made.

It could be hypothesized that this caldera-like cavity originated due to strong earthquake. The only one known analogue – the so called “Bitut” structure was formed during the 1957 catastrophic ($M > 8$) Gobi Altai, earthquake in Mongolia [Gobi Altai ..., 1963]. However, to explain the nature and mechanism of such dislocations we should, at first, understand were the tremendous amount of rocks that initially occupied the cavities "disappeared" (Figure 143) since erosion has removed a small portion of material only, incomparable with the total volume of the cavity.

Geology of the mountain ranges where the cavity is located excludes its karst origin. The morphology of its bottoms and of the upper reaches of the gorge that cut its southern edge don't allow to explain the cavity's genesis as the result of glacial or erosion processes. It is really a caldera-like collapse, though its volcanic origin should be excluded as well.

One more caldera-like collapse, much smaller in size and, likely, much older, is located 30 km west from the Kyzylkiol one at 41.81° N, 73.38° E, outside the area shown on Figure 2 [Strom, 2000].

It is hypothesized that such tremendous subsurface cavities – hundreds millions and billions cubic meters in volume – could appear in the course of the detachment basement folding in the tectonically stratified rigid upper crust (Figure 144) that could last for dozens of millennia. This model of the geologically long-term deformations preceding rapid single-event collapse. Such model, though

being quite exotic, seems to be the only one, that could explain sudden 'disappearance' of hundreds million and billions of cubic meters of rocks in the mountain ridge interior in the specific tectonic environment.



Figure 140. Upper reaches of the Kyzylkiol creek, eroding the cavity bottom
Note none-erosive flat relief of the cavity bottom outside the eroded part

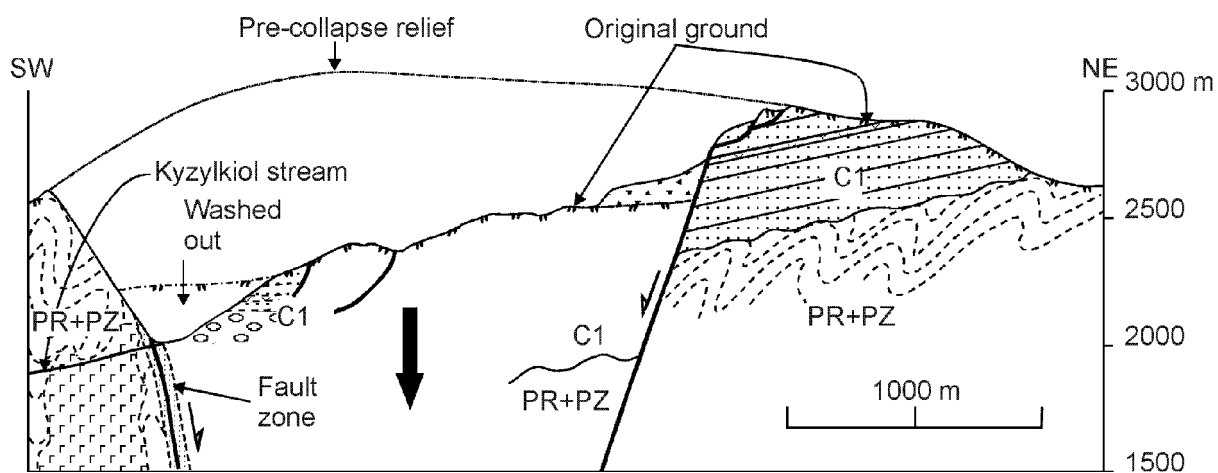


Figure 141. Cross-section of the Kyzylkiol caldera-like collapse
C₁ - Carbon sandstone and conglomerate with gypsum interbeds;
PR+PZ - Proterozoic and Palaeozoic metamorphic and igneous rocks

Anyhow further detail mapping and geophysical investigations are necessary to reveal real mechanism of these unique features' origin.

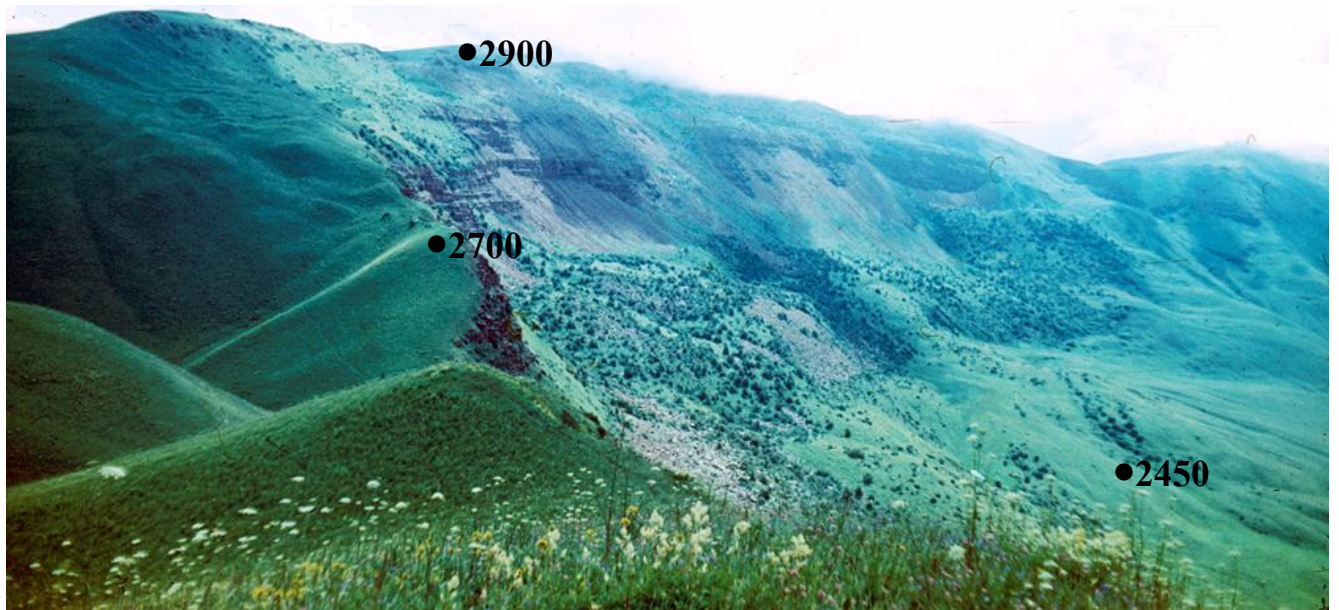


Figure 142. Torn topographic features at the northern edge of the Kyzylkiol cavity



Figure 143. View of the Santash Ridge at the Kyzylkiol section from the north

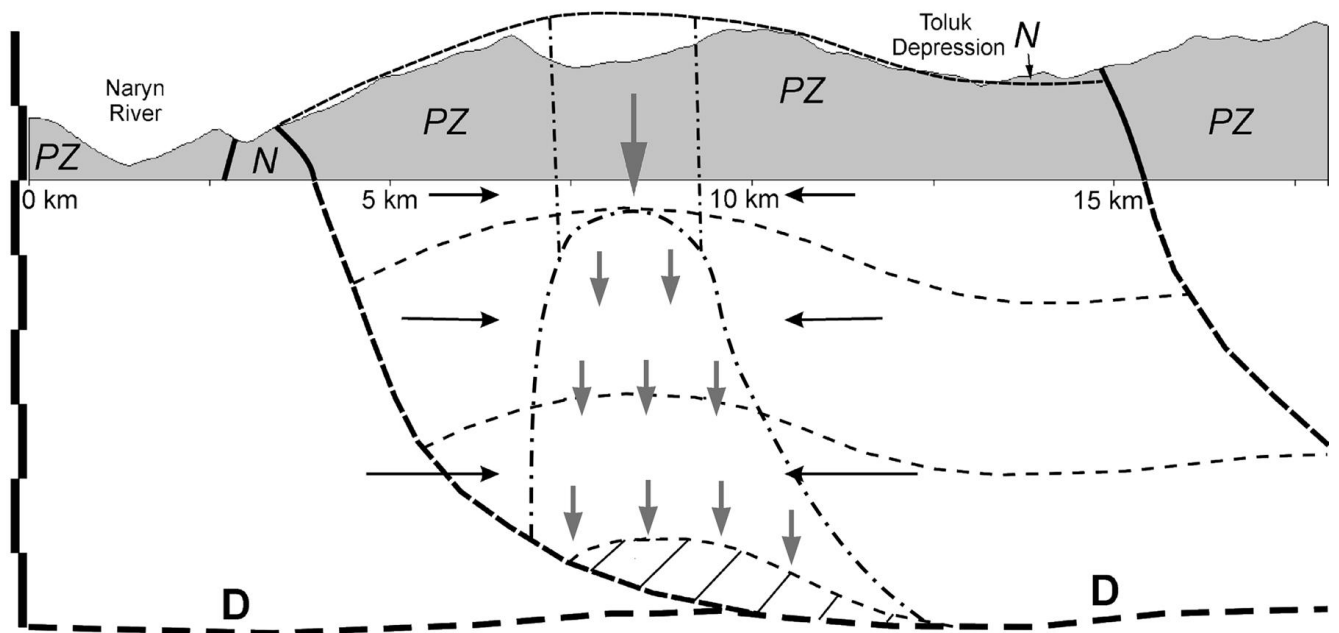


Figure 144. Schematic model of the 'tectonic cave' formation due to basement folding associated with the deep-seated detachment. The upper part is the cross-section of the Santash ridge with reconstructed deformed pre-orogen planation surface indicating well-pronounced basement folding. Shaded area – the assumed 'initial free space' in the core of an anticline above the detachment zone (D); black arrows show qualitative

distribution of the horizontal stress; small gray arrows below the dashed-dotted line – gradual failure and formation of the cavity roof arch; large gray arrow – final catastrophic collapse

4 CONCLUSIONS

Case studies described above represent various types of rockslides and landslides, which differ in volume, age, runout, morphology, style and extent of river damming, etc. They can be classified according to various classification systems proposed by Zolotariov, et al. [1969], Emelianova [1972], Varnes [1978], Costa & Schuster [1988], Nicoletti & Sorriso-Valvo [1991], Hermanns, et al. [2004], Dunning et al. [2005], Strom [2006].

Most of features described in this Guidebook are large-scale bedrock landslides (rockslides), and many of them had converted into highly mobile rock avalanches, they were classified into three main types, according to Strom [2006]: "Primary" rock avalanches in unconfined (the Seit rock avalanche – see section 3.1) and confined (the Mini-Köfels rockslide – see section 3.10) conditions; "Jumping" rock avalanches exemplified by the Kashkasu (see section 3.7) and the Northern Karakungey (see section 3.11) case studies; and the most widely developed "Secondary" rock avalanches. The latter belong to two subtypes: secondary rock avalanches with prominent "secondary" scar above the avalanche-like part (the Chongsu – see section 3.4, the Southern Karakungey – section 3.11, and the Mingteke – section 3.12 case studies) and those, which originated, likely, due to the "bottle-neck effect" (the Snake-head – see section 3.1 and the Sarysu – section 3.5 rock avalanches). It is evident that extensive further studies, including physical and numerical modeling are necessary to understand real mechanisms of rock avalanches' formation and their high mobility.

It is likely that most of the studied features originated due to strong past earthquakes. In some cases, such as the Snake-head and the giant Kokomeren rockslide, such assumption has enough grounds (see sections 2.2, 3.1, 3.8), while in many other cases additional studies should be performed to prove (or disprove) this assumption.

No one land/rockslide, except those formed by the 1992 Suusamyр earthquake have been dated precisely up to now. Their age estimates are based on their morphological freshness and on the relationships with other geomorphic elements such as river terraces mainly. The upper limit of the Seit ans Karakungey rock avalanches age was estimated by tree-ring dating. Along with geomorphic data it allows assumption of their origin in the Late Holocene time. Several large-scale rock slope failures, namely the Kokomeren rockslide, the Displaced Peneplain rockslide, the Kara-Kungey-Old and the Pre-Karakungey rock avalanches, and, presumably, the Sarysu rock avalanche are Late Pleistocene features.

Lack of rockslide ages is a critical gap in our knowledge preventing reliable rockslide risk assessment of the upper part of the Kokomeren River basin. Thus, dating is one of the main fields of further rockslide investigations in the this region.

5 ACKNOWLEDGEMENTS

We want to express out gratitude to Prof. Kyoji Sassa for his kind attention to our activities in the Tien Shan Region. Preparation of Summer School Guidebook was strongly supported by the UNESCO IPL grants provided by ICL in 2004-2009. This work was also supported by the Scientific Program of the Presidium of Russian Academy of Sciences No 16 (Catastrophic Processes) and we want to thank Director of IDG RAS Julius Zetzer and IDG Programme leader Sergey Turuntaev for their help in organization of field trips.

We had useful discussions with Mikhail Akhmetiev, Stuart Dunning, Stephen Evans, Reginal Hermanns, Hans-Balder Havenith, Oldrich Hungr, Oliver Korup, Mauri McSaveney, Tim Davies, Gabriele Scarascia Mugnozza.

We were glad to host participants of the 2006-2008 Summer Schools from Czech Republic, Italy, USA, Russia, Kyrgyzstan and hope to see them in the Tien Shan in future.

Field investigations that provide most of data described in the Guidebook, could not be performed without hard work and overall assistance of Atyr Djumabaeva, Zhyldyz Dyikanalieva, Cholponbek Ormukov, Kazbek Abdrakhmatov, Kyzylgul Beishekova, Sagyn Mukambetov, Mukhtar Isaev.

6 REFERENCES

- Abdrakhmatov, K., Lemsin, I., Strom, A. 1994. Neotectonics of the Ketmen-Tiube depression. In: The Tien Shan in the Recent Orogeny Period. Bishkek, Ilim, 86-96 (in Russian).
- Abdrakhmatov, K., Strom, A., 2006. Dissected rockslide and rock avalanche deposits; Tien Shan Kyrgyzstan. In Evans, S.G.; Scarascia Mugnozza, G.; Strom, A.; Hermanns, R.L. (Eds.) Landslides from Massive Rock Slope Failure. NATO Science Series: IV: Earth and Environmental Sciences, Springer, Vol. 49, 551-572.
- Alford, D. and Schuster R. (Eds.) 2000. Usoi Landslide Dam and Lake Sarez. An assessment of Hazard and Risk in the Pamir Mountains, Tajikistan.. UN Publication. Sales No. E.00.III.M.1.
- Belousov T.P., Skobelev S.F., and Strom A.L. 1994. On estimation of the recurrence period of strong earthquakes of the central Tien Shan (according to the data of absolute geochronology). Journal of Earthquake Prediction Research, 3, 226-236.
- Bogachkin, B.M., Korjenkov, A.M., Mamyrov, E., Nechaev, Yu.V., Omuraliev, M., Petrosian, A.E., Pletniov, K.G., Rogozhin, E.A., Charimov, T.A. 1997. Structure of the 1992 Suusamyr earthquake source on the basis of its geological and seismological effects analysis. Physics of the Earth., No 11, 3-18 (in Russian, English translation).
- Bogdanovich, M.C., Kark, J. Korolkov, B. and Muchketov D. 1914. Earthquake of the 4th January 1911 in the northern districts of the Tien Shan, Transactions Geol. Com., New Series 89: 270 p. (in Russian).
- Bull, W.B. 1996. Prehistorical earthquakes on the Alpine fault, New Zealand. Journal of Geophysical Research, 101 No B3, 6037-6050.
- Cassie, J.W., Van Gassen, W., Cruden, D.M. 1988. Laboratory analogue of the formation of mollards, cones on rock-avalanche debris. Geology, 16, 735-738.
- Chedia, O.K. 1986. Morphostructures and Neotectonic of the Tien Shan. Frunze, Ilim Publishing House, 314 p. (in Russian).
- Costa, J.E., and Schuster, R.L. 1988. The formation and failure of natural dams, Geol. Soc. Am. Bull. 100, 1054-1068.
- Cui, P., Chen, X., Chen, Z. 2009. The Barrier Lakes created during the Wenchuan Earthquake and its disaster mitigation works. Rock Characterisation, Modelling and Engineering Design Methods. Proc. of the ISRM-Sponsored International Symposium on Rock Mechanics, Hong Kong, 19-22 May 2009, CDROM.
- Delvaux, D., Abdrakhmatov, K.E., Lemzin, I.N. and Strom A.L. 2001. Landslides and surface breaks of the 1911, Ms 8.2 Kemin earthquake, Kyrgyzstan, Russian Geology and Geophysics 42(10): 1167-1177.
- Dunning, S.A., Petley, D.N., Rosser N.J., Strom, A.L. 2005. The morphology and sedimentology of valley confined rock-avalanche deposits and their effect on potential dam hazard. In: Hungr, O, Fell, R., Couture, R., and Eberhardt, E. Landslide Risk Management, A.T. Balkema, Amsterdam, 691-704.
- Emelianova, E.P. 1972. Main regularities of landslide processes. Moscow, Nedra Publishing House, 310 p. (in Russian).
- Erismann, T.H. 1979. Mechanisms of large landslides, Rock Mechanics 12, 15-46.
- Evans, S.G., Clague, J.J., Woodsworth, G.J, and Hungr, O. 1989. The Pandemonium Creek rock avalanche, British Columbia. Can. Geotechnical Journal 26, 427-446.
- Evans, S.G., Hungr, O., & Enegren, E.G. 1994. The Avalanche Lake rock avalanche, Mackenzie Mountains, Northwest Territories, Canada: description, dating and dynamics. Can. Geotechnical Journal 31, 749-768.

- Gaziev, E., 1984. Study of the Usoi Landslide in Pamir. Proc. 4th Int. Symp. on Landslides, Toronto, 1, 511-514.
- Ghose, S., Mellors, R.J., Korjenkov, A.M., Hamburger, M.W., Pavlis, T.L., Pavlis, G.L., Mamyrov, E. and Muraliev, A.R., 1997. The Ms = 7.3 1992 Suusamy, Kyrgyzstan earthquake: 2. Aftershock Focal Mechanisms and Surface Deformation. Bulletin of the Seismological Society of America, 87: 23-38.
- Gobi Altai earthquake, 1963. N.A. Florensov, V.P. Solonenko (eds.) Publishing House of the Academy of Sciences of the USSR, Moscow, 391 p. (in Russian, English edition is available).
- Hartvich, F., Mugnai, F., Proietti, C., Smolkova, V., Strom, A. 2008. A reconstruction of a former rockslide-dammed lake: the case of the Kokomeren River valley (Tien Shan, Kyrgyzstan). Poster presentation at the EGU conference, Vien.
- Havenith, H.-B., Strom, A., Caceres, F., Pirard, E., 2006. Analysis of landslide susceptibility in the Suusamy region, Tien Shan: statistical and geotechnical approach. Landslides, 3, 39-50.
- Heim, A. 1882. Der Bergsturz von Elm. Deutsch. Geol. Gesell. Zeitschr. 34, 74-115.
- Heim, A. 1932, Bergsturz und Menschenleben. Fretz and Wasmuth, Zürich.
- Hermanns, R.L., Niedermann, S., Gonzales Diaz, F.E., Faugue, L., Folguera, A., Ivy-Ochs, S., Kupic, P. 2004. Landslide dams in the Argentine Andes. In: Security a Natural and Artificial Rockslide Dams. NATO ARW Extended Abstracts, 79-85.
- Hewitt K., 2002 Styles of rock avalanche depositional complex in very rugged terrain, Karakoram Himalaya, Pakistan. In Evans S.G. (ed.) Catastrophic Landslides : effects, occurrence and mechanisms, Reviews in Engineering Geology. Geological Society of America, Boulder, Colorado, 345-378
- Hsü, K.J. 1975, Catastrophic debris streams (sturzstroms) generated by rock falls. Geological Society of America, Bulletin 86, 129-140
- Ignatiev, I.V. 1886. The earthquake in the Tokmak district in the 1885. Proceedings of the Russian Imperial Geographic Society, 22, Issue 2. (in Russian).
- Korup, O., Strom, A.L., and Weidinger, J.T. 2006. Fluvial response to large rock-slope failures – examples from the Himalayas, the Tien Shan and the New Zealand Southern Alps. Geomorphology, 78, 3-21.
- Kuchai, V.K., 1969. The results of repeated inspection of residual deformations in the pleistoseismal area of the Kebin earthquake. Geology and Geophysics, 1969, N°8 (116), 101-108. (in Russian).
- Kuchai, V.K. 1971. Use of paleoseismic dislocations for studying seismic regime (exemplified by the pleistoseismal zone of the 1946 Chatkal earthquake). Geology and Geophysics, No 4, 124-129 (in Russian).
- Lee C.F. and Dai F.C. The Dadu River Landslide Dam, Sichuan, China (in press)
- Leonov, N.N., 1960. The Khait 1949 earthquake and geological conditions of its origin. Proceedings of Academy of Sciences of the USSR Geophysical Series 3, 409-424 (in Russian).
- Leonov, N.N. 1970. The 1946 Chatkal earthquake. Problems of the engineering seismology, Issue 13, Moscow, Nauka, 64 - 77. (in Russian).
- Litovchenko, A.F. 1964. Catastrophic debris flow along the Issyk River. Meteorology and Hydrology. No 4, 39-42 (in Russian).
- Makarov, V.I. 1977. Newest Tectonic Structure of Central Tien Shan. Transactions of Geological Institute of RAS, Vol. 307 (in Russian).
- Mushketov, I.V., Orlov, A.P. 1893. Catalogue of Earthquakes of Russian Empire. Proceedings of Russian Geographic Society, 26. (in Russian).
- Nichol, S., Hungr, O., Evans, S.G. 2002. Large-scale brittle and ductile toppling of rock slopes. Canadian Geotechnical Journal, Vol. 39, 773-780.
- Nicoletti, P.G. and Sorriso-Valvo M. 1991. Geomorphic controls of the shape and mobility of rock avalanches, Geol. Soc. Am. Bull. 103, 1365-1373.
- Nikitin, M., Huggel, C., Schwarz, M., Goncharenko, O., and Galushkin, I.V. 2006. The analysis of the remotely sensed materials for the reconstruction of the Kolka Glacier collapse. In: Proc. Of the

- International Conference on High Mountain Hazard Prevention, Vladikavkaz – Moscow, June 23-26, 2004, 160-171.
- Orlov, L.N. 1980. On the kinematics and dynamics of the overthrusts at the boundary of the Northern and Middle Tien Shan. *Seismotectonics and seismicity of Tien Shan*. Ilim Publishing House, Frunze, 50-59. (in Russian).
- Sadybakasov, I. 1972. *Neotectonics of the Central part of the Tien Shan*. Frunze, Ilim, 116 p.
- Sadybakasov, I. 1990. *Neotectonics of High Asia*. Moscow, Nauka, 180 p.
- Shultz, S.S. 1948. Analysis of Newest Tectonics and Relief of the Tien Shan. *Proceedings of the All-Union Geographic Society. New Series, Vol. 3*, 222 p.
- State Water Inventory. Perennial data on the mainland superficial water regime and resources. Volume IX, Kyrgyz SSR. 1987. Leningrad, *Gidrometeoizdat Publishing House*, 450 p. (In Russian).
- Strom, A.L. 1982. About new zone of paleoseismodislocations in the Northern part of the Central Tien Shan. *Main problems of seismotectonics*. Moscow, 4-13, deposited in VINITI, No 3290-83. (in Russian).
- Strom, A.L. 1996. Some morphological types of long-runout rockslides: effect of the relief on their mechanism and on the rockslide deposits distribution, in K. Senneset (Ed.) *Landslides. Proc. of the Seventh International Symposium on Landslides, 1996, Trondheim, Norway, Rotterdam, Balkema, 1977-1982*.
- Strom, A.L. 2000. Caldera-like collapses at the watersheds in the Central Tien Shan, in *Landslides in Research, Theory and Practice*. Balkema.
- Strom, A.L. 2006. Morphology and internal structure of rockslides and rock avalanches: grounds and constraints for their modelling. In Evans, S.G.; Scarascia Mugnozza, G.; Strom, A.; Hermanns, R.L. (Eds.) *Landslides from Massive Rock Slope Failure. NATO Science Series: IV: Earth and Environmental Sciences, Vol. 49*, 305-328.
- Strom, A.L., Abdrakhmatov, K.E. 2004. Clustering of large rockslides: the phenomenon and its possible causes. In: Lacerda, W.A., Ehrlich, M., Fontoura, A.B., Sayao, A. (Eds.), *Landslides: Evaluation and Stabilization*. Taylor and Francis Group, London, 317–320.
- Strom, A.L., Groshev, M.E. 2009. *Mysteries of Rock Massifs Destruction*. In: M. Abbie and J.S. Bedford (Eds.) *Rock Mechanics: New Research*. Nova Science Publishers.
- Strom, A.L., Korup, O. 2006. Extremely Large Rockslides and Rock Avalanches in the Tien Shan, Kyrgyzstan. *Landslides, Vol. 3*, 125-136.
- Strom, A.L., Stepanchikova P. 2008. Seismic triggering of large prehistoric rockslides: Pro and Con case studies. *Proceedings of the International Conference on Management of Landslide Hazard in the Asia-Pacific Region (Satellite symposium of the First World Landslide Forum, Tokyo), Sendai, 11th – 12th November 2008*, 202-211.
- Varnes, D.J., 1978, Slope Movement types and processes, in Schuster, R.L. and R.J. Krizek (ed.), *Landslides – Analysis and Control: National Academy of Sciences Transportation Research Board Special Report No. 176*, p. 12-33.
- Wang, F., Cheng, Q., Highland, L., Miyajima M., Wanmg, H., Yan, C. 2009. Preliminary investigation of some large landslides triggered by the 2008 Wenchuan earthquake, Sichuan Province, China. *Landslides, 6*, 47-54.
- Yin, Y., Wang F., Sun, P. 2008. Landslide hazards triggered by the 12 May 2008 Wenchuan earthquake, Sichuan, China. *Proc. of the First World Landslide Forum., 18021 November 2008, UNU, Tokyo, Japan. Parallel Session Volume*, 1-17.
- Zolotariev, V.S., Kalinin, E.V., Fedorenko, V.S., Sheshenia, N.L. 1969. *Engineering-geological study of rockfalls and other gravitational phenomena on mountainous slopes*. Moscow State University, 188 p.